N82-18603

CR 165554
PWA-5515-165

NASA

JT9D Ceramic Outer Air Seal System Refinement Program

by

W. O. Gaffin

UNITED TECHNOLOGIES CORPORATION
PRATT & WHITNEY AIRCRAFT GROUP
COMMERCIAL PRODUCTS DIVISION

Prepared for

NATIONAL AERONAUTICS AND SPACE ADMINISTRATION
Lewis Research Center
Contract NAS3-20630

1. Report No.	2. Government Accession No.	3. Recipient's Catalog No.
NASA-CR-165554		

4. Title and Subtitle	5. Report Date
JT9D Ceramic Outer Air Seal System Refinement Program	January 27, 1982
	6. Performing Organization Code
7. Author(s)	8. Performing Organization Report No.
W. O. Gaffin	PWA-5515-165
	10. Work Unit No.
9. Performing Organization Name and Address	
United Technologies Corporation Pratt & Whitney Aircraft Group - CPD East Hartford, Connecticut 06108	11. Contract or Grant No. NAS3-20630
	13. Type of Report and Period Covered Contractor 1/79-2/81
12. Sponsoring Agency Name and Address NASA Lewis Research Center 21000 Brookpark Rd. Cleveland, Ohio 44135	14. Sponsoring Agency Code

15. Supplementary Notes
NASA Project Manager, Mr. J. E. McAulay Project Engineer, T. N. Strom
Engine Component Improvement Office
NASA - Lewis Research Center, 21000 Brookpark Rd., Cleveland, Ohio 44135

16. Abstract

The abradability and durability characteristics of a plasma sprayed ceramic outer air seal system have been improved to the point of being a strong candidate for incorporation in the high pressure turbine of JT9D engines. These improvements were accomplished by refinement and optimization of the plasma spray process and the metal substrate design.

An interactive analytical and rig test evaluation program provided direction for the refinement and optimization effort. The acceptability of the final seal system for engine testing was demonstrated by an extensive rig test program which included thermal shock tolerance, thermal gradient, thermal cycle, erosion, and abradability tests. An interim seal system design was also subjected to 2500 endurance test cycles in a JT9D-7 engine.

17. Key Words (Suggested by Author(s))	18. Distribution Statement
JT9D high pressure turbine Ceramic outer air seal Plasma sprayed zirconia Abradable outer air seal Durability improvement	

19. Security Classif. (of this report)	20. Security Classif. (of this page)	21. No. of Pages	22. Price*
UNCLASSIFIED	UNCLASSIFIED		

* For sale by the National Technical Information Service, Springfield, Virginia 22161

Foreword

The JT9D Ceramic Outer Air Seal program is part of the ECI-PI Project conducted by the Commercial Products Division of Pratt & Whitney Aircraft Group, United Technologies Corporation, under sponsorship of the National Aeronautics and Space Administration - Lewis Research Center. The seal system refinement effort presented in this report was conducted from January 2, 1979 to February 13, 1981. Mr. J. E. McAulay and Mr. T. N. Strom of the NASA Lewis Research Center were the Project Manager and Project Engineer respectively for the contract. Dr. R. C. Bill of the U. S. Army R&D Lab served as technical advisor.

This program was under the technical direction of Mr. L. T. Shiembob of Pratt & Whitney Aircraft who was assisted by Sr. Engineers David Cloud and James Hyland. Senior engineering advice and consultation was provided by Mr. J. T. McCabe and Mr. F. H. Mahler.

This report was prepared under the direction of William O. Gaffin, Pratt & Whitney Aircraft Program Manager. This report has been assigned the Commercial Products Division, Pratt & Whitney Aircraft Group Internal Report Number PWA-5515-165.

TABLE OF CONTENTS

TABLE OF CONTENTS (Continued)

1.0 Summary

The ceramic outer air seal system was refined to be a strong candidate for incorporation in the high pressure turbine of the JT9D engine.

The initial demonstration of sprayed ceramic seals for gas turbine engine sealing was demonstrated by engine test under NASA ECI-PI project support, Reference 2. Engine test of that design demonstrated potential but indicated the advisability of improving the durability of the system.

Durability of the sprayed ceramic seal system was addressed by this program by refinement and optimization of the plasma spray process and the metal substrate design. The advancements were guided by an interactive analytical/-experimental evaluation effort. Many combinations of seal system design and fabrication parameters were screened by physical property measurements, rig tests, and analytical evaluations. The characteristics of one interim selection were verified by engine endurance tests, and a similar test of the final selection is in progress. The final seal system demonstrated an improvement of 231°C (415°F), from 1301°C (2375°F) to 1532°C (2790°F), in thermal shock tolerance rig tests relative to the best system available at the start of the program.

A typical engine seal segment resulting from this effort is shown in Figure 1. It consists of a porous abradable ceramic surface layer applied over three graded layers of dense ceramic with increasing percentages of metal alloy in the lower layers. The metal substrate is a nickel alloy casting designed for compatibility with the thermal growth properties of the ceramic and with the existing seal support structure in the JT9D high pressure turbine. A typical engine segment resulting from this effort is shown in Figure 1.

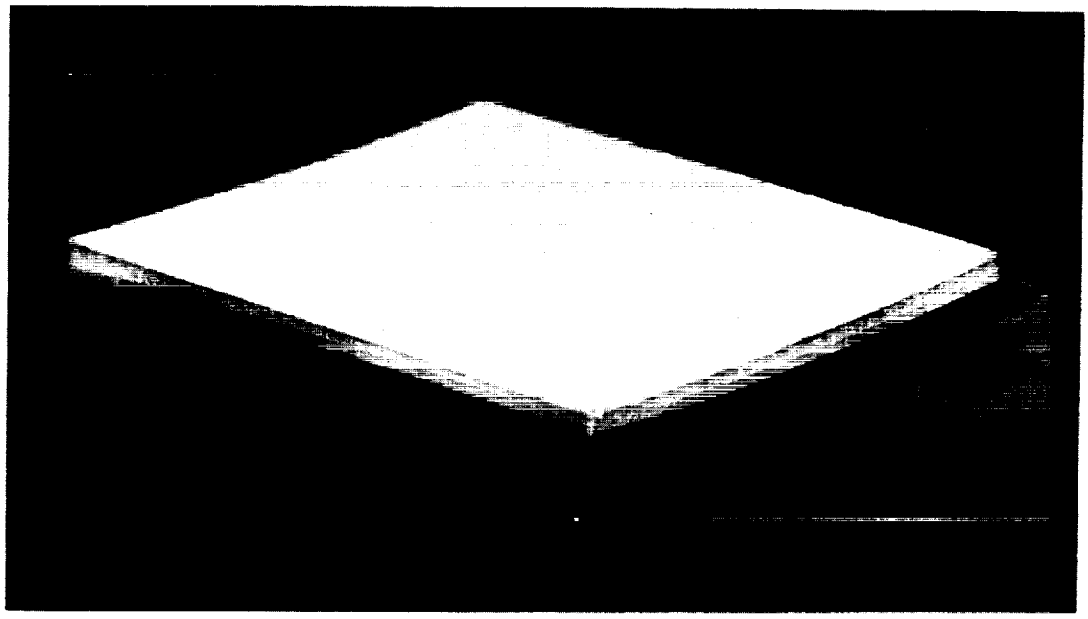

Figure 1 JT9D-7 Ceramic Turbine Seal to be Engine Tested

2.0 Introduction

National energy demand has outpaced domestic supply, creating an increased U.S. dependence on foreign oil. This increased dependence was dramatized by the OPEC oil embargo in the winter of 1973-74. In addition, the embargo triggered a rapid rise in the cost of fuel which, along with the potential of further increases, brought about a changing economic circumstance with regard to the use of energy. These events were felt in the air transport industry as well as other forms of transportation. As a result of these experiences, the government, with the support of the aviation industry, initiated programs aimed at both the supply (sources) and demand (consumption) aspects of the problem. The supply problem is being investigated by looking at increasing fuel availability from such sources as coal and oil shale. Efforts are currently underway to develop engine combustor and fuel systems that will accept fuels with broader specifications.

An approach to the demand aspect of the problem is to evolve new technology for commercial aircraft propulsion systems which will permit development of a more energy efficient turbofan, or the use of a different approach such as a turboprop. Although studies have indicated large reductions in fuel consumption usage are possible with advanced turbofan or turboprop engines (e.g., 15 to 40 percent), any significant fuel savings impact of these approaches is at least fifteen years away. In the near term, the only practical fuel savings approach is to improve the fuel efficiency of current engines. Examination of this approach has indicated that a five percent fuel reduction goal, starting in the 1980-82 time period, is feasible for current commercial engines. Inasmuch as commercial aircraft in the free world are using fuel at a rate in excess of 80 billion liters of fuel per year, even five percent represents significant fuel savings.

Accordingly, NASA is sponsoring the Aircraft Energy Efficient (ACEE) Program (based on a Congressional request), which is directed at reduced fuel consumption of commercial air transports. The Engine Component Improvement (ECI) Program is the element of the ACEE Program directed at reducing fuel consumption of current commercial aircraft engines. The Engine Component Improvement (ECI) Program consists of two parts: Engine Diagnostics and Performance Improvement. The Engine Diagnostics effort is to provide information to identify the sources and causes of engine deterioration. The Performance Improvement (PI) effort is directed at developing engine components having performance improvement and retention characteristics which can be incorporated into new production and existing engines.

The Pratt & Whitney Aircraft Performance Improvement effort was initiated with a Feasibility Analysis, which identified engine performance improvement concepts. These concepts were then assessed for technical and economic merit. This assessment included a determination of airline acceptability (measured by the amount of time the concept would require to pay for itself, or "payback period"), the probability of introducing the concepts into production by the 1980 to 1982 time period, and their retrofit potential. Since a major portion of the present commercial aircraft fleet is powered by the JT8D and JT9D engines, performance improvements were investigated for both engines. The study was conducted in cooperation with Boeing and Douglas aircraft companies, and American, United and Trans World Airlines, and is reported in reference 1.

In the Feasibility Analysis, the JT9D Ceramic Outer Air Seal concept was selected for development and evaluation because of its fuel savings potential and attractive airline payback period. Under the feasibility study, the concept was predicted to have a potential fuel savings of 1,953,000,000 liters (516,000,000 gallons), and a payback period under a year for installations in both new and existing engines in all aircraft. This is well within the five year payback period defined as the acceptability limit in the study.

The goal of the Ceramic Outer Air Seal Program was to produce a cost effective and durable seal system that can reduce engine operating clearances by at least 0.025 cm (0.010 in). The seal should have a life of 5000 hours under typical engine operating conditions without compromising any of the other desirable properties of the bill-of-material configuration.

The ceramic outer air seal refinement effort described in this report was preceded by a ceramic seal technology effort also sponsored by the ECI-PI Project. This technology effort, which is reported in Reference 2, established the baseline for the further improvement of ceramic seals described herein. The technology effort culminated in a test of ceramic outer air seals in a JT9D engine that demonstrated encouraging abradability (three ceramic seals were rubbed to a maximum depth of 0.060 cm (0.024 in) with an insignificant amount of blade wear) and good hardware condition (the seals sustained very minor laminar cracking). The baseline design is composed of three layers plasma sprayed over a thin bond coat on a metal casting. The three layers are formed by spraying ceramic and metallic powder; the top layer is 100 percent zirconia powder, the middle layer, 85 percent zirconia and 15% CoCrAlY, and the lower layer, 40% zirconia and 60% CoCrAlY. The bond coat is NiCrAl. The metal casting is similar in configuration and the same material (MAR-M-509) as the JT9D Bill-of-Material high pressure turbine outer air seal segments.

This report describes the refinement of the baseline seal system toward the goal of production engine acceptability. Section 3.0 is a general description of the refinement approach used to improve the ceramic outer air seal concept. Section 4.0 describes the design that resulted from the improvement effort under this phase of the program. Section 5.0 describes test equipment and methods used to evaluate the ceramic seal system, and Section 6.0 provides the results of these tests. Section 7.0 summarizes what was learned and the future course of action that will be taken on the concept.

3.0 Refinement Approach

The baseline ceramic seal system was refined during a 19 month effort using a combination of analytical and experimental methods, first in an iterative process and later in a screening process. The baseline design which performed well during engine test under the earlier NASA program was carefully analyzed. Properties of each of the individual layers as well as the substrate were defined. A two dimensional finite element program was used to define the stresses expected throughout the seal system which resulted from the thermal environment at various transient and steady state operating conditions. Stresses generated throughout the seal at various critical thermal conditions were compared with the strength of the material at the location of the stresses at the temperature associated with that stress. A stress to strength ratio was then used for evaluation purposes. If the stress generated by thermals at a particular point in the seal exceeded the strength of the material at that temperature it was expected that a crack would be generated. Using this criteria the approach was to develop a ceramic seal system which would have a stress to strength ratio less than one throughout the seal at all engine operating conditions - a seal system which would not crack during engine use.

The approach used to refine this system is shown schematically in Figure 2. The baseline design tested under the earlier NASA program was used as a model for an analysis to define the significance of various properties of each of the sprayed layers on stresses generated during a typical engine thermal cycle. This effort identified which properties of which layers would be the most significant in reducing stress in the seal system.

An experimental program was conducted simultaneously (to be time effective) to provide specimens of each of the sprayed layers utilizing variations in spray parameters. These specimens were used for material property measurement to define the relationship between properties and spray parameters. This effort identified the direction and magnitude of spray parameter changes to produce a desired change in layer properties.

The effect of exposure to the engine thermal environment on properties was also evaluated to determine if exposure had an adverse effect on thermal rupture resistance. This was done by subjecting the specimen to specified temperatures for defined periods of time which were consistent with expected engine conditions for each of the layers considered.

Results of these analytical and experimental efforts provided the basis for identifying the changes to spray parameters offering the most potential for reducing stresses.

Combinations of spray parameters providing material properties giving the best stress-strength ratio for each layer were used to fabricate complete ceramic-system, multi-layer specimens. These specimens were subjected to thermal rupture resistance tests which imposed increasingly severe thermal stresses on the ceramic system. The combination of spray parameters that showed the best thermal rupture resistance with the baseline substrate configuration was selected as the "improved" ceramic seal system.

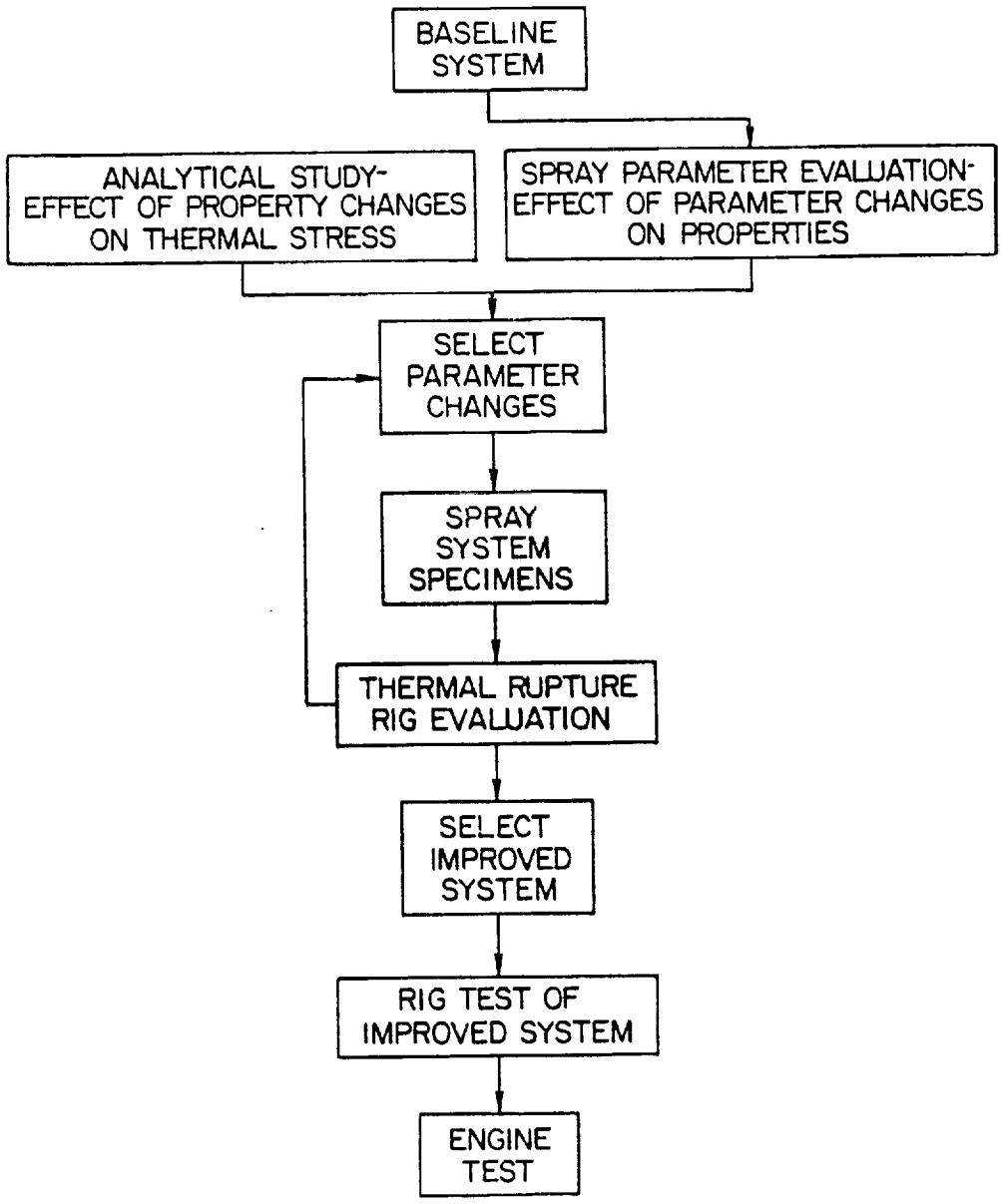

Figure 2 Refinement Process

In an attempt to optimize the design of the metallic substrate to be compatible with the improved ceramic system, various design refinements were evaluated. Variations in the overall substrate thickness, thickness around the periphery specifically at corner locations and substrate surface treatment to promote bonding were considered. Parts were fabricated and tested in the thermal rupture rig to identify beneficial design refinements.

4.0 Design

4.1 Overview

The ceramic outer air seal concept is designed to reduce high pressure turbine clearances. The concept consists of layers of ceramic material applied to a metal structural support, or substrate. The ceramic material is abradable when rubbed by the high pressure turbine blade tips, which contain abrasive material. Blade wear is reduced significantly compared to metal seal designs, improving performance and performance retention. The improved design described in this section evolved from a previous design, referred to as the baseline design, developed under an earlier NASA contract (reference 2).

The JT9D-7J was chosen as the demonstrator engine for the ceramic outer air seal, because it was available as a test vehicle in the time frame of the Ceramic Outer Air Seal Program. The ceramic seal and blades were required to have the same envelope as the bill-of-material seals and blades to allow interchangeability in the engine. The attachment hardware also had to be identical, along with the general cooling scheme. This approach led to a sprayed ceramic seal segment design which was interchangeable with bill of material metallic seal segments to facilitate retrofit possibility in the future.

4.2 Ceramic Layers

The ceramic abradable seal system consists of five layers: two layers ceramic (yttria stabilized zirconia) which serve as the abradable layer to absorb blade rubs and as insulation to reduce heat transfer to the seal substrate. Two intermediate layers sprayed of a mixture of zirconia and CoCrAlY (cobalt, chromium, aluminum, and yttrium powder) to match the thermal expansion characteristics of the zirconia layer to the substrate. A NiCrAl layer bonds the ceramic layers to the metal substrate. These five layers will be called the porous zirconia, 100%, 85%, 40%, and bond layers, respectively, for the remainder of this report. The percentage refers to the weight percent of zirconia in the powder used to spray each layer. Figure 3 is a cross-section of the ceramic seal, showing the composition and thickness of each layer.

The structure of each of the layers is highlighted in Figure 4 which shows the homogeneous distribution of metallic and ceramic particles in the intermediate layer and the random distribution of porosity in the top zirconia layer.

The thicknesses and compositions of all the layers except the top layer of porous zirconia were determined under a previous NASA contract (reference 2) using analytical and experimental methods. The structure and properties of the layers is controlled by the plasma spray process parameters used to fabricate each layer. The program described in this report was primarily concerned with the choice of these parameters, to improve the thermal resistance capability of the ceramic system. The porous zirconia layer was added primarily to increase the abradability of the system. This effort is discussed in detail in Section 6.0.

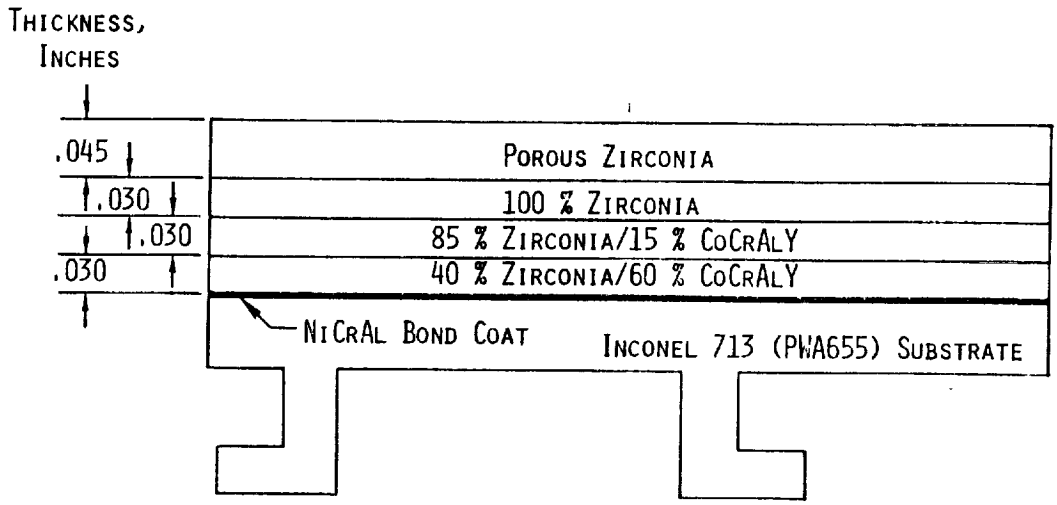

Figure 3 Ceramic Seal System is Composed of Graded Layers

4.3 Substrate

Inconel 713 was chosen as the substrate material for the improved design, compared with the cobalt-based MAR-M-509 used in the baseline design. Inco 713 contains no cobalt, which is a critical material. Inco 713 is as durable, easily cast, and more machinable than MAR-M-509. It cannot withstand temperatures as high as MAR-M-509, but this is acceptable since the sprayed ceramic system will insulate the substrate from the severe thermal environment of the engine.

The substrate is attached to its support structure and ultimately to the turbine case by the rails. These rails add to the stiffness of the substrate. Since analysis had indicated that reduced substrate stiffness would reduce stresses, several slotting configurations to reduce stiffness were examined. Two approaches were considered; a large number of thin slots and a smaller number of wide slots or "scallops." The wide slot "scallop" design was selected because it was effective in reducing circumferential stiffness and was easier and less expensive to manufacture. The seal segment length was designed to be approximately 5.0 cm (2.0 in) long with 60 seal segments required for the JT9D first stage seal. This number of seal segments is the same as in the current B/M material of advanced versions of the JT9D engine.

The exact placement and size of the slots were compromises between several competing factors. The closer the slots are to each other, the greater the reduction in circumferential stiffness. However, low cycle fatigue life is reduced as the slots get closer together.

To eliminate mechanical loads on the ends of the ceramic system, the system layers were cut back from the edge, as shown in Figure 5. This prevents the ceramic layers of adjacent segments from touching, eliminating the possibility of delamination and cracking due to mechanical loads.

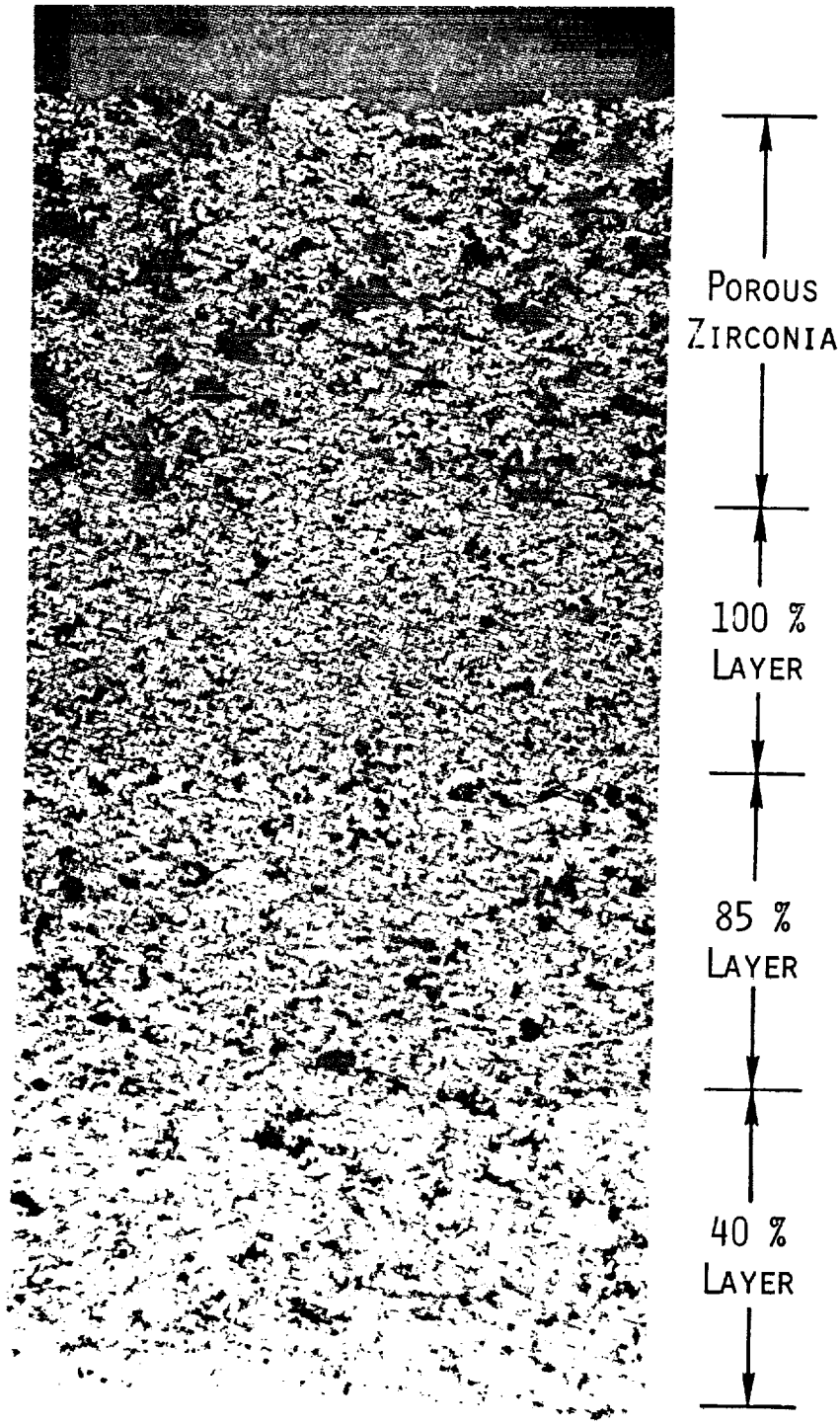

Figure 4 Metallography Depicting the Ceramic and Ceramic/Metallic Composition of Each Layer

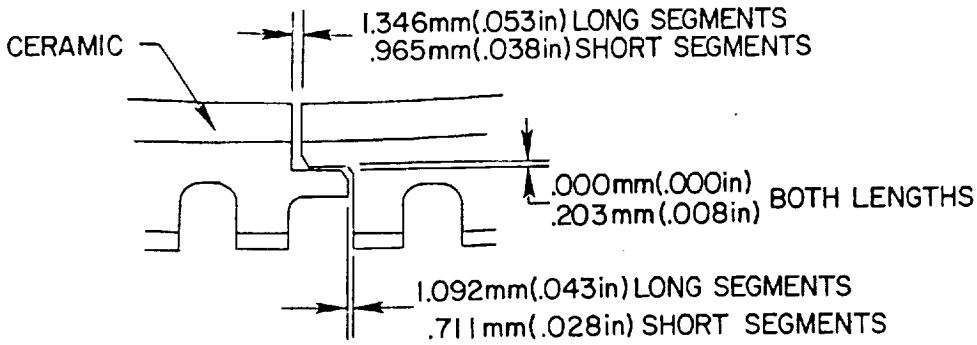

Figure 5 Design Ensures Against Ceramic Contact

A seal was also designed with the same ceramic system but twice as long as the one described above. A longer seal reduces the number of fabrication steps and assembly costs. Performance also should benefit, since there are fewer axial seal gaps for air to leak through. Less leakage improves turbine efficiency and fuel consumption. Because of the higher thermal environment in advanced JT9D engines, the length of conventional seals has been reduced to minimize thermal distortion during engine operation. Because of the insulative and abradable properties of the ceramic seal system, however, it is anticipated that length can be increased without adversely effecting engine performance. The scheduled engine test will provide the necessary assessment of this design feature. A comparison of the circumferential view of the long and short seals with the final slotting configuration is shown Figure 6.

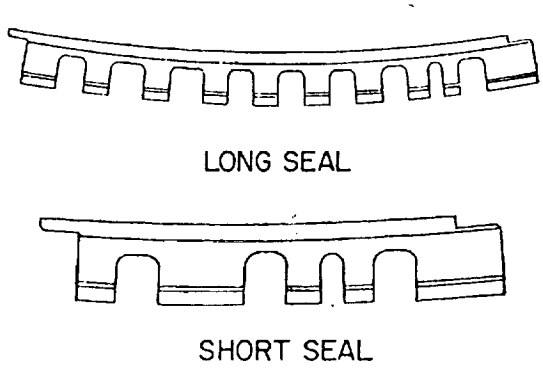

Figure 6 Circumferential View of Two Type Seals to be Engine Tested

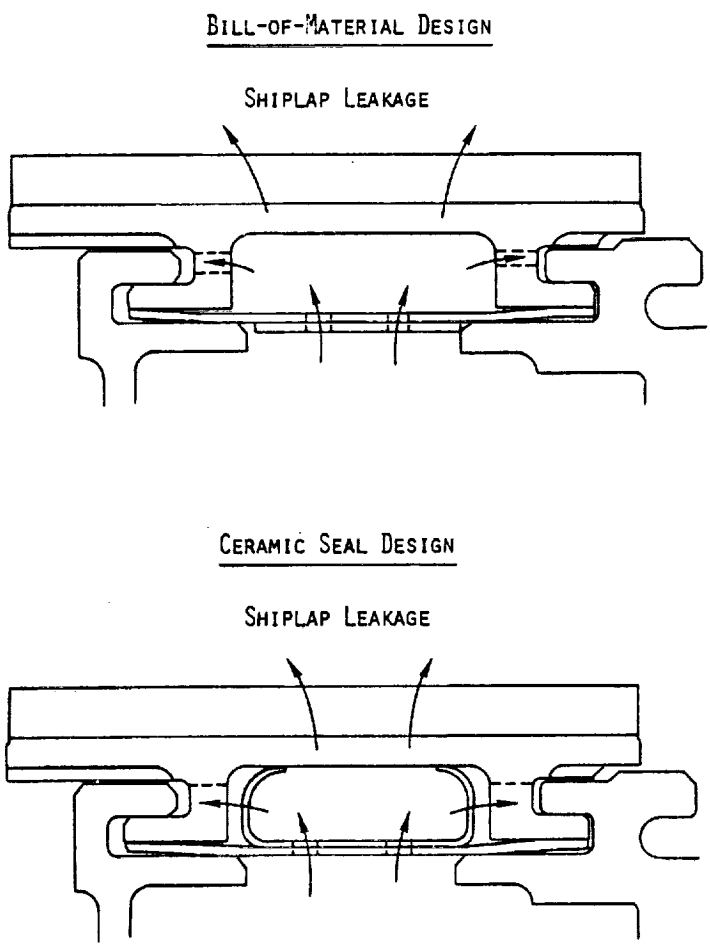

Figure 7 Bathtub Seal Controls Cooling Flow in Ceramic Seal Design

The long seals were designed to be intermixed with the short seals so that they could be tested in the same engine. Because of the intermixing requirement for this test, the slotting arrangement for both the long and short seal design was established to be compatible with the same engine seal support hardware. The removal of the intermixing requirement would allow the long seal slotting configuration to be modified to further optimize seal stiffness and provide all slots of equal size and equally spaced.

4.4 Cooling

The seal is cooled using the same cooling flow rate as the bill-of-material design. The improved ceramic seal design required some changes to the cooling airflow control system. In the bill-of-material design, cooling air is directed on the outer surface of the seal substrate by an impingement plate. The cooling air is metered through exit holes in the rails, as shown in Figure 7, where it continues on to cool the rails and outer edges of the seal.

The slots in the ceramic outer air seal design are much too large to control cooling airflow. A metal seal, called a "bathtub seal" due to its shape, was designed to partially block flow through the slots. The bathtub seal is loaded against the substrate by the impingement plate, and contacts the substrate outer surface, creating a chamber for cooling air to flow through. The flow is metered through holes in the sides of the bathtub seal, impinging upon the ceramic seal rails and outer flanges and cooling them. This design is also illustrated in Figure 7.

Leakage of secondary flow into the gaspath between the segments of the ceramic outer air seal is controlled by the use of overlapping joints, or "shiplaps". Details of the shiplap joint is shown in Figure 8. This design is essentially the same as that used in the bill-of-material seal, with slight adjustments to accommodate the ceramic layer.

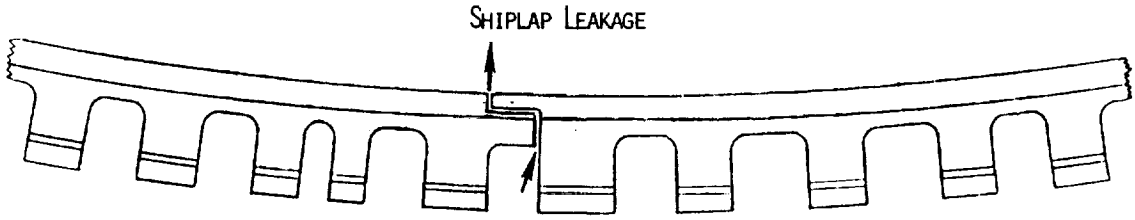

Figure 8 Ceramic Turbine Seal Shiplap Detail

4.5 Blade Tip

Abrasive tips are bonded to the high pressure turbine blades to minimize blade wear when rubbing the seals. The blade tips are composed of a metal/abrasive grit mixture consisting of 20% (by volume) 0.038 cm (0.015 in) diameter silicon carbide grits in a Tipaloy^{R} matrix (a nickel-based superalloy). The blade tips are fabricated using the hot isostatic pressing technique and then attached to the blades using the transient liquid phase (TLP^{R}) bonding process. A typical blade tip is shown in Figure 9.

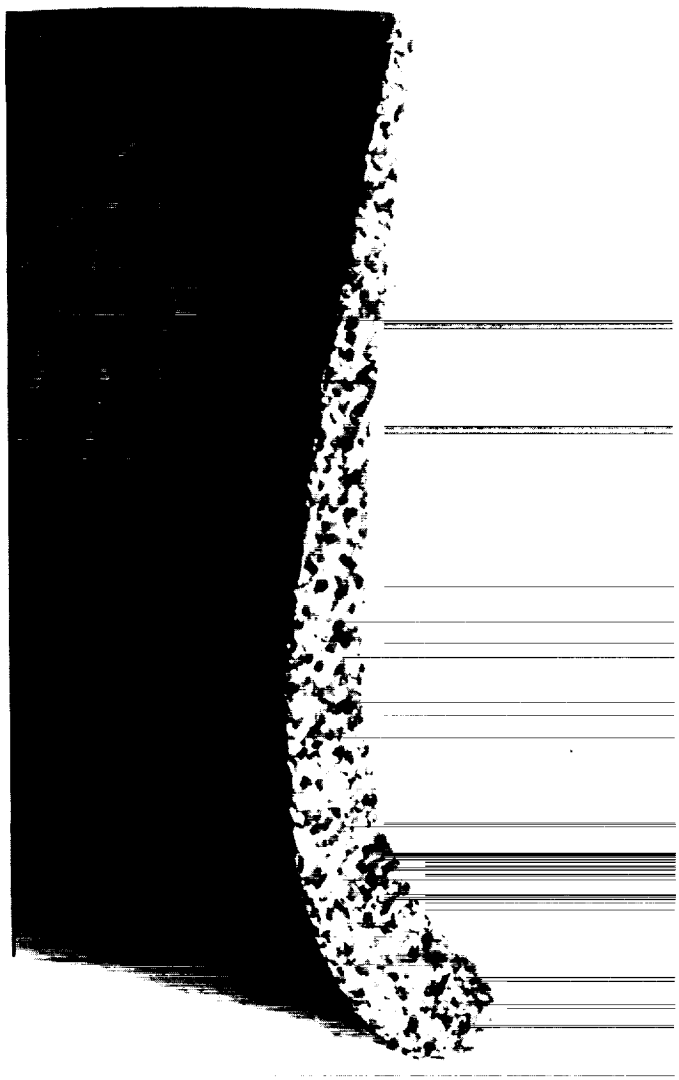

Figure 9 JT9D-7 Abrasive Blade Tip to be Engine Tested

5.0 Evaluation Techniques

5.1 Analytical Studies

The objective of the analytical studies was to determine the effect of significant ceramic seal material property variations on thermal stresses generated during the JT9D engine thermal cycle. The analysis considered ±50% variations in modulus of elasticity, tensile strength, thermal conductivity, and thermal expansion to define the stress/property relationship for the sprayed ceramic seal system during JT9D engine operating conditions. This sensitivity study provided stress/property relationships which, together with the results of evaluation of spray parameter effects, provided the means to improve the thermal stability of the ceramic seal system .

The analytical design system used in the study consisted of three analytical computer programs. The first program provided a two dimensional finite element nodal breakup of the seal design. Both axial and circumferential breakups were generated.

The temperature distribution through the seal was calculated using a second program which performed a finite difference heat transfer analysis for transient and steady state temperature distributions based on JT9D-7 operating cycle boundary conditions. The required input for the heat transfer program included 1) the finite element breakup, 2) appropriate thermal boundary conditions and, 3) thermal conductivity as a function of temperature for each of the layers of the ceramic seal system and the substrate. Temperature distributions were calculated through the seal in both the axial and circumferential directions for four engine operation conditions: idle, acceleration from idle to sea level take-off, maximum power, and deceleration from sea level take-off to idle.

The temperature distribution resulting from the heat transfer program was used to calculate the stress distribution through the seals by means of a third analytical program which conducted a two-dimensional stress analysis. The required input for this program includes the seal temperature distribution, the modulus of elasticity and the coefficient of thermal expansion for each of the layers and the substrate. Additionally, a description of the residual stress in the seal is needed. The residual stress is incorporated into the stress analysis by means of the stress free temperature (SFT) which is the temperature distribution through the part for which no internal stresses exist.

Stresses resulting from the engine's thermal environment were initially calculated in the axial and circumferential plane for the four engine operating conditions. Early analytical results revealed that stresses in the axial plane and for engine operating conditions other than acceleration were less critical. As a result, subsequent analysis concentrated on the acceleration to maximum thrust operating condition and the circumferential plane of the seal segment.

5.2 Spray Parameter Evaluation

The objective of the spray parameter evaluation effort was to determine the effect of spray parameter changes on material properties. This effort provided data which was used in concert with the analytical studies described previously. By identifying the property modifications most beneficial with respect to reducing stresses and the spray parameter changes most effective in providing those modifications, combinations of spray parameters offering the most improvement in the stress/strength ratio of the ceramic seal system were selected for thermal rupture rig evaluation.

Single layer flat plate property specimens were fabricated by varying the plasma spray parameters from their baseline values. The four spray parameters chosen to vary were plasma spray gun power, primary gas flow rate, powder feed rate, and gun distance from the surface to be sprayed. A review of existing in-house experience substantiated by existing technical literature had indicated that these were the most influential spray parameters. These parameters were varied around the baseline values as shown in Table I.

The properties measured for each of the variations were modulus of elasticity, tensile strength, compressive strength and thermal expansion.

Spray parameter variation testing was only done for the 100% and 85% ceramic layers because the sensitivity study had shown that variations in the 40% ceramic layer had little significance with respect to the stress to strength ratio in all the layers. The spray parameter variations evaluated are listed in Table I.

TABLE I
SPRAY PARAMETER VARIATIONS EVALUATED

	Gun Power Level, KW	Gun Standoff Distance cm,(in)	Primary Gas Flow CMH,(CFH)	Powder Feed Rate, gpm
100% Layer	29,36*,46	6.3,12.7*,19.0 (2.5,5.0*,7.5	1.7,2.1*,2.8 (60,75*,100	60,90*,120
85% Layer	26,36*,46	6.3,12.7*,15.2 (2.5,5.0*,6.0	1.4,2.1*,2.8 (50,75*,100	20,45*,90

*Baseline values

A ring of specimens was sprayed for each variation of the four spray parameters. Material property measurements were conducted on three sets of flat plate test specimens from each ring to determine the repeatability of the material properties for each spray parameter variation.

Metallography was performed on the single layer test specimens fabricated for the material property measurements for the purpose of identifying structural changes, as produced by the variations in the spray parameters. Metallography was also helpful in determining that successive test specimens employing the same spray parameter variations reproduced the same structural characteristics.

The elastic modulus and tensile strength were determined from single layer specimens placed in a fixture supported at each end with varying loads applied at two distinct points, as shown in Figure 10. A strain gage, placed at mid span and center of each specimen, was used to measure deflection over a temperature range from room temperature to approximately 315°C (600°F), the strain gage temperature limit. A deflectometer was also used from room temperature to 315°C (600°F) for calibration purposes, and was used alone at higher temperatures. The specimen was subjected to progressively higher loads until failure, producing a curve of load versus deflection. These measurements were taken at a minimum of three different temperature levels for each layer. The test specimen was 0.2 cm (0.1 in) thick x 0.952 cm (0.375 in) wide x 3.0 cm (1.2 in) long with a sprayed material thickness of 0.63 cm (0.25 in).

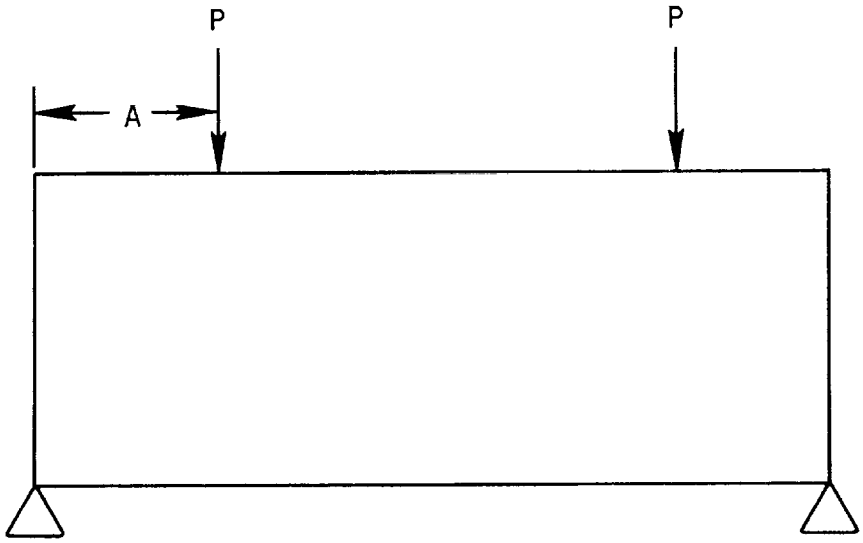

Figure 10 Four Point Bend Specimen Loading

The elastic modulus was determined by:

$$E = \frac{1}{8bh^3} \quad \frac{p}{\delta}$$

where b = specimen width perpendicular to the load application

h = specimen thickness coincident with the load direction

p/δ = slope of the load versus deflection curve

The tensile strength was calculated by:

$$T = \frac{6PA}{bh^2}$$

where P = maximum load prior to specimen failure

A = distance between load applied at fixture and next applied load (See Figure 10)

Compressive strength was measured in the circumferential direction on single layer specimens measuring 1.98 x 0.60 x 0.55 cm (0.78 x 0.24 x 0.22 in) in length, width and thickness respectively. Measurements were taken at the same temperature levels, using the same combination of strain gage and deflectometer instrumentation as the elastic modulus/tensile strength test for each material. The specimen is supported at one end and loads applied at the other end until failure. The compressive strength was determined by dividing the applied load by the cross-sectional area over which the load was applied.

Tensile and compressive strength, modulus of elasticity and strain at failure measurements were repeated three times for each fabrication trial and averaged to minimize the effect of variations in the measurement set-up and techniques. The accuracy of the measurement technique is $\pm$5%.

Thermal conductivity measurements were not taken on this part of the spray parameter evaluations because of the relative insensitivity of stress to changes in that property. When required later in the program, however, it was determined by measuring the thermal diffusivity, density, and specific heat, and taking the product of the three measurements. The thermal diffusivity was measured by a laser flash technique. A flash of radiant energy is deposited uniformly over one surface of a homogeneous sample during a negligible time duration, and the heat pulse was allowed to diffuse unidirectionally to the opposite face. The diffusivity is calculated from the sample thickness and the time required for the rear face temperature rise to reach a known percentage of its maximum value. These specimens were shaped in the form of a disk, with a diameter of 1.79 cm (0.705 in) and a thickness of 0.12 cm (0.05 in). The accuracy in measuring the thermal diffusivity is $\pm$2%.

Specific heat was measured in a argon gas environment using a differential scanning calorimeter. A reference and a sample holder were equipped with heaters and temperature sensors. As the samples are heated, the sensors detect temperature fluctuations of the sample with respect to the reference. A high gain, closed-loop electronic system provides differential electrical power to the heaters to compensate for fluctuations. This differential power was read

out directly in millicalories per second and is equivalent to the rate of energy absorption of the sample. By comparing this rate with the rate measured during the heating of a known mass of sapphire, the specific heat was calculated. The accuracy of this device, using a 0.63 cm (0.025 in) diameter test disk, is ±3%. The upper limit for this test equipment was 726°C (1340°F). Above this temperature, values were determined by extrapolation.

Density was determined by weighing a specimen, calculating its volume and dividing the weight by the volume. The accuracy of the measurement technique is ±1%.

The coefficient of thermal expansion of each layer was determined using a dilatometer. This instrument can operate to 1537°C (2800°F) in air, inert atmosphere, or vacuum. Tests at elevated temperatures were done in an argon gas environment. The specimens were 2.5 x 0.5 x 0.2 cm (1.0 x 0.2 x 0.1 in) in length, width and thickness, respectively, with the ends flat and parallel within 0.0012 cm (0.0005 in). A suitable standard was placed in parallel with the specimen so that the measurement data corresponded to the difference in expansion between the specimen and the standard.

Each sample was cycled three times, with data recorded during the heat up and cool down portion of each cycle. The accuracy associated with this procedure is +1%.

The effect of the engine thermal environment on properties, and thereby thermal rupture resistance of the system, was also investigated. Specimens of the various layers comprising the baseline and improved systems were heated in an oven at a temperature and for a time consistent with expected engine conditions and then used for property measurements. The 100% layer was heated for 50 hours at 1371°C (2500°F). The 85% layer for 300 hours at 871°C (1600°F) and the 40% layer for 500 hours at 760°C (1400°F).

5.3. Thermal Rupture Rig Tests

The thermal rupture rig was designed to subject multi-layer, sprayed ceramic system, test specimens to calibrated thermal conditions to screen methods of improving the thermal capability of the ceramic system. By subjecting the specimen to a known gas stream temperature for a specified time, a thermal gradient is produced through the ceramic. This gradient is an exaggerated version of the transient thermal condition produced during engine acceleration, which is the limiting thermal condition for the ceramic outer air seal system.

The specimen is mounted in the thermal rupture rig, as shown in Figure 11, by an air cooled, metal holding fixture. The hot gas stream temperature is set to one of the five levels of severity available by setting the air and jet A fuel flows to the prescribed levels. The specimen is shielded from the hot gas stream during this operation by a metal shutter. The backside temperature is stabilized at a prescribed level by adjusting cooling air flow to the backside of the holding fixture. After these conditions are established, the specimen

is tested by lifting the metal shield and exposing the front surface to the hot gas stream for 15 seconds. The back surface temperature is continuously recorded during the actual test run. After the test cycle has been completed the specimen is removed from the holding fixture and inspected for cracks. The test specimen is considered to have "failed" when cracks visible under inspection at 60X magnification have developed. The specimen is tested at progressively higher levels of severity until failure or maximum rig capability is reached.

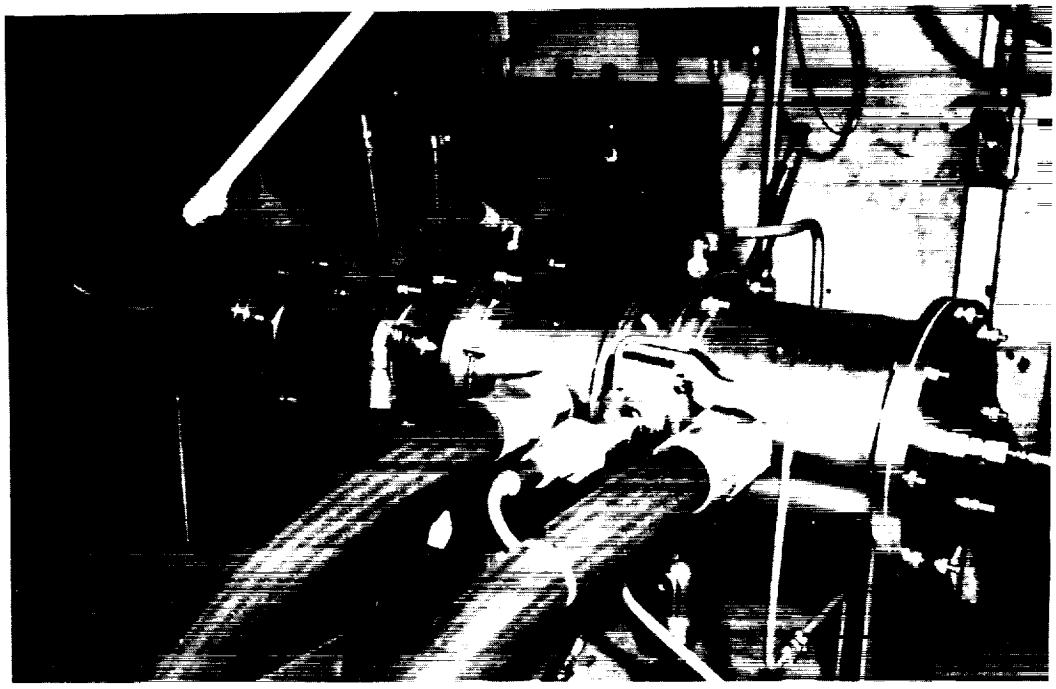

Figure 11 JT9D Ceramic Outer Air Seal Thermal Rupture Rig Facility was Used to Evaluate Thermal Stability Improvement

The specimen's thermal rupture resistance is measured by calculating the temperature differential required to cause failure. This temperature differential is defined as the burner temperature minus the specimen backside temperature at the end of the test. Comparing the thermal resistance capability of the various specimens in this manner accounts for any differences which may exist in thermal conductivity.

The thermal rupture rig was used to evaluate specimens of the complete ceramic seal system which incorporated the potentially beneficial spray parameters and metal substrate design changes shown in Table II.

Over 250 thermal rupture rig tests were conducted during this program.

TABLE II

CERAMIC SPRAY PARAMETER AND SUBSTRATE STIFFNESS VARIATIONS SELECTED FOR EVALUATION IN THE THERMAL RUPTURE RIG

Layer	Spray Parameter or Substrate Stiffness Variation	Ceramic Seal System Identification No. 1	2	3	4	5	6	7	8	9	10	11	12	13	14
100%	Increased Porosity			X	X	X	X	X	X	X	X	X	X	X	X
	Reduced Gun Distance (6.3 cm, 2.5 in)	X	X					X			X	X	X	X	X
	Reduced Powder Feed Rate (60 gpm)		X												
	Reduced Gun Power (29 kW)									X					
85%	Increased Gun Distance (15 cm, 6 in)	X	X				X								
	Incr Powder Feed Rate (90 gpm)		X		X				X						
	Reduced Gun Distance (6.3 cm, 2.5 in)					X		X		X	X	X	X	X	X
	Reduced Gun Power (26 kW)								X						
Substrate															
	Machined Grooves										X				
	Machined Cross Grooves											X			
	Machined Edges												X		
	Machined Corners													X	
	Reduced Thickness														X

5.4 Other Rig Tests

The baseline and the improved ceramic seal systems were subjected to thermal gradient, thermal cycle, erosion, and abradability rig tests to further evaluate their relative acceptability for engine use. The tests are described below.

5.4.1 Thermal Gradient

Long term durability of the sprayed ceramic seal system in an engine application depends on the ability of the structure to withstand the physical and chemical changes which take place due to exposure of the system to the operating thermal environment. The major concerns are oxidation of the metallic constituents and sintering of the ceramic portions and the effect of both on structural integrity of the ceramic system.

A study was performed to determine the expected exposure time and thermal environment in the area of the ceramic seal for both the cruise and sea level takeoff conditions for a JT9D engine. It was determined that a 50 hour thermal gradient test with a front and back side temperature of 1090°C (1995°F) and 543°C (1010°F) respectively for cruise and 1273°C (2325°F) and 662°C (1225°F) for sea level take-off would provide the required exposure time and thermal environment for evaluating the ceramic seal system.

The specimen was mounted in the test rig, shown in Figure 12, using a fire brick holding fixture held by a water cooled copper fixture. A combination of oxygen-propane torches and cooling air jets are used to achieve the desired environment.

Figure 12 Cyclic Thermal Shock Rig Simulates Engine Thermal Cycles and Steady State Thermal Gradients

5.4.2 Thermal Cycle

Thermal stresses are generated by temperature differentials through the seal system. The analytical studies (Section 5.1) showed that the thermal condition at engine acceleration, a transient condition, generated the greatest stresses. The ability of the ceramic to withstand repeated stresses generated during this transient condition was evaluated in a rig which simulates the engine's thermal cycle from idle to sea level take-off and back to idle.

The test rig used for this program was the same as the Thermal Gradient Rig. To provide the required thermal cycle, the torches were mechanically moved toward or away from the specimen at controlled rates. Fixed cooling air jets were turned on and off, or the flow was changed at predetermined intervals, to meet the cycle requirements. The ceramic and metal substrate surface temperatures were monitored continuously with an optical pyrometer and thermocouples, respectively, and recorded on a strip chart.

The typical rig test thermal cycle is shown in Figure 13. An engine cycle is shown for comparison to illustrate the closeness of simulation.

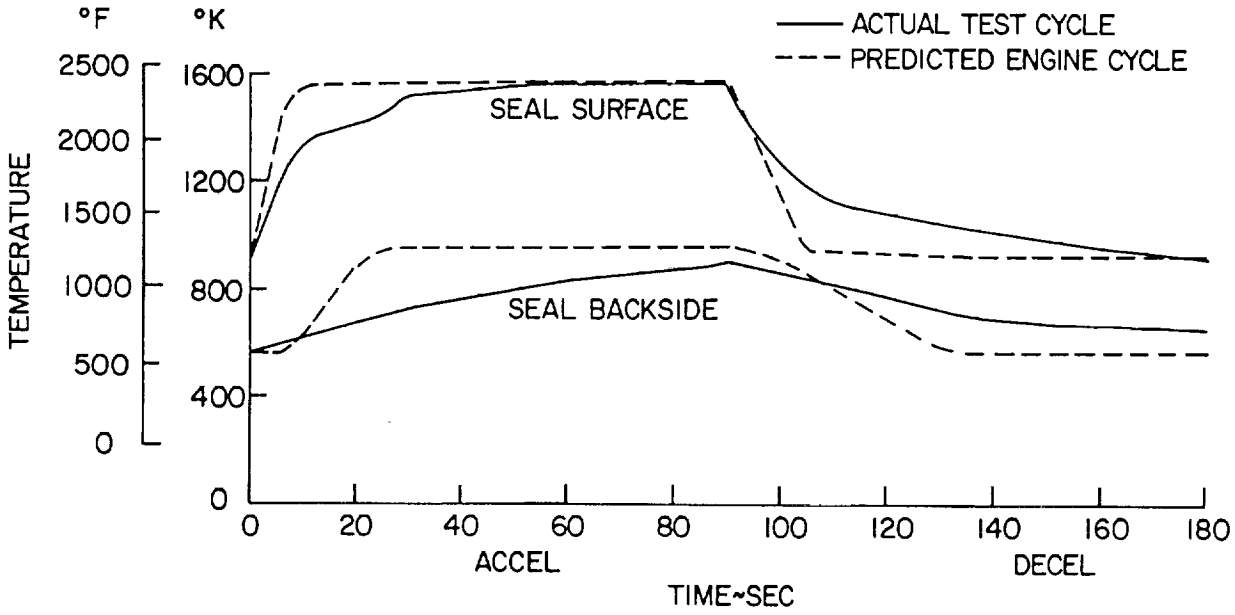

Figure 13 Thermal Shock Test Cycles Simulate Engine Operating Conditions

5.4.3 Erosion

Erosion resistance was evaluated in the hot particulate erosion rig shown in Figure 14. This rig enables the erosion resistance of the sprayed system to be evaluated at various impingement angles and temperatures. The specimens were positioned at the various impingement angles relative to the end of the combustor exit nozzle by a compound vise. The specimen was heated by impinging JP-5 fuel and air combustion products on the surface of the specimen through a 1.9 cm (0.75 in.) diameter exit nozzle. The temperature of the specimen and the exit gas velocity were controlled by varying fuel and air flows.

After stabilization of the specimen surface temperature and gas velocity, particulate flow was initiated. The Al_2O_3 particulate was gravity fed into a tube connected into the combustor exit nozzle approximately 5.1 cm (2.0 in.) upstream of the nozzle end. The particulate was picked up and accelerated to the specimen surface by the hot gas stream. The flow rate of the particulate was controlled by a precalibrated orifice placed in the storage hopper discharge line. The particulate flow rate was checked by monitoring the weight of the particulate used and the duration of the particulate flow during the test.

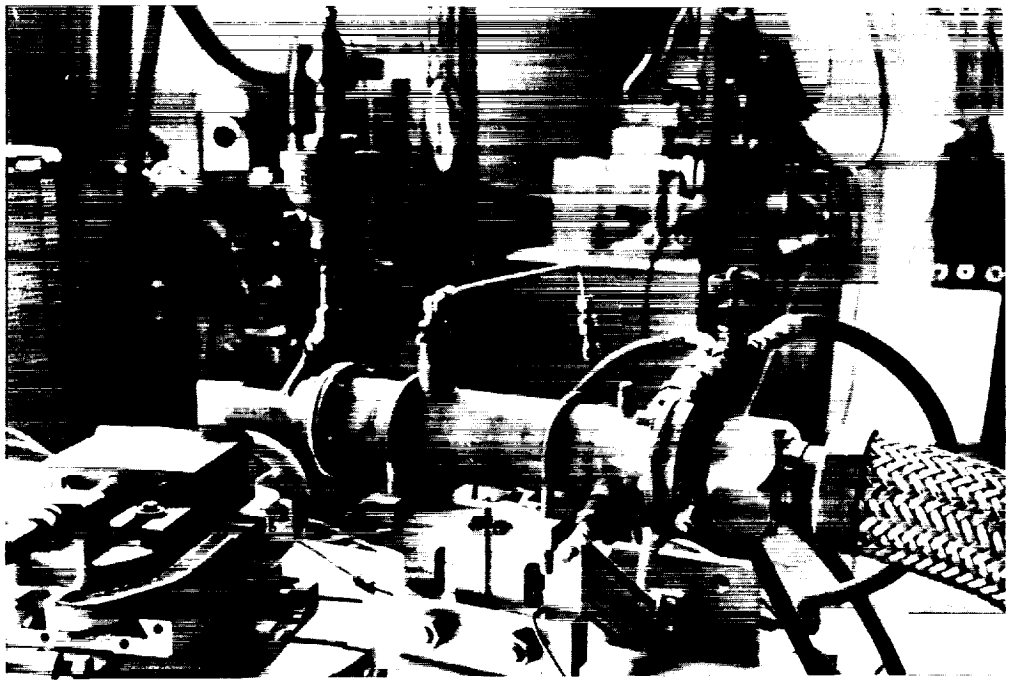

Figure 14 Hot Particulate Erosion Rig Simulates Long Term Engine Erosion Effects

Specimen temperature was measured on the ceramic surface by an optical pyrometer. Erosion wear was determined by measuring the weight loss of the specimen at five minute intervals.

The erosion specimen consisted of the composite seal system sprayed on a flat Hastelloy-X plate, 5.0 x 6.8 cm (2.0 x 2.7 in). A cap screw was welded to the center of the plate for mounting in the test fixture.

Erosion tests were performed on both the baseline and the improved ceramic seal systems at four impingement angles, 15, 30, 45, and 85 degrees. Specimens aged at elevated temperatures were also tested at an impingement angle of 15 degrees. All of the tests were run under the following conditions:

Gas Velocity	0.35 Mach number
Surface Temperature	1589°K (2400°F)
Nozzle-to-Specimen distance	3.81 cm (1.5 in.)
Particulate Type	Aluminum Oxide
Particulate Flow Rate	9 gm/min (1.2 lb/hr)

An 80 grit, average diameter 0.0266 cm (0.0105 in), particulate size was used for all of the baseline system testing. Most of the improved system testing was conducted with 90 grit, average diameter 0.020 cm (0.008 in) particulate size because of an availability problem with the 80 grit particulate. The switch was made after preliminary tests on the improved system indicated this small difference in particulate size had a negligible effect on erosion rate.

5.4.4 Abradability

The abradability tests were performed with the high temperature abradability test rig shown in Figure 15. Rig blades, with abrasive tip caps, are rubbed against the ceramic seal test specimens at different incursion rates, representative of engine interaction rates. Six blades are mounted in a disk driven at the required speed by a compressed air turbine. Blades were refurbished after use to provide an acceptable abrasive tip for subsequent tests. The seal segment specimen is mounted in a fixture at the end of a horizontal post. The post is attached to a moving carriage assembly designed to push the specimen radially into the rotor assembly at the required incursion rate. The seal specimen is heated by an oxygen/jet fuel burner directed at the front surface of the seal and an electric hot air heater directed at the rear surface of the seal. Gas flow, fuel flow, and current flow are varied to control the seal surface temperature. Seal surface temperature is monitored by optical pyrometers. Carriage travel is monitored by a linear differential transformer. All data is recorded continuously on a strip chart.

Figure 15 High Temperature Abradability Rig Simulates Engine Conditions

The differences in abradability for various test conditions and test specimens were assessed on the basis of the volume wear ratio (VWR), the seal wear volume divided by the blade wear volume. Blade tip and seal wear were determined through pre and post-test measurements. The higher the volume wear ratio the better the abradability of the system. Accuracy of the assessment is limited at high volume wear ratio (700 and up) by blade tip wear measurement techniques. Blade tip wear of 0.0005 cm (0.0002 in) is the smallest that can be measured accurately.

The tests were conducted at a seal surface temperature of 1315°C (2400°F), with one exception which was run at 1093°C (2000°F), and at a blade tip speed of 305 m/sec (1000 ft/sec) to simulate engine operating condition. An incursion depth of 0.05 cm (0.02 in) was set for all tests. Twelve abradability tests were conducted on the baseline ceramic seal system design to evaluate the effect of the incursion rates: 0.0002, 0.002, and 0.020 cm/sec (0.0001, 0.001 and 0.010 in/sec). In addition, these tests were used to evaluate the effect on the ceramic of time at temperature on abradability at the 0.002 cm/sec (0.001 in/sec) incursion rate condition. Six abradability tests were also performed on the improved ceramic seal system design to evaluate the effect of the incursion rates: 0.0002, 0.002, and 0.020 cm/sec (0.0001, 0.001, and 0.010 in/sec).

5.5 Engine Test

As part of a related in-house program, sprayed ceramic seals were tested in an engine. The objectives of the test were to assess the effects of engine thermal cycles on the seal system, compare these results with results of thermal rupture rig testing, and obtain additional information on the abradability of the abrasive tip blade and ceramic seal.

Thirty-six first stage turbine sprayed ceramic seal segments and 23 abrasive tip blades were tested in a JT9D-7 test engine (X-596). The seal was an interim design, since the test occurred prior to completion of the seal refinement process.

The configuration tested was similar to the improved seal. The geometry was approximately the same and a porous zirconia top layer was provided over a dense zirconia layer.

The engine was cycled according to the schedule shown in Figure 16. The high pressure turbine was removed from the engine and the seals inspected after 500 and 2500 cycles. The results of this engine test and the results of the rig tests and analytical studies described earlier are presented in Section 6.

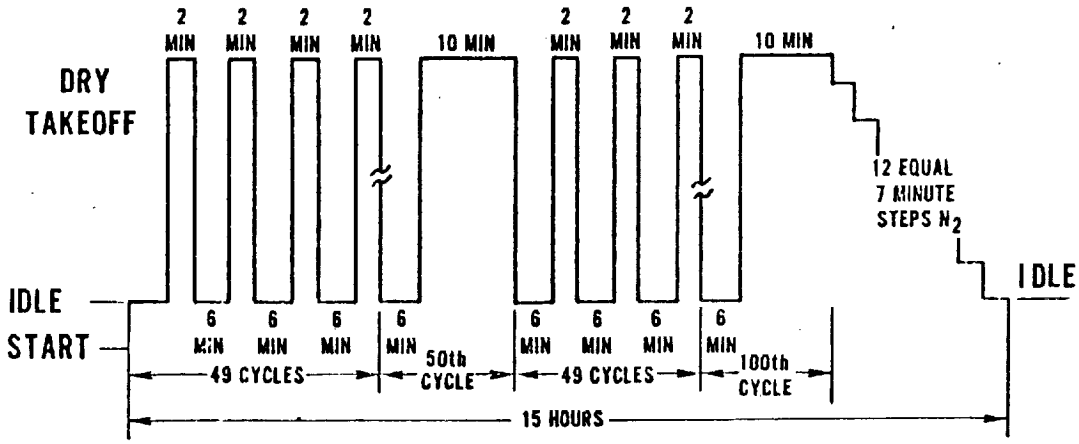

Figure 16 Accelerated Engine Endurance Test Cycle was Used to Evaluate Ceramic Outer Airseals

6.0 Evaluation Results

6.1 Analytical Studies

An initial analysis was conducted to determine the stresses generated in the baseline ceramic seal system in the 0.76 cm (0.030 in) 40% layer, 0.76 cm (0.030 in) 85% layer and 0.165 cm (0.065 in) 100% top layer. Engine operating conditions of 6 seconds and 8 seconds into acceleration from idle to sea level takeoff (acceleration 1 and 2), steady state sea level takeoff and 8 and 10 seconds into deceleration (deceleration 1 and 2) from takeoff to idle were analyzed. The axial and circumferential planes through the segment were analyzed at each engine operating condition.

The stresses at each of the 1800 nodes of the analytical model at each operating condition were scanned in comparison with the strength of the material at that node at the operating condition temperature. The greatest ratio of stress to strength, an indication of the potential of crack initiation, for each of the three ceramic system layers is presented in Table III. The stress at that location is also presented. Results indicated that the acceleration 1 condition, in the circumferential plane, produced the greatest potential of crack initiation, a stress to strength ratio of 1.3 in both the 100% and 85% layers.

As a result, the circumferential plane and 6 second acceleration was selected to be used for the property sensitivity study. The study defined the change in stresses in the ceramic system for changes in modulus of elasticity, tensile strength, thermal conductivity and thermal expansion for each of the three layers of the ceramic system. Results are presented in Figures 17-25. Curves presented in those figures show the trend of change in maximum stresses in each of the layers corresponding to changes in the value of the property for each of the layers. The trend lines have been generated on the basis of three points, the actual value of the property and plus and minus changes of 50%.

The curves shown in Figure 17-19, show the effect of changes in modulus of elasticity in the 100%, 85% and 40% layers respectively on the maximum stress in each layer generated during the JT9D acceleration transient. As expected, a modulus change in a layer has the greatest effect on the stresses in that layer with an increase in modulus producing an increase in stress. A change in the 100% layer modulus, Figure 17, had the most effect on stresses in the other two layers, a decrease in 100% layer modulus resulted in a reduction in stress in both the 85% and 40% layers. A modulus change in either the 85% or 40% layers had no significant effect on the stress in either of the other two layers as shown in Figures 18 and 19.

The effect of changes in the coefficient of thermal expansion of 100%, 85% and the 40% layers on the stresses in each of the three layers is presented in Figures 20-22. The most significant effect on stresses was again in the layers with the changed property, the less the coefficient of thermal expansion, the less the stress.

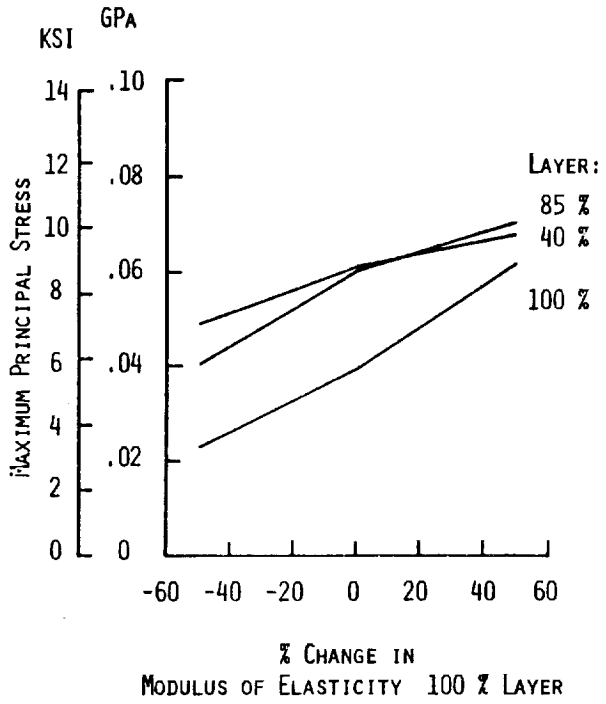

Figure 17 A Reduction in the Modulus of the 100% Layer Reduces the Stresses in All Three

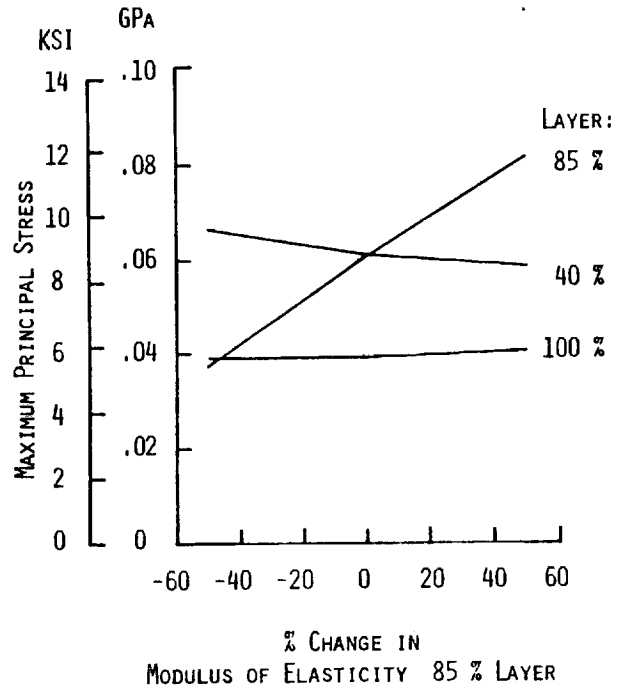

Figure 18 Reduction in the Modulus of the 85% Layer Reduces Stresses in that Layer and Has No Appreciable Effect on the Stress in the Other Two Layers

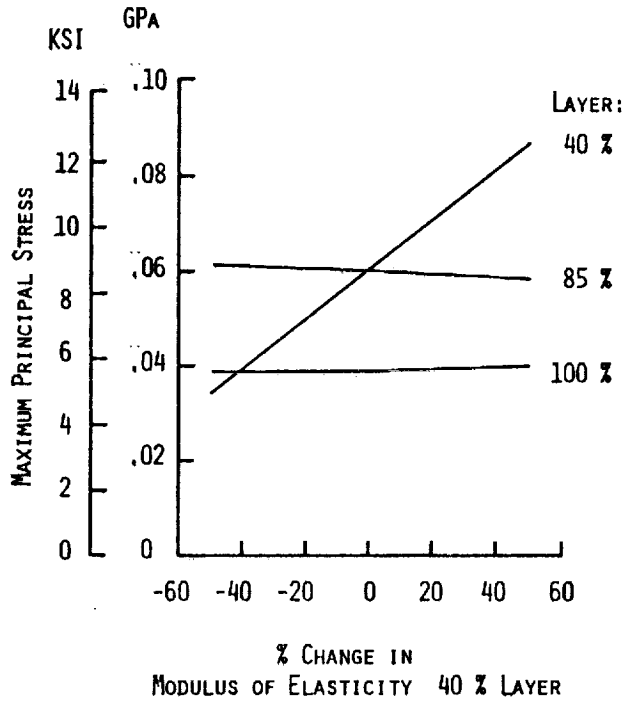

Figure 19 Reduction in the Modulus of the 40% Layer Reduces the Stresses in That Layer and Has No Effect on the Stresses in the Other Two Layers

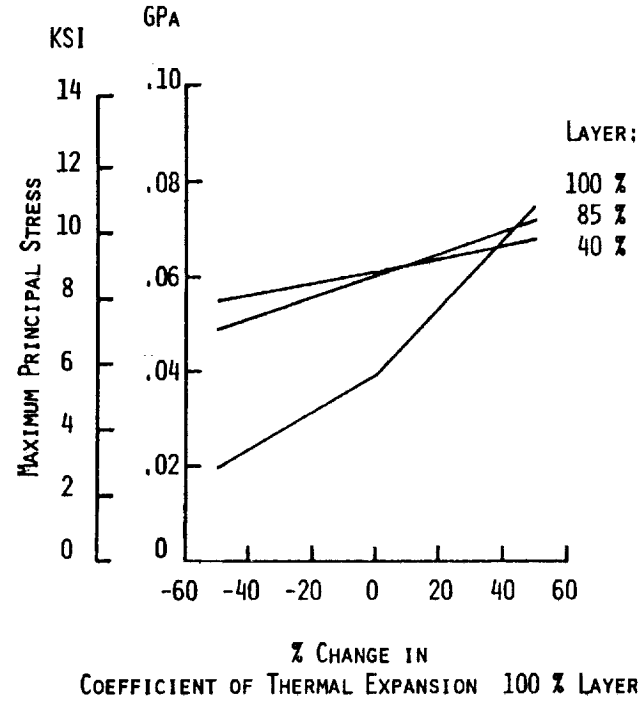

Figure 20 A Reduction in the Thermal Expansion of the 100% Layer Reduces the Stresses in All Three Layers

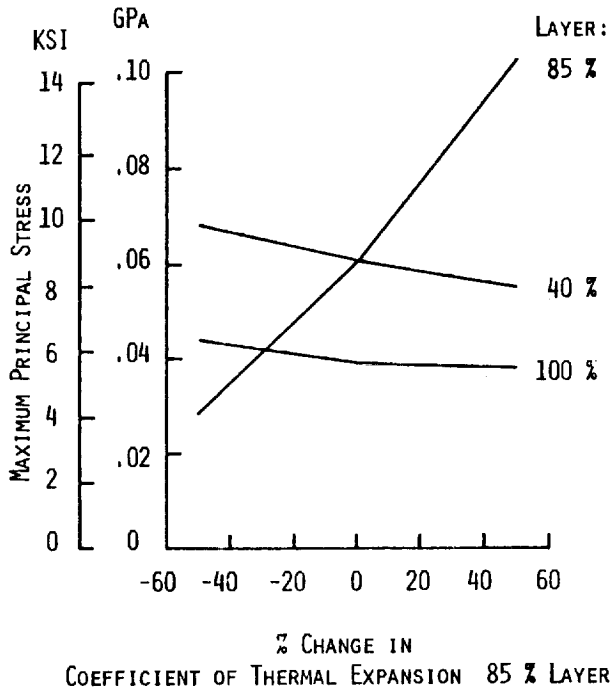

Figure 21 A Reduction the Thermal Expansion of the 85% Layer Only Significantly Effects (reduces) the Stresses in that Layer

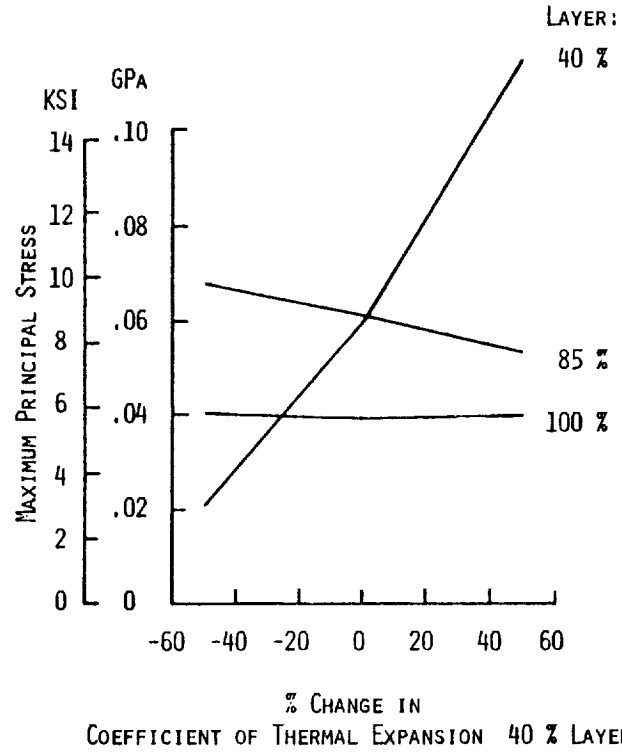

Figure 22 A Reduction in the Thermal Expansion of the 40% Layer Reduces Stresses in that Layer with no effect on the Other Two Layers

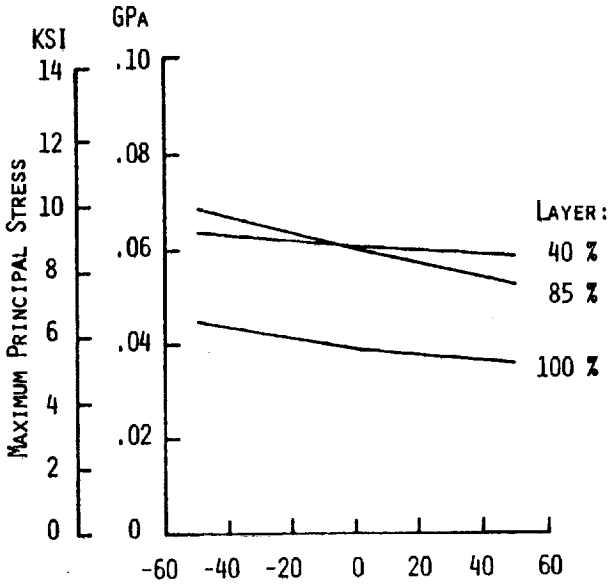

Figure 23 A Change in Thermal Conductivity of the 100% Layer has a Minimal Effect on the Stress of All Layers

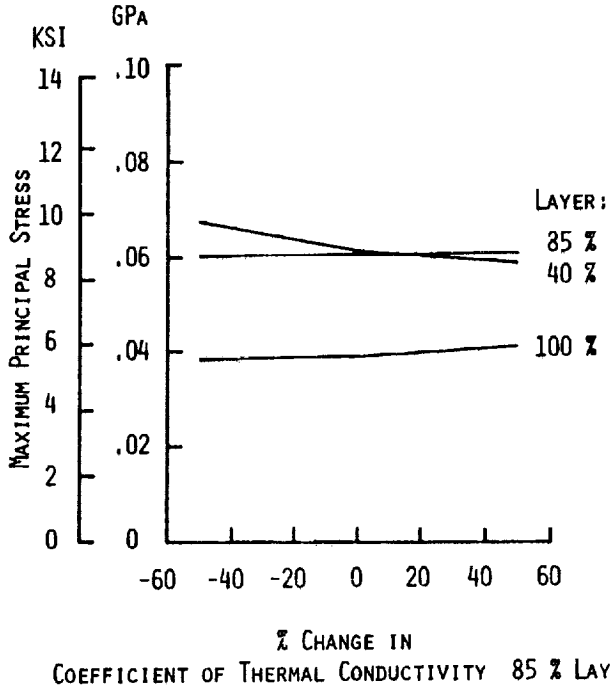

Figure 24 A Change in Thermal Conductivity of the 85% Layer has a Minimal Effect on the Stresses of All Layers

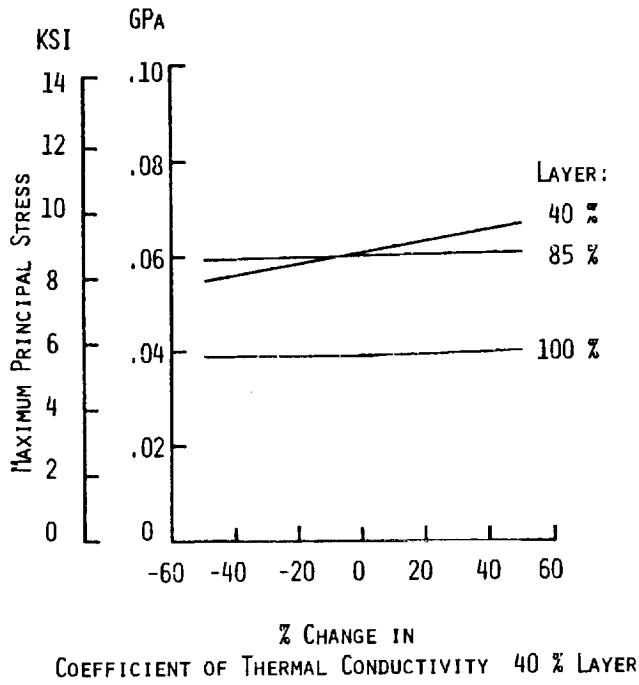

Figure 25 Variation in the Thermal Conductivity of the 40% Layer has a Minimal Effect on Stresses in the Three Layers

The effect of changes in thermal conductivity had the least effect of the three properties evaluated. Figures 23-25 show that changes in thermal conductivity did change stresses but only slightly.

In using a stress to strength criteria for acceptability, the strength is a significant property in that an increase or decrease directly influences the ratio on a one to one basis. The other properties evaluated in this analysis effect stresses and, thereby, the stress-to-strength ratio shown by the slope of the trend lines in Figure 17-25. The significance of the stresses shown in those plots were judged on the basis of strength of 26.2, 51.0, and 124.1 MPa (3.8, 7.4, and 18.0 ksi) for the 100%, 85%, and 40% layers respectively.

A review of all the data presented in Figures 17-25 revealed that the four changes in properties that would reduce stresses were 1) reducing modulus of elasticity in the 100% layer, 2) reducing modulus of elasticity in the 85% layer, 3) increasing thermal conductivity in the 100% layer and 4) reducing the coefficient of thermal expansion in the 100% layer.

It should be noted that the trend lines, by their slope, indicate that changes to the 40% layer were significant to stresses generated in that layer. However, the margin available in consideration of its strength of 124.1 MPa (18.0 ksi) was considered sufficient, so improvements in this layer were not pursued.

The trends shown in Figures 17-25 for the more significant properties were confirmed by more detailed analysis. The same circumferential plane model used in the analysis resulting in Table III data was used but with the modulus of the 100% and 85% layer reduced by 50%, increasing thermal conductivity of the 100% layer and reducing the coefficient of thermal expansion in the 100% layer. Results are presented in Table IV and indicate a reduction in stress to strength ratio of a factor of 2+, producing a maximum value of 0.4, well below the design evaluation criteria of 1.

TABLE III
MAXIMUM STRESS/STRENGTH RATIOS FOR
BASELINE CERAMIC SEAL SYSTEM

Engine Operating Condition/ Seal Plane	Graded Ceramic Layer					
	Zirconia		85% Layer		40% Layer	
	Stress MPa (psi)	Stress/ Strength	Stress MPa (psi)	Stress/ Strength	Stress MPa (psi)	Stress/ Strength
Acceleration 1/ Axial	33.3 (4828)	1.1	46.7 (6775)	1.0	61.4 (8905)	0.5
Acceleration 1/ Circumferential	39.0 (5661)	1.3 (max)	60.0 (8704)	1.3	60.6 (8791)	0.5
Acceleration 2/ Axial	32.8 (4751)	1.1	50.0 (7246)	1.1	50.2 (7285)	0.4
Acceleration 2/ Circumferential	38.3 (5559)	1.2	59.0 (8555)	1.3	44.7 (6483)	0.4
Sea Level Take-off/ Axial	14.5 (2100)	0.5	30.2 (4373)	0.6	21.3 (3095)	0.2
Sea Level Take-off/ Circumferential	20.7 (2999)	0.8	37.6 (5458)	0.8	23.9 (3464)	0.2
Deceleration 1/ Axial	25.9 (3762)	0.8	14.6 (2111)	0.3	15.0 (2173)	0.1
Deceleration 1/ Circumferential	17.8 (2588)	0.6	10.1 (1471)	0.2	17.3 (2504)	0.1
Deceleration 2/ Axial	21.1 (3064)	0.7	12.9 (1865)	0.3	14.9 (2168)	0.1
Deceleration 2/ Circumferential	13.1 (1896)	0.4	8.7 (1255)	0.2	16.6 (2408)	0.1

6.2 Spray Parameter Evaluation

Based on Pratt & Whitney Aircraft's experience in sprayed ceramics, and available literature, four spray parameters were determined to be the most significant effecting deposited material. The four parameters evaluated were 1) gun stand-off distance, 2) gun power, 3) powder feed rate and 4) primary gas flow. Values were selected for each parameter which were below and above the value used in spraying the baseline. Baseline property values used in this evaluation are those shown as a function of temperature in Appendix B. All parameters other than the change being evaluated were kept at baseline values. The plots in Figures 17-25 were used to identify influence factors which related the change in property to change in stress to estimate the net improvement in stress to strength ratio for each spray parameter change. No values are shown for the 19.0 cm (7.5 in) standoff for the 100% layer because deposition rate was decreased significantly and even after an extended period of spraying the specimen was too thin for measurements.

TABLE IV
MAXIMUM CIRCUMFERENTIAL STRESS/STRENGTH
RATIOS FOR THE CERAMIC SEAL SYSTEM
MODULUS OF THE 100% AND 85% LAYER REDUCED 50%
THERMAL CONDUCTIVITY OF THE 100% LAYER INCREASED 50% AND
THERMAL EXPANSION OF THE 100% LAYER REDUCED 50%

Engine Operating Condition	Graded Ceramic Layer					
	Zirconia		85% Layer		40% Layer	
	Stress MPa (psi)	Stress/ Strength	Stress MPa (psi)	Stress/ Strength	Stress MPa (psi)	Stress/ Strength
Acceleration 1	12.1(1760)	0.3	18.1 (2627)	0.4	28.9 (4190)	0.2
Acceleration 2	9.7(1402)	0.2	14.0 (2037)	0.3	20.2 (2933)	0.1
Sea Level Take-off	10.6(1533)	0.3	4.9 (716)	0.1	9.5 (1377)	0.1
Deceleration 1	4.2(613)	0.1	4.8 (690)	0.1	10.5 (1524)	0.1
Deceleration 2	2.9(425)	0.1	4.6 (673)	0.1	10.7 (1556)	0.1

A total of sixteen different fabrication runs were conducted initially; eight of each of the 100% and 85% layers. Table V contains the values for each of the four parameters and the resulting effect on tensile strength, modulus of elasticity and thermal expansion at the engine operating conditions.

The data in Table V formed the basis for selecting changes in spray parameters for both the 100% and 85% layers for evaluation in thermal rupture rig testing of system parts. For the 100% layer, decreased stand-off distance and reduced powder feed rate offered the greatest potential for reducing stresses in that layer. Increasing and decreasing stand off distance and a decreased power level offered most potential for reducing stresses in the 85% layer. Various combinations of these parameter changes as well as increasing the porosity of

a top section of the 100% layer, determined by an in-house program to improve abradability, were tested in the thermal rupture rig. Details of property measurements associated with spray parameter changes are presented in Appendix B.

TABLE V
COMPARISON OF SPRAY PARAMETER
VARIATIONS WITH BASELINE SYSTEM

Plasma Spray Parameter	Net Change, %			
	Tensile Strength	Modulus of Elasticity	Thermal Expansion	Stress/ Strength Ratio
100% Layer				
Gun Standoff Distance				
Increase to 19.0 cm*(7.5 in*)	-	-	-	-
Decrease to 6.3 cm(2.5 in)	+49%	+26%	No effect	-20.4%
Gun Power Level				
Increase to 46 KW	+33%	+48%	No effect	+19.8%
Decrease to 29 KW	- 6%	-21%	No effect	-15%
Powder Feed Rate				
Increase to 120 gpm	+ 9%	+22.2%	No effect	+15%
Decrease to 60 gpm	+26%	+ 5.1%	No effect	-20.3%
Primary Gas Flow				
Increase to 2.8 CMH (100 CFH)	+25%	+54%	No effect	+34.4%
Decrease to 1.7 CMH (60 CFH)	+17%	+38%	No effect	+24.8%
85% Layer				
Gun Standoff Distance				
Increase to 15.2 cm (6.0 in)	+26%	-7.5%	-3%	-30.5%
Decrease to 6.3 cm (2.5 in)	0	-18%	+11%	-29%
Gun Power Level				
Increase to 46 KW	-2%	-7%	+6.5%	-11.5%
Decrease to 26 KW	-2%	-19%	+3%	-24%
Powder Feed Rate				
Increase to 90 gpm	+16%	-2%	-3%	-15%
Decrease to 20 gpm	-10%	-4%	+8%	-2%
Preliminary Gas Flow				
Increase to 2.8 CMH (100 CFH)	+7%	-9.1%	+3%	-19.1%
Decrease to 1.4 CMH (50 CFH)	-15%	-18.5%	+8%	-11.5%

*The increase in gun stand off distance to 19.0 cm (7.5 in) for the 100% layer dramatically decreased the deposition rate resulting in a specimen too thin to test.

6.3 Thermal Rupture Rig Evaluation

Over 250 thermal rupture tests were conducted during the program to evaluate the effects of spray processing and design changes on the thermal rupture resistance of the sprayed ceramic seal system. The combination of spray parameters evaluated by thermal rupture rig changes is shown in Table VI. Seal system number 1 and 2 represented combinations of spray parameter changes which by analysis offered greater benefit. System No. 3 was tested because of in-house program data indicating it to have greater thermal rupture resistance than the baseline system as well as a decreased density at the surface to promote improved abradability. Thereafter the parameters selected for test evaluation were based on results of these tests and analysis as discussed below.

TABLE VI
CERAMIC SEAL SYSTEMS SELECTED FOR
THERMAL RUPTURE RIG EVALUATION

Seal System Number	Layer	Spray Parameter Variation
1	100%	Reduced gun distance, 6.3 cm (2.5 in)
	85%	Increased gun distance, 15.2 cm (6.0 in)
2	100%	Reduced gun distance, 6.3 cm (2.5 in)
	100%	Reduced powder feed rate, 60 gpm
	85%	Increased gun distance, 15.2 cm (6.0 in)
	85%	Increased powder feed rate, 90 gpm
3	100%	Increased porosity, top 0.076-0.114 cm (0.030-0.045 in) only
4	100%	Increased porosity
	85%	Increased powder feed rate, 90 gpm
5	100%	Increased porosity
	85%	Reduced gun distance, 6.3 cm (2.5 in)
6	100%	Increased porosity
	85%	Increased gun distance, 15.2 cm (6.0 in)
7	100%	Increased porosity
	100%	Reduced gun distance, 6.3 cm (2.5 in)
	85%	Reduced gun distance, 6.3 cm (2.5 in)
8	100%	Increased porosity
	85%	Increased powder feed rate, 90 gpm
	85%	Decreased gun power level, 26 kW
9	100%	Increased porosity
	100%	Reduced gun power, 29 kW
	85%	Decreased gun distance, 6.3 cm (2.5 in)

Test results are summarized in Figure 26 in comparison with baseline system test data. Maximum temperature change, the difference between combustor gas temperature and temperature on the back of the specimen of the test condition initiating a crack in the specimen was averaged for all tests of a given system and plotted. Results of the tests of the two initial systems indicated that the anticipated benefits of the individual parameter changes were not additive in that testing did not show the system specimens to be able to withstand a greater temperature gradient. The third system a 0.114 cm (0.045 in) porous top layer of zirconia did show a slight improvement.

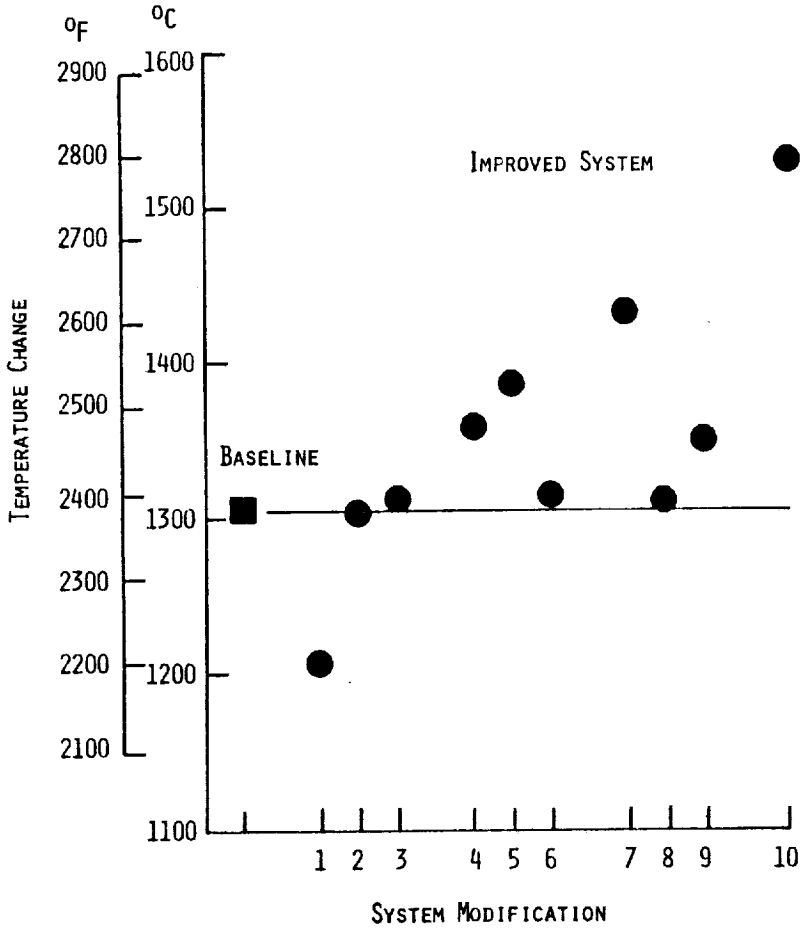

Figure 26 Improved Systems Showed 231°C (416°F) Improvement in Thermal Rupture Resistance

Because the effect of parameter changes was not additive, individual changes in spray parameters were then evaluated. Inspection of parts from testing to this point in the program indicated that cracks were concentrated primarily in the 85% layer. For that reason parameter changes were selected to decrease the stress to strength ratio in the 85% layer while maintaining the benefit associated with the 0.114 cm (0.045 in) porous zirconia layer. Systems 4, 5, and 6 accomplished that objective revealing that an increase of an additional 83°C (150°F) in thermal resistance could be achieved by decreasing gun distance to 6.3 cm (2.5 in) during spraying of the 85% layer. Systems 7

through 9 testing substantiated the improvement offered by adding a gun distance change to 6.3 cm (2.5 in) for the zirconia to the other two changes (a porous zirconia and 6.3 cm gun distance for the 85% layer) previously incorporated.

Improvements to the spray process involving mainly more accurate instrumentation and controls were incorporated and used to spray the improved system (noted as system modification No. 10). These improvements contributed significantly to increasing the average thermal resistance of the parts during spraying. An increase of 231°C (415°F) in temperature was demonstrated to be achievable with the improved system selected for engine test.

The improved system involves the following three changes to the baseline system.

1) 0.114 cm (0.045 in) porous zirconia top layer
2) 6.3 cm (2.5 in) gun stand off for the 100% layer
3) 6.3 cm (2.5 in) gun stand off for the 85% layer

The improvement in thermal rupture resistance as demonstrated by these rig tests was considered to be significant for JT9D engine use because of a rig/engine correlation developed under an in-house program. Seals fabricated with system 3 parts, with 222°C (400°F) less capability than the improved system, had been tested in a JT9D engine and completed engine cycling without spalling. The added benefit of the improved system would be expected to provide greater cyclic capability at similar engine temperatures or equivalent cycle capability at higher temperatures.

A typical specimen crack produced in the improved system by thermal rupture rig testing is shown in Figure 27. The crack typically angles through the 40% layer and becomes laminar near the interface of the 40% and 85% layers.

In addition to improving the spray process, effort was directed toward using the thermal rupture rig to evaluate several different substrate design features that could be incorporated to optimize the seal system durability. All previous thermal rupture rig testing had been done on specimens fabricated on 0.228 cm (0.090 in) flat stock Hastelloy X or Inconel 718. The attempt now was to identify engine seal substrate design modifications which could be demon- strated by rig tests of flat plate specimens to offer potential to reduce stresses. The designs investigated included 1) partial cross grooves as well as the baseline and a thinner substrate, 2) cross grooves, 3) picture frame and 4) cut corners. (Figure 28 shows modification 1-4).

The thin substrate design modification reduced the thickness of the flat plate from the baseline 0.228 cm (0.090 in) thickness to an approximate thickness of 0.152 cm (0.060 in). Both the cut corner and picture frame substrate modification attempted to reduce the effective thickness of the substrate at the most highly stressed parts of the seal, the leading and trailing edge and at the corners, where cracks occurred during rig and engine test. The cross groove and partial cross groove design modifications not only attempted to reduce the effective thickness but also attempted to introduce irregularities into the substrate surface to provide a torturous path for laminar crack progression.

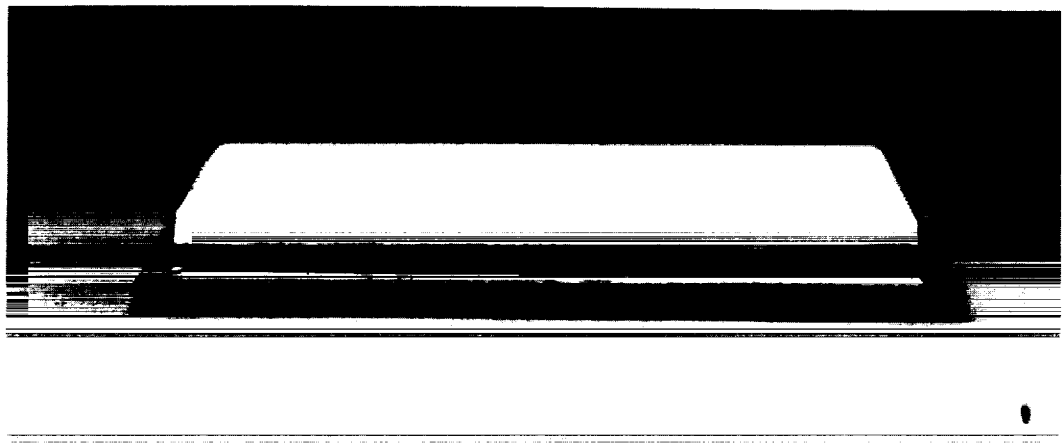

Figure 27 Typical Thermal Rupture Rig Crack Angles Through 40% Layer to 40%-85% Layer Interfaces

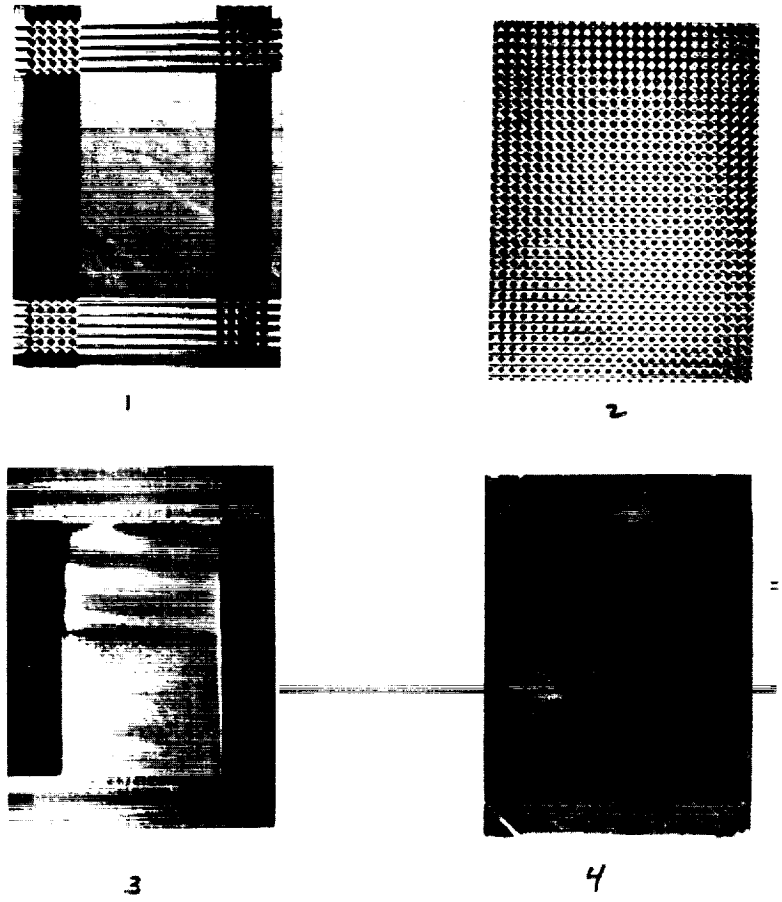

Figure 28 Four Seal Substrate Surface Design Modifications were Evaluated

All the specimens fabricated on the different substrate designs utilized the improved ceramic system with a gun standoff of 6.3 cm (2.5 in) for the 85% and 100% layers and a porous zirconia top layer

Since the majority of the improved system parts survived the maximum thermal rupture cycle testing did not identify any one configuration as being superior to the others.

In order to determine the relative merits of the substrate modifications a much thicker substrate was employed. Previous work had shown that a thicker substrate with its greater stiffness reduced thermal rupture resistance and therefore testing would result in crack initiation at a less severe thermal cycle. It was expected that by evaluating all alternative substrate design modifications with a thicker substrate susceptability to thermal stress would be increased. Cracks would be initiated at a lower test condition and differences between design modifications could be identified.

Testing was conducted but results did not conclusively prove that any design change offered thermal rupture resistance benefit. An attempt to further evaluate cross grooving was not successful. Difficulties in machining cross grooves on seals for cyclic thermal shock rig testing and successful engine test of seals without cross grooving provided the basis for a decision not to incorporate the cross groove feature in the ceramic seal design.

6.4 Other Rig Tests

6.4.1 Thermal Gradient

Two multi-layer specimens of the improved ceramic seal system were fabricated for thermal gradient testing. The specimens were machined to remove overspray of the edges and provide the final overall thickness required to match actual engine segment dimensions. The first test, simulating the thermal gradient at engine cruise conditions with a 1090°C (1995°F) zirconia and 543°C (1010°F) back temperature, completed 50 hours without cracking. The second test, simulating the thermal gradient at engine sea level takeoff condition with a 1273°C (2325°F) surface temperature and 662°C (1225°F) back temperature completed 33.33 hours of testing before aborting because of equipment failure. The equipment failure resulted in a very severe temperature decrease on both surfaces. Inspection of the part revealed cracks at the 100%-85% layer interface.

The results of the analytical study of this test indicate that the cracking observed would be expected to result from the abnormal temperature decrease encountered with the equipment failure, and probably was not the result of 33.33 hours of exposure to the normal test temperature gradient. On the basis of this analysis, and the results of the cruise temperature gradient tests, it was concluded that the improved ceramic seal system was stable under expected temperature gradients. Previous testing resulted in the same conclusion regarding the baseline ceramic seal system.

6.4.2 Thermal Cycle

Thermal cycle testing of the improved ceramic seal system was concluded after the first acceleration cycle. Visual inspection of the segment revealed cracking in the ceramic as shown in Figure 29. Maximum surface temperature recorded was 1537°C (2800°F) which is greater than the expected nominal engine conditions. Post-test analysis indicated that thermally induced stresses could produce the observed cracking in the porous zirconia and 85% regions as shown in Figure 30. All three time points (acceleration, sea level take-off and deceleration) were examined in the analysis. A summary of this data is presented in Table VII. showing that the acceleration cycle was the most severe. The predicted crack locations correlate favorably with the actual test data, and differences are attributable to the localized stiffening effect of the slotted mounting rails. A repeat of the test of expected nominal engine conditions was not pursued because of the limited value of such a rig test considering the fact that engine test results would be available soon.

TABLE VII

ANALYTICAL RESULTS OF THERMAL CYCLE TESTING

Subset	Material	Thermal Time Point: Accel		SLTO		Decel	
		Stress MPa (psi)	Stress/ Strength	Stress MPa (psi)	Stress/ Strength	Stress MPa (psi)	Stress/ Strength
1	Porous zirconia	-6.0 (-877)		-2.4 (-347)		8.9 (1288)	0.6
2		11.9 (1731)		3.7 (537)		4.6 (674)	
3		20.9 (3032)	1.5	8.1 (1170)	0.7	3.1 (450)	
4	100%	27.5 (3983)		11.9 (1720)		4.7 (681)	
5		33.4 (4840)		16.9 (2450)		5.6 (815)	
6		27.8 (4035)		17.0 (2472)		3.2 (460)	
7		41.0 (5944)	1.0	26.9 (3905)	0.7	12.1 (1752)	0.3
8	85%	39.2 (5685)		14.1 (2041)		7.6 (1107)	
9		38.4 (5565)		19.7 (2863)		7.4 (1068)	
10		36.2 (5247)		26.8 (3880)		4.8 (701)	
11		45.6 (6619)	1.0	54.8 (7946)	1.2	24.3 (3526)	0.5
12	40%	49.2 (7140)		15.2 (2201)		3.2 (465)	
13		47.7 (6924)		15.3 (2218)		4.0 (575)	
14		58.0 (8415)		23.9 (3473)		8.3 (1209)	
15		69.3 (10044)	0.5	86.7 (12572)	0.6	13.8 (2004)	0.1
16	Bond coat	217.2 (31503)		45.9 (6659)		10.2 (1475)	
17	Substrate	185.6 (26925)		89.7 (13014)		19.5 (2829)	

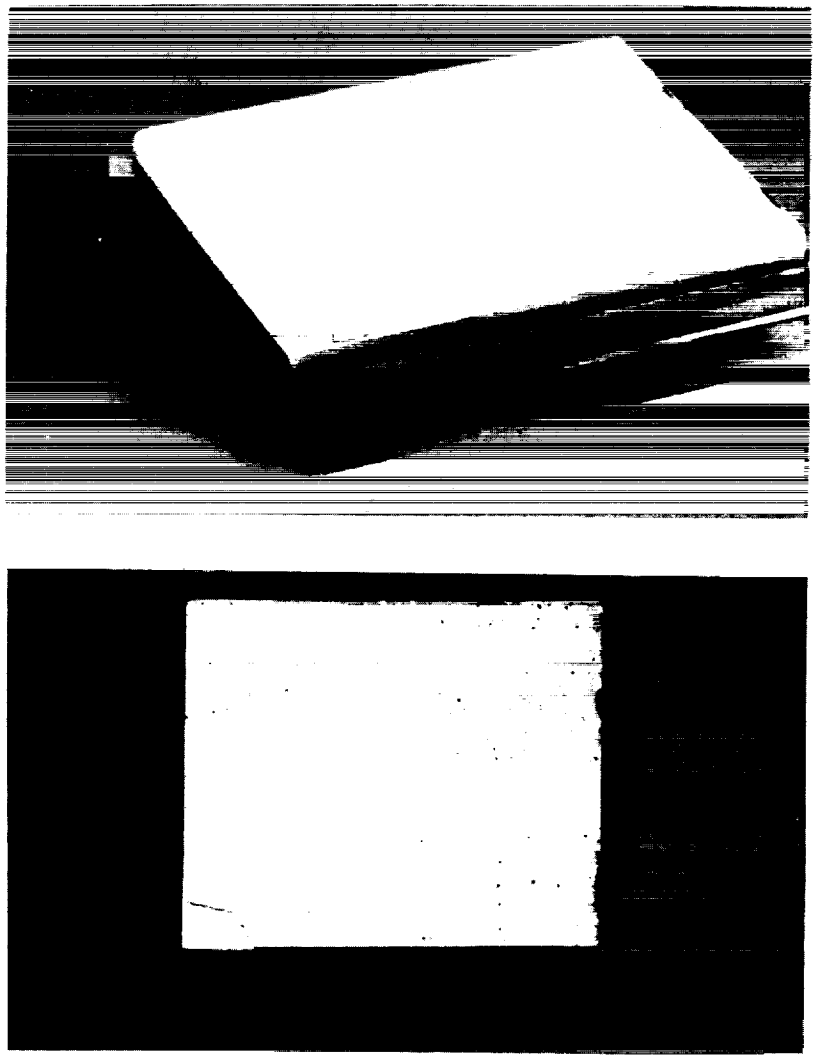

Figure 29 Ceramic Seal Cracks After First Accel of Thermal Cycle Testing are Shown

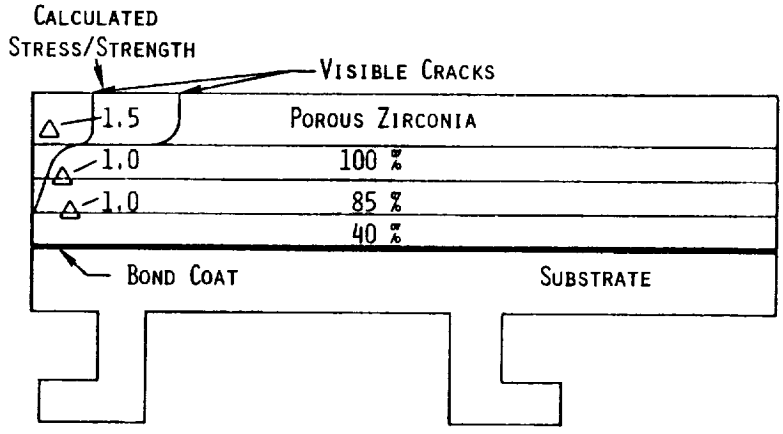

Figure 30 Analysis Predicts Identical Crack as Engine Result

6.4.3 Erosion

The results of erosion rig testing of the baseline and improved ceramic seal systems at 1315°C (2400°F) are summarized in Table VIII, and photographs showing typical post test condition of tested specimens are presented in Figure 31 (numbers in the figure correspond to Table VIII). Comparison of the unaged results with the two systems at the higher impingement angles (30, 45, and 85 degrees) shows that the erosion rate of the improved system is slightly higher (4%). Comparison of the unaged results at 15 degrees impingement angle shows the erosion rate of the improved system to be significantly higher (85%). However, whereas aging increases the erosion rate of the baseline system, the data from the improved system is not conclusive because of the limited amount of data, as shown on Figure 32. The higher erosion rate of the improved system is expected because of the more porous top surface used in the improved system to increase abradability. It should be noted that in-house engine testing has indicated that the demonstrated erosion rate is acceptable for initial engine evaluation for the intended application.

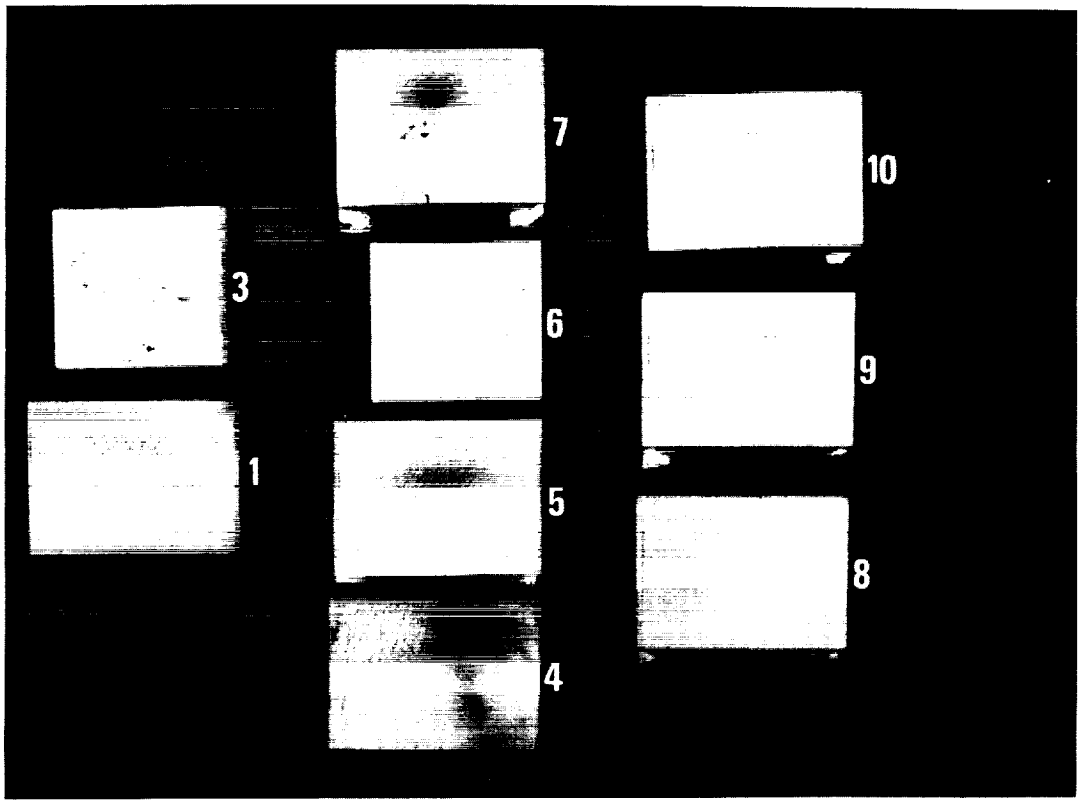

Figure 31 Erosion Rate Demonstrated by Rig Testing is Acceptable for Initial Engine Evaluation

TABLE VIII

RESULTS OF EROSION RIG TESTING

Number	Seal System	Aging Time Hrs	Aging Temp, °C (°F)	Impingement Angle Degree	Particulate Size	Erosion Rate* gm/min (lb/hr)
	Baseline		Unaged	15	80 Grit	0.0045 (0.00060)
	Baseline		Unaged	30	80 Grit	0.0154 (0.00204)
	Baseline		Unaged	85	80 Grit	0.0522 (0.00690)
	Baseline	100	760 (1400)	15	80 Grit	0.0050 (0.00066)
	Baseline	200	760 (1400)	15	80 Grit	0.0055 (0.00073)
	Baseline	500	760 (1400)	15	80 Grit	0.0068 (0.00090)
	Baseline	100	871 (1600)	15	80 Grit	0.0069 (0.00091)
1	Improved		Unaged	15	90 Grit	0.0083 (0.00110)
2	Improved		Unaged	15	80 Grit	0.0149 (0.00197)
3	Improved		Unaged	15	80 Grit	0.0089 (0.00118)
4	Improved		Unaged	30	90 Grit	0.0127 (0.00168)
5	Improved		Unaged	45	90 Grit	0.0449 (0.00594)
6	Improved		Unaged	45	80 Grit	0.0630 (0.00833)
7	Improved		Unaged	85	90 Grit	0.0636 (0.00841)
8	Improved	100	760 (1400)	15	90 Grit	0.0097 (0.00128)
9	Improved	200	760 (1400)	15	90 Grit	0.0082 (0.00108)
10	Improved	100	871 (1600)	15	90 Grit	0.0109 (0.00144)

* Seal Surface temperature of 2400°F

Examination of the data in Table VIII also shows that the switch from 80 grit to 90 grit particulate, which was necessary part way through the program because of an availability problem, had a negligible effect on the results. Comparison of test numbers 2 and 3, which are identical in every respect including grit size (80 grit), shows a potential repeatability error of ±25 percent in erosion rate. Comparison of the erosion rate of test number 1, which differs from test numbers 2 and 3 only in grit size (90 grit), with the average erosion rate of test numbers 2 and 3 show that the 90 grit test is 30 percent less. Comparing test numbers 5 and 6, which are identical except for grit size, also show the erosion rate with 90 grit particulate to be about 30 percent less. Since the results in these two examples fall in the same range as the repeatability error, it was concluded that the general comparisons of the two seal systems were reasonable.

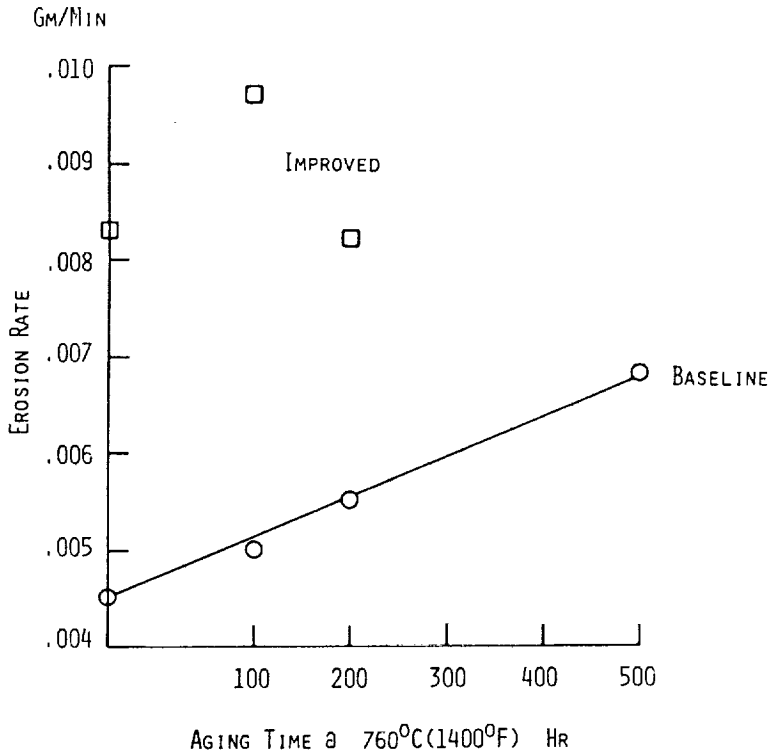

Figure 32 Results of Erosion Tests After Aging of Improved System are Inconclusive

6.4.4 Abradability

The results of the abradability rig testing of the baseline and improved ceramic seal systems are summarized in Table IX. The high values of VWR shown for most of the cases in this table indicate excellent abradability. Values of volume wear ratio above 700 were not calculated because they corresponded to blade wear measurements lower than 0.0005 cm (0.0002 in) which was within blade wear measurement accuracy. Comparing test 6 with tests 16 and 17 shows

that the improved system, which includes a more porous surface layer, resulted in a significant abradability increase at slow interaction rates where the baseline system is poorest. This conclusion is based on unaged specimens of both seal systems. A comparison of test 4 with tests 7, 8, 9, 10 and 11 indicates that aging of the baseline system resulted in no change in abradability within the accuracy of the measurements. This conclusion is also expected to apply to the improved system, which was not tested after aging.

TABLE IX

RESULTS OF ABRADABILITY RIG TESTING

Test No.	Seal System	Aging Time Hrs	Aging Temp, °C (°F)	Incursion Rate, cm/sec (in/sec)	Max Seal Wear cm (in)	Avg Blade Tip Wear cm (in)	VWR
1	Baseline	Unaged		0.025(0.010)	0.040(0.016)	Negligible	700+
2	Baseline	Unaged		0.025(0.010)	0.040(0.016)	Negligible	700+
3	Baseline	Unaged		0.005(0.002)	0.058(0.023)	0.012(0.005)	600
4	Baseline	Unaged		0.002(0.001)	0.058(0.023)	0.012(0.005)	700+
5	Baseline	Unaged		0.002(0.001)	0.020(0.008)	0.0302(0.0119)	1.4
6	Baseline	Unaged		0.0002(0.0001)	0.020(0.008)	0.0302(0.0119)	1.4
7	Baseline	50	760(1400)	0.002(0.001)	0.043(0.017)	Negligible	700+
8	Baseline	200	760(1400)	0.002(0.001)	0.033(0.013)	Negligible	700+
9	Baseline	500	760(1400)	0.002(0.001)	0.043(0.017)	Negligible	700+
10	Baseline	50	860(1600)	0.002(0.001)	0.048(0.019)	Negligible	700+
11*	Baseline	50	1095(2000)	0.002(0.001)	0.043(0.017)	Negligible	700+
12*	Baseline	33.5	1315(2400)	0.002(0.001)	0.015(0.006)	0.0134 (0.0053)	3.4
13	Improved	Unaged		0.025(0.010)	0.055(0.022)	Negligible	700+
14	Improved	Unaged		0.002(0.001)	0.058(0.023)	0.0040 (0.0016)	700+
15	Improved	Unaged		0.002(0.001)	0.0416(0.0164)	0.0124 (0.0049)	35.2
16	Improved	Unaged		0.0002(0.0001)	0.033(0.013)	0.0114 (0.0045)	13
17	Improved	Unaged		0.0002(0.0001)	0.0690(0.0272)	0.0523 (0.0206)	265
18**	Improved	Unaged		0.025(0.010)	0.073(0.029)	Negligible	700+

* Aging of these specimens was the result of exposure to a thermal gradient test.

** Seal surface temperature of 1093°C (2000°F) instead of the 1315°C (2400°F) used in all other cases.

A comparison of tests 11 and 12 relates the abradability of an engine segment aged at a cruise condition (test 11) with a segment aged at take off conditions (test 12). Test 12 shows a significant reduction in abradability compared to the other aged tests. While this may be at least partly attributable to its very high aging temperature (1315°C, 2400°F), it is more likely due to the fact that the specimen was cracked when subjected to a rapid temperature reduction when the rig equipment failed during a prior thermal gradient test.

Comparison of test 4 with 5 and 14 with 15 shows substantial variation of abradability results in repeated testing. The 700+ VWR result from each pair of tests is believed to be the correct result because of its consistency with the results of tests 7, 8, 9 and 10, which were run with the same incursion rate.

Test 18 was conducted with a seal surface temperature at 1093°C (2000°F), while all other tests were at 1315°C (2400°F). This test may be compared to tests 13, 1, and 2 to show that abradability is not affected significantly by this range of surface temperature.

6.5 Engine Test

This test provided the opportunity to compare the results of 500 and 2500 cycles of engine tests with the thermal rupture rig test results of the ceramic system with porous zirconia top layer. Visual inspection revealed that most of the 36 seal segments were unaffected by exposure to the engine environment, as shown in Figure 33. Only six segments showed small areas of edge chipping, as shown in Figure 34. Microscopic inspection showed that small, tight cracks were generated on only 15% of the segment corners. The porous zirconia top layer in combination with improvements made to the 85% and 100% layer and improved processing techniques demonstrated improved thermal rupture resistance as shown by comparing system modifications numbers 3 and 10 in Figure 26. It is anticipated, therefore, that engine testing of the improved design which includes these additional features will result in less cracking than exhibited by these parts.

A total of nine seal segments were rubbed during the test to a maximum depth of 0.033 cm (0.013 in). Twenty-two of the twenty-three blades participated in the rub with a maximum measured blade tip wear of 0.139 cm (0.055 in). A volume wear ratio, seal volume removed to blade tip volume worn, of 22 to 1 was calculated from the measured data. The seal rub is shown in Figure 35. A typical blade tip showing results of the test is also shown in Figure 36. These rub results substantiated the potential engine clearance reduction benefit attributable to the abradability of the sprayed ceramic seal system.

Eighteen of the thirty-six seals which were unaffected by the 500 cycles were subsequently tested for another 2000 cycles resulting in only 10 very local areas of edge chipping similar to that shown in Figure 34.

The engine test also demonstrated that the seal system with the 100% layer top coat would abrade sufficiently and cleanly without chipping and cracking during a blade tip rub. This feature is included in the improved seal design and comparable rub performance in subsequent engine test of the design is anticipated.

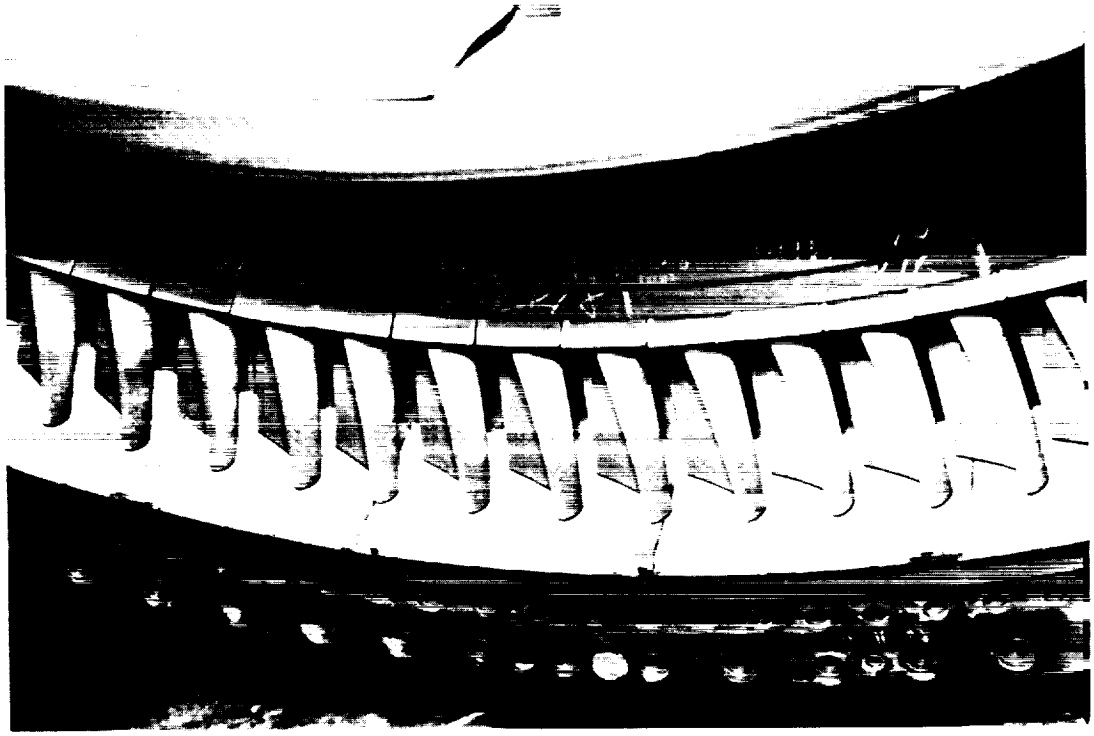

Figure 33 Most Seal Segments were Unaffected by Exposure to 2500 Engine Cycles

Figure 34 Six Segments Showed Some Edge Chipping after Exposure to 2500 Engine Cycles

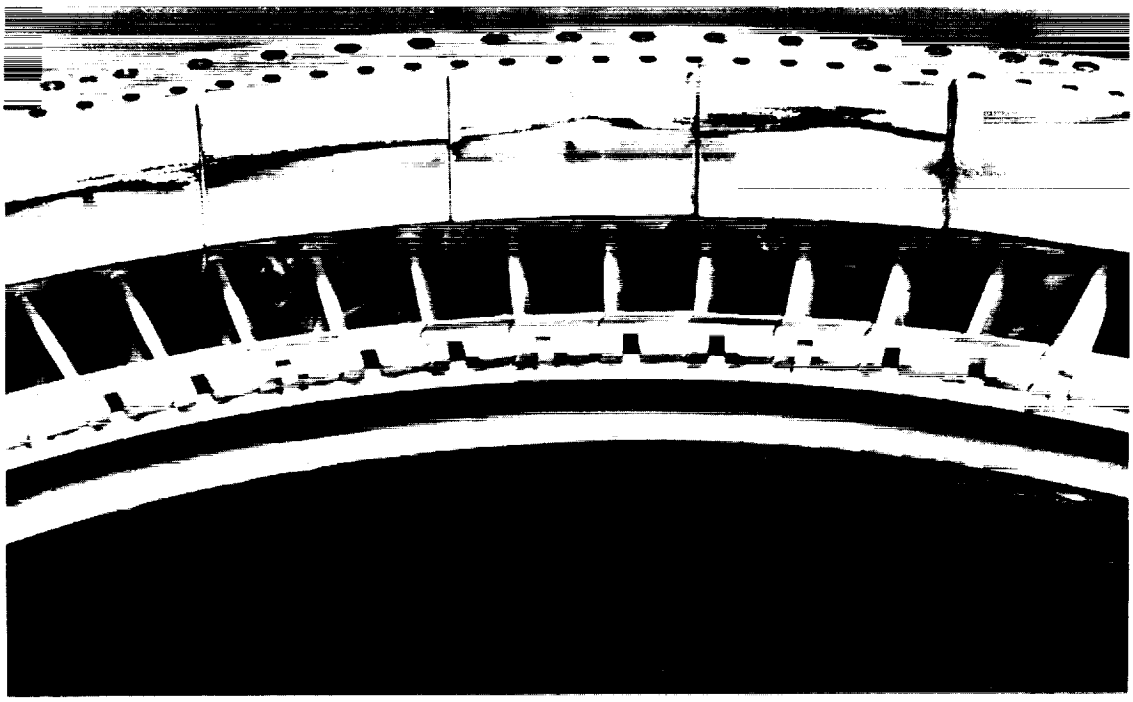

Figure 35 Seal Rub is Consistent with a Volume Wear Ratio of 22 to 1

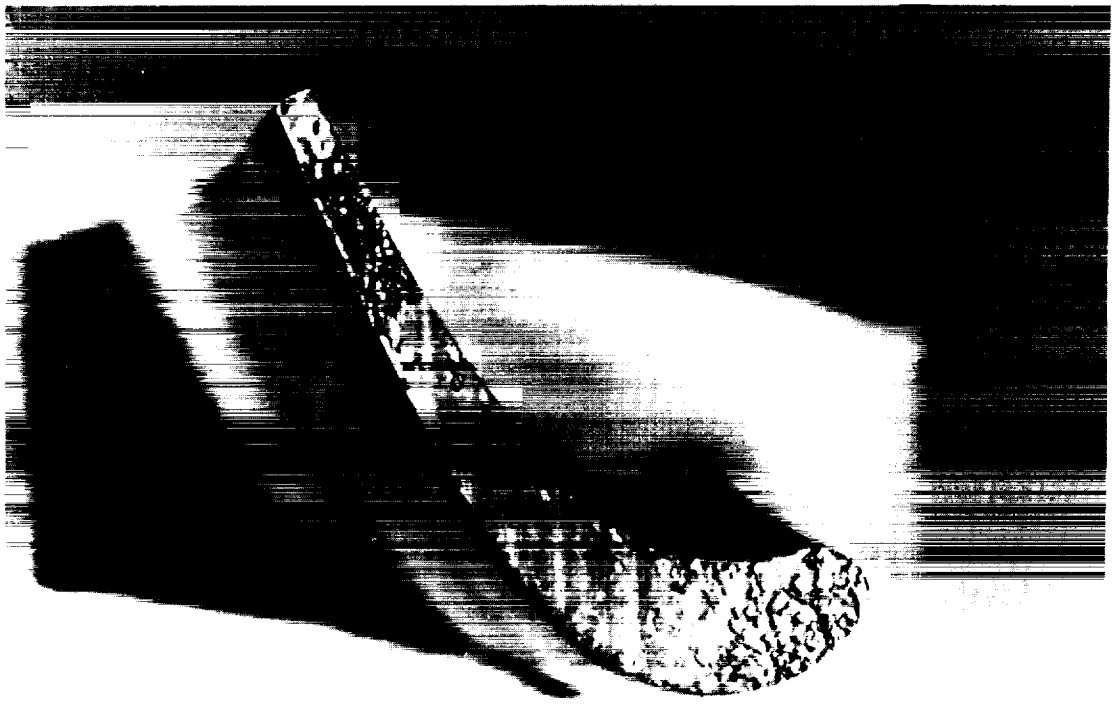

Figure 36 Blade Tip Wear is Consistent with a Volume Wear Ratio of 22 to 1

7.0 Concluding Remarks

Significant improvements in the critical characteristics of the ceramic seal system have been accomplished under this NASA sponsored ECI-PI project. With these improvements, the seal system is expected to perform successfully in two upcoming engine tests under Phase II of the ECI project. One test will demonstrate the abradability and durability characteristics of the final seal system in a 1000 cycle endurance test of a JT9D-7J engine. The other test is an FAA-monitored 150 hour, maximum exhaust gas temperature test of a JT9D-7R4 engine, which is expected to qualify the seal system for subsequent airline service evaluation.

Airline service evaluation is the ultimate test of the acceptability of the seal system, marking completion of the transition from the concept to the application stage. Application to new production engines and retrofit in existing engines would be expected to follow rapidly, allowing at least 0.025 cm (0.010 in) reduction in turbine tip clearance and an estimated fuel saving of 0.4 percent.

Recommendations for further work on ceramic seal systems will be formulated based on the results of engine testing scheduled in Phase II of this program.

Appendix A

Plasma Spray Equipment

Pratt & Whitney Aircraft's Metal Joining Development Group of Manufacturing Research and Development is developing plasma spray equipment which will have capabilities superior to any currently available. The first generation of this equipment was used for a majority of the plasma spray work performed under this contract. The control panel and holding fixture used are shown in Figures A-1 and A-2 respectively. The use of this equipment provides an added degree of spray parameter control which has helped in the identification and optimization of significant spray parameters that are key to the successful development of the improved ceramic seal design. Future generations of equipment are being developed to further improve the ability to optimize complex plasma sprayed systems of this type and fabricate them with consistency.

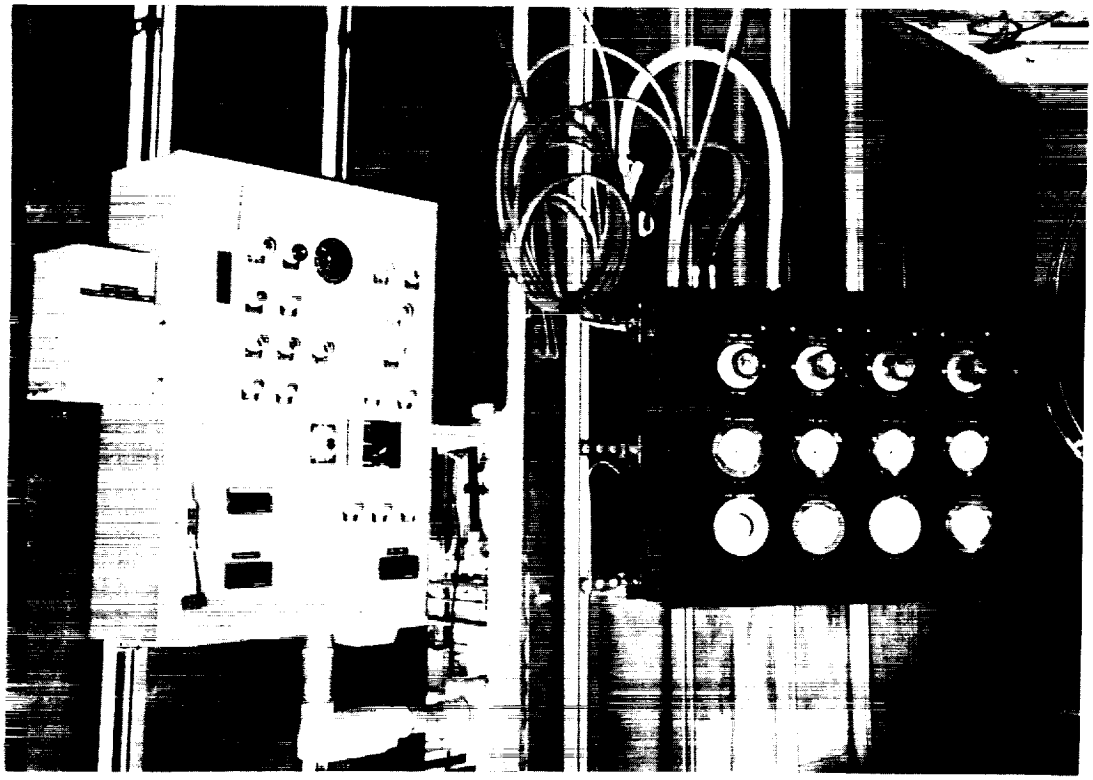

Figure A-1 Plasma Spray Control Panel Used in the Evaluation and Optimization of Significant Spray Parameters

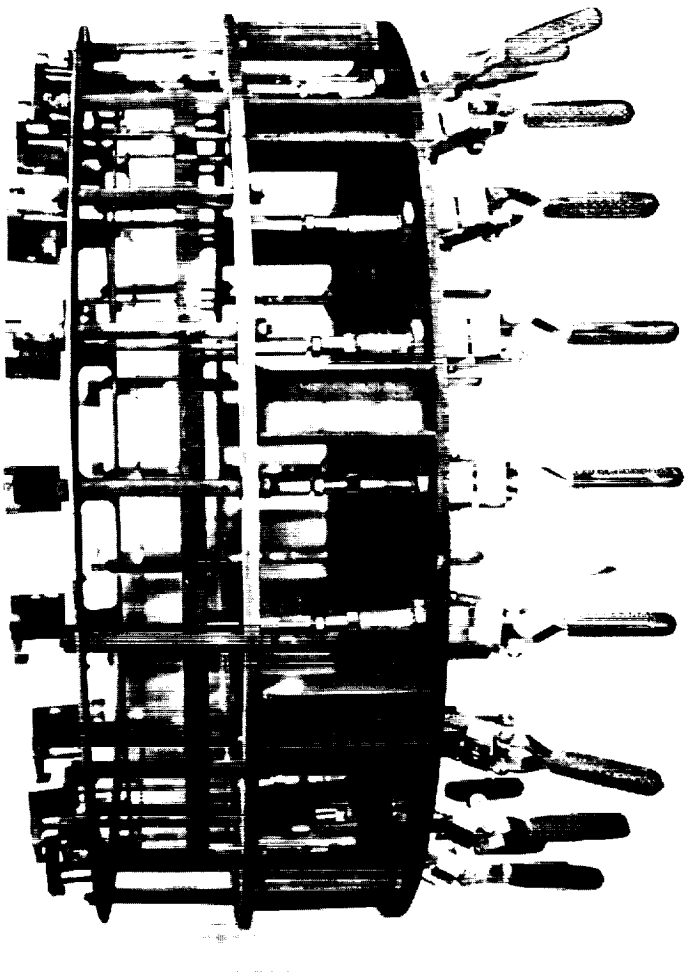

Figure A-2 Production Type Holding Fixture Used in Spraying Property Specimens, and Rig and Engine Parts

Additional equipment consisted of the powder delivery system shown in Figure A-3. This system utilizes 5 Plasmadyne powder feeders which allows for continual spraying of the system's 5 layers. Two Plasmadyne 40 kilowatt power supplies are tied together and are used to supply the power to the 3M Micro Plasma Spray Gun, Figure A-4.

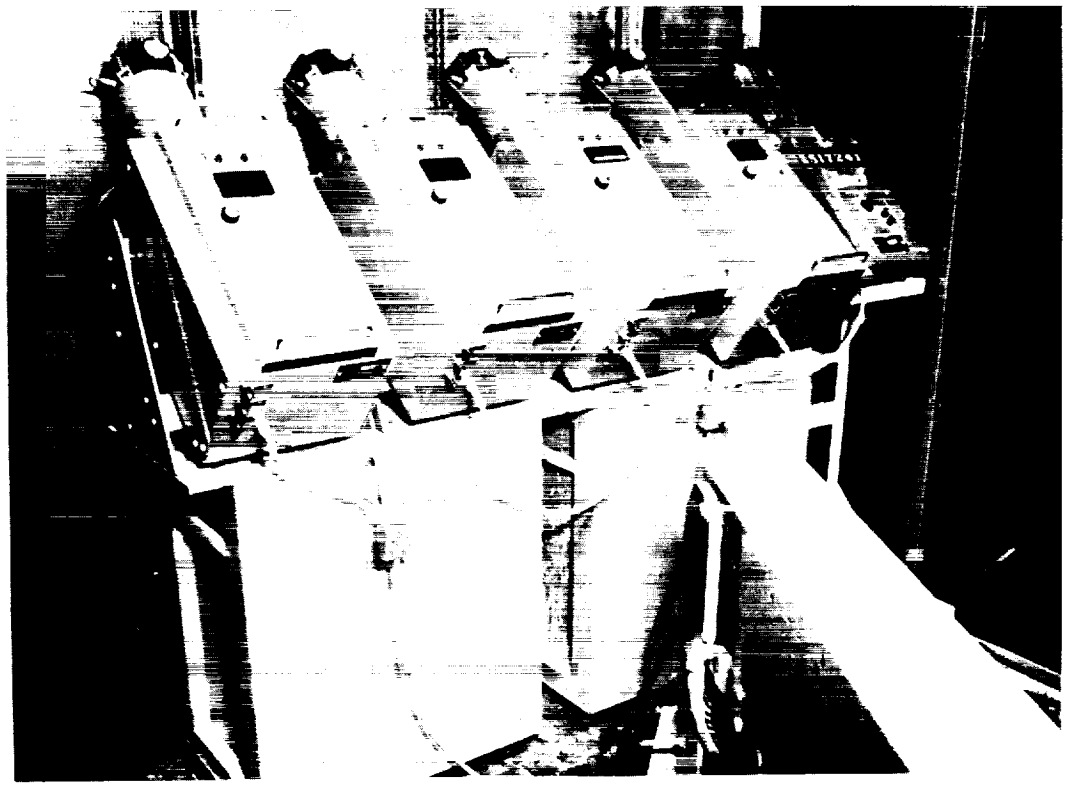

Figure A-3 Powder Feed System Providing Continuous Powder Flow During Spraying of Ceramic System Specimens and Parts

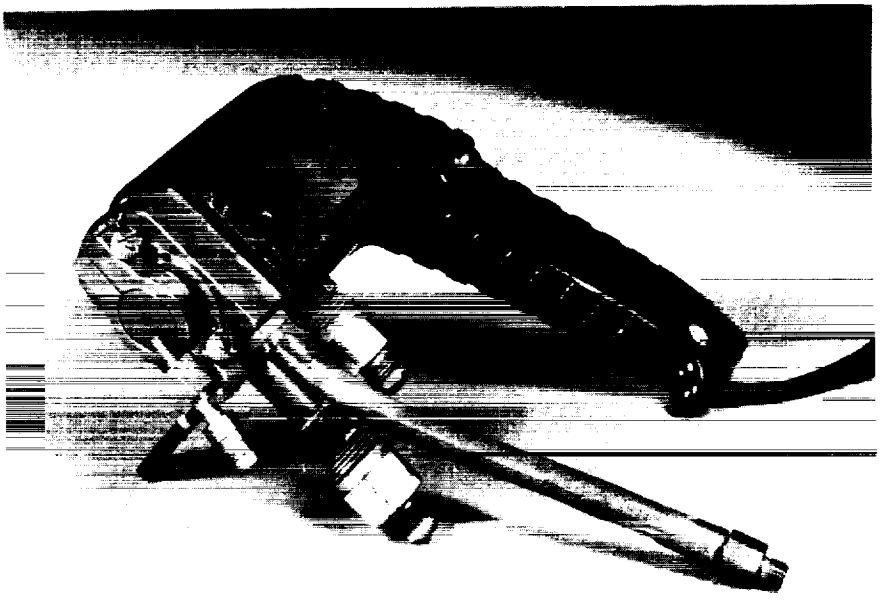

Figure A-4 Metco Plasma Spray Gun

Appendix B

Material Properties

I Material Properties and the Effects of Aging of the Baseline Ceramic Seal System

Single layer flat-plate specimens were prepared of the baseline ceramic seal system for each of the ceramic/metallic layers. The specimens were machined and thermally aged at temperatures and times representative of the engine environment. Aged specimens were then subjected to property measurements for modulus, tensile strength, compressive strength, thermal conductivity and thermal expansion.

Property measurements were evaluated on the 100% layer after a 50 hour aging period at a temperature of 1371°C (2500°F). Figure B-1 is a comparison of the tensile strength of aged and non-aged specimens versus temperature. In the temperature range of 1037°C (1900°F) to 1371°C (2500°F) the tensile strength is increased by a factor of 2 after aging. At the lower temperatures the increase in tensile strength approaches three times that of baseline. Compressive strength increased more dramatically in the temperature range of room temperature to 537°C (1000°F) for the aged specimens. At 1037°C (1900°F) to 1371°C (2500°F) the increase was one and a half times greater than the unaged specimens. Figure B-2 is a comparison of the compressive strength of aged and non-aged test specimens versus temperature. The elastic modulus of the 100% layer after aging, determined from the tensile and compressive strengths, is shown in Figure B-3.

Property measurements for the 85% layer were evaluated after an aging period of 300 hours at a temperature of 871°C (1600°F). Figure B-4 is a comparison of the tensile strength of aged and unaged specimens versus temperature. The aged material did not increase in strength. In the temperature range of 537°C (1000°F) to 760°C (1400°F) the tensile strength of the unaged specimens was approximately 50 percent greater than the aged. The compressive strength (Figure B-5) exhibits the same trend in data as for the tensile strength. Within the temperature range of 537°C (1000°F) to 760°C (1400°F) the unaged specimens were approximately two times stronger. The elastic modulus, calculated from tensile and the compressive strength (Figure B-6) showed an increase over the baseline data.

Property measurements for the 40% layer were evaluated after an aging period of 500 hours at a temperature of 760°C (1400°F). Before considering the data obtained for this material, it should be noted that the ring used for aging was fabricated with a higher ceramic content than was intended. This was confirmed by analysis of the metallic content The result was an expected decrease in strength and elastic modulus. Therefore, the following discussion deals in terms of general trends. Figure B-7 is a comparison of the aged tensile strength to earlier baseline data. An increase in strength after aging was noted at all test temperatures. The data from the compressive strength exhibits the same trend (Figure B-8). The elastic modulus also showed an increase over the unaged data (Figure B-9).

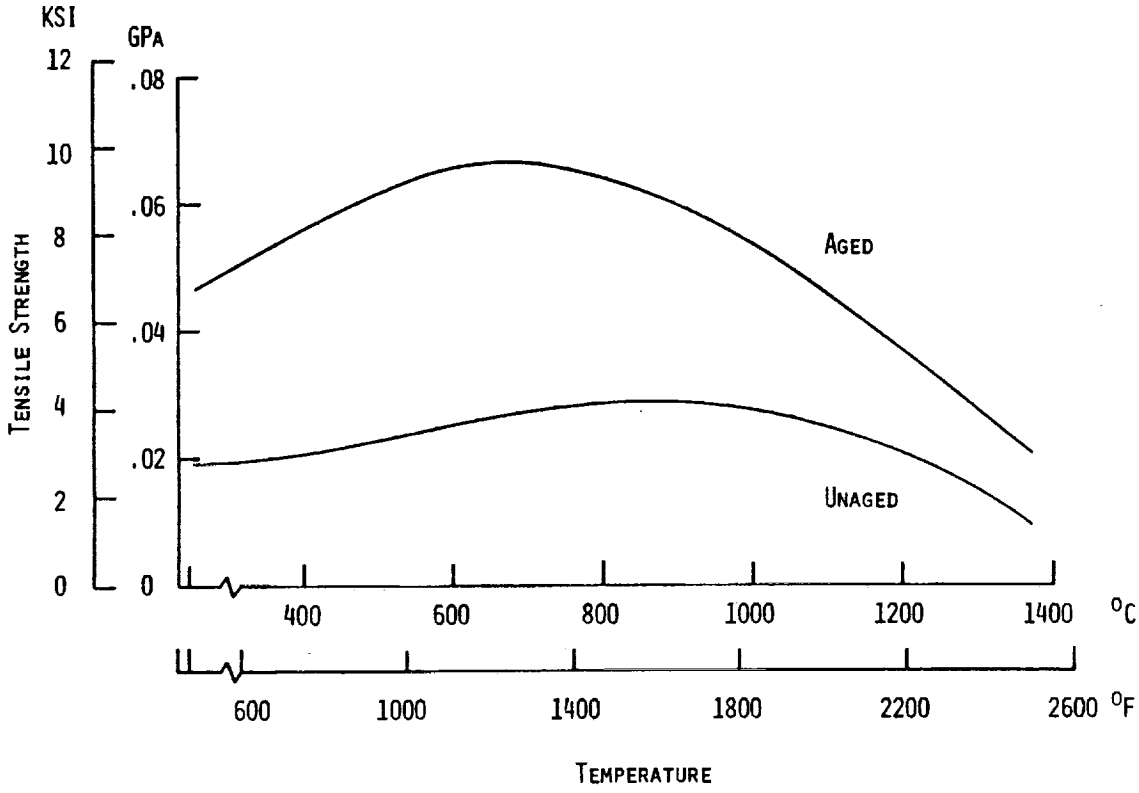

Figure B-1 Aging of the Baseline 100% Layer for 50 Hours at 1371°C (2500°F) Increases the Tensile Strength Through Entire Temperature Range

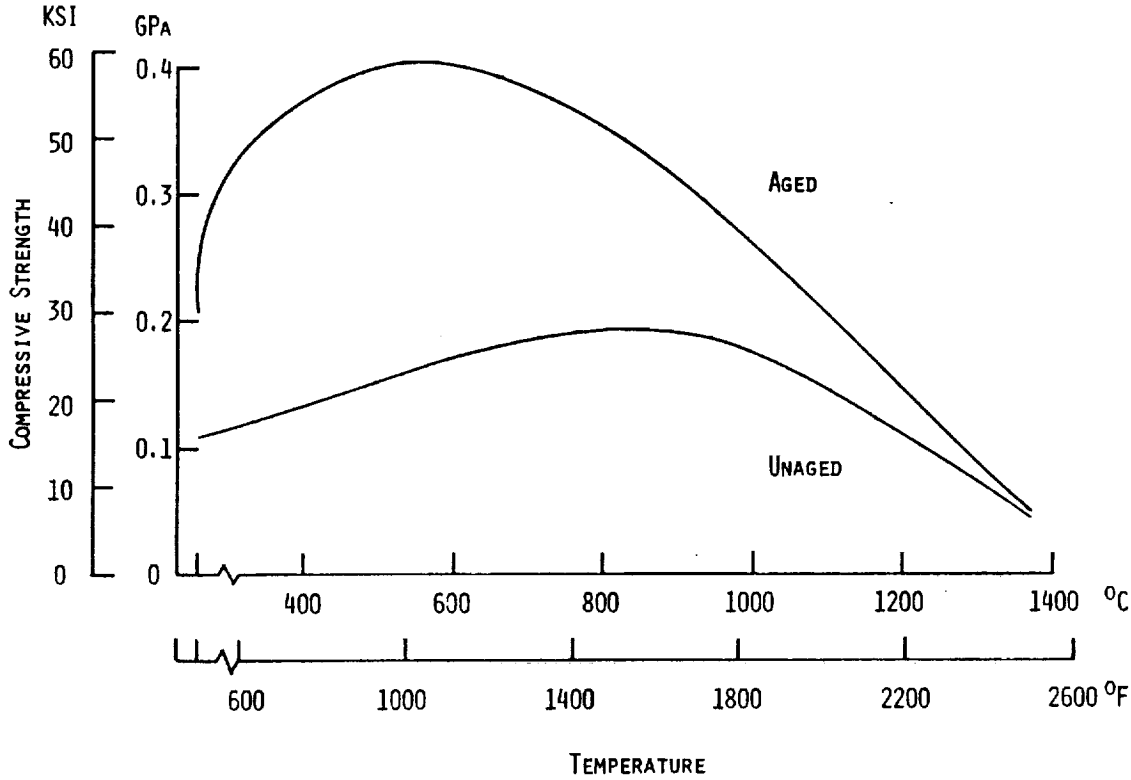

Figure B-2 Aging of the Baseline 100% Layer for 50 Hours at 1371°C (2500°F) Increases the Compressive Strength Over Entire Temperature Range

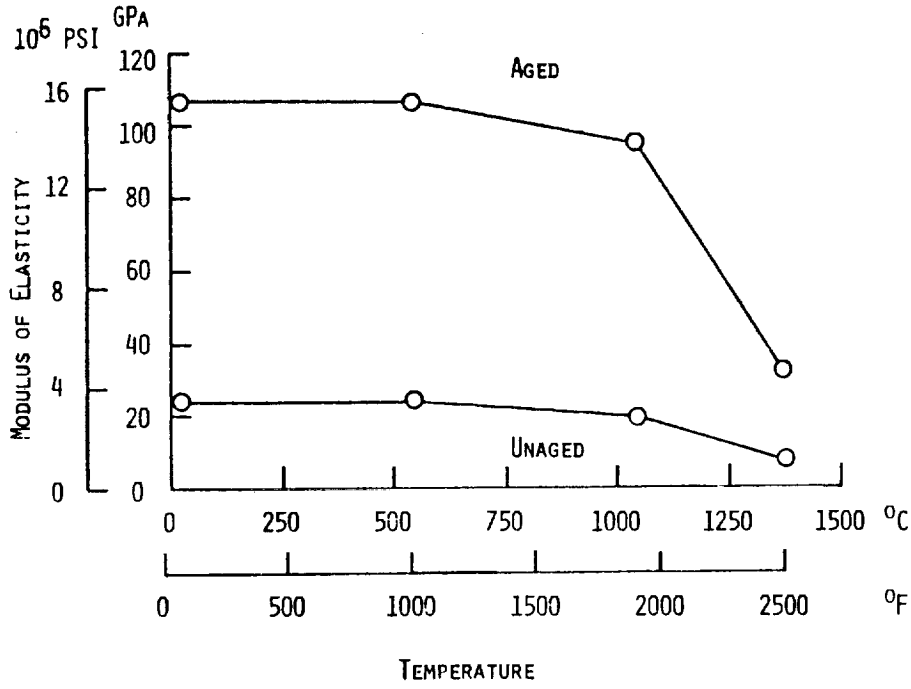

Figure B-3 Modulus of Elasticity of the Baseline 100% Layer Increases with Aging, 50 Hours at 1371°C (2500°F)

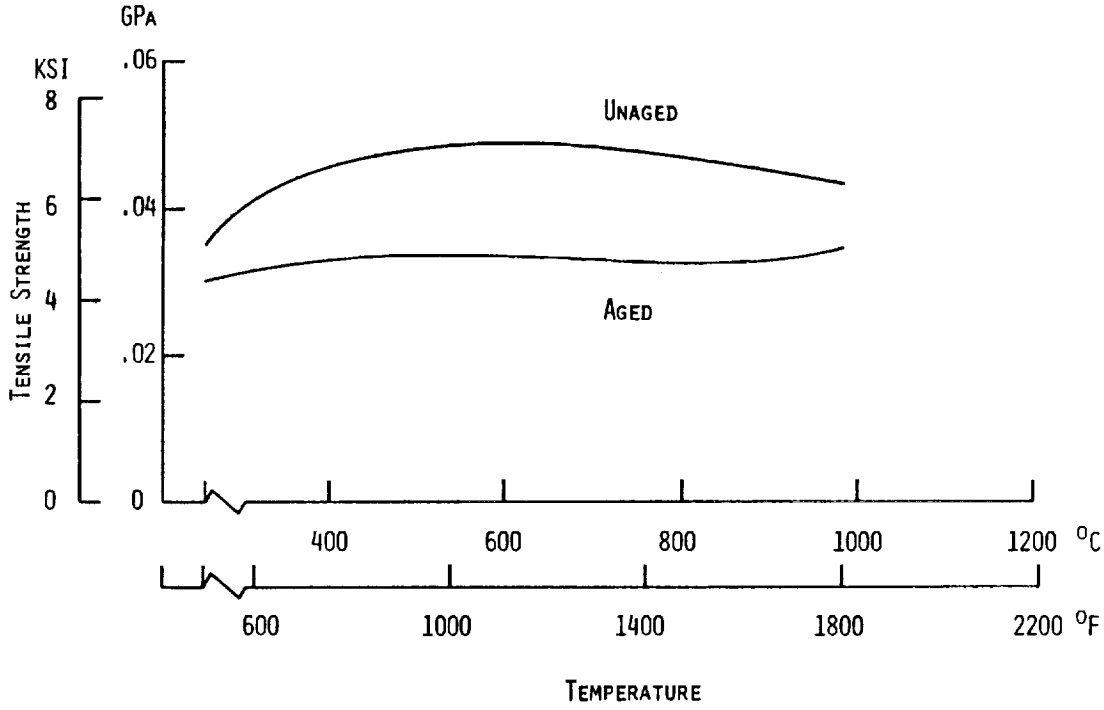

Figure B-4 The Tensile Strength of the Baseline 85% Layer Decreases with Aging, 300 Hours at 871°C (1600°F)

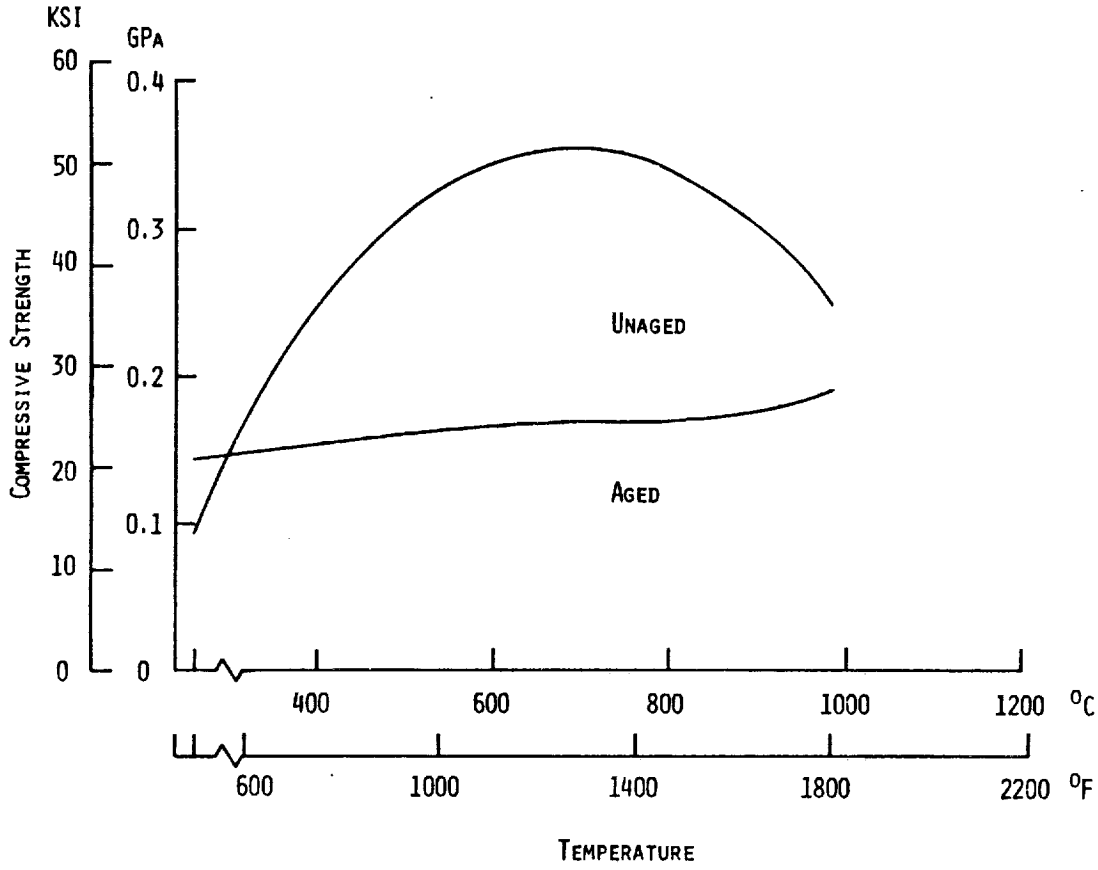

Figure B-5 Aging of the Baseline 85% Layer for 300 Hours at 871°C (1600°F) Decreases the Compressive Strength Except at Room Temperature

Figure B-10 is a comparison of thermal conductivity of the baseline 100% layer unaged and aged for 50 hours at 1371°C (2500°F). The results show a factor of 2 increase in thermal conductivity for the aged over the unaged material. This is due to an increase in diffusivity. No change was noted in the values obtained for specific heat. The thermal expansion data (Figure B-11) is essentially the same as the unaged baseline data taken after the first heat-up cycle. The shrinkage typically seen during the first heat up cycle of the as-sprayed material at temperatures above 1093°C (2000°F) was not observed.

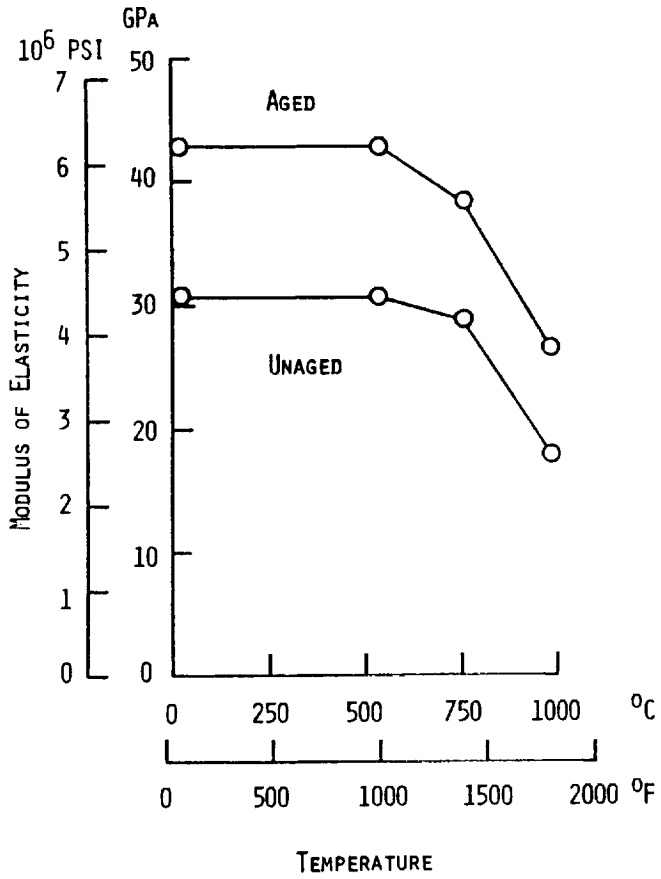

Figure B-6 Aging of the Baseline 85% Layer for 300 Hours at 871°C (1600°F) Increases the Modulus of Elasticity Over the Entire Temperature Range

The thermal conductivity of the aged 85% layer (Figure B-12) was essentially identical to the unaged data except at elevated temperatures where the conductivity of the aged material was 5% less than the unaged. The thermal expansion data of the aged material is within ±5% of the unaged material (Figure B-13).

The thermal conductivity of the 40% layer after aging increased by 50% (Figure B-14). This was due to an increase in density, specific heat and diffusivity. The thermal expansion was slightly less than the unaged baseline data as shown in Figure B-15. The metallic content of the aged material was less than that found in the unaged baseline rings, which could have contributed to the difference.

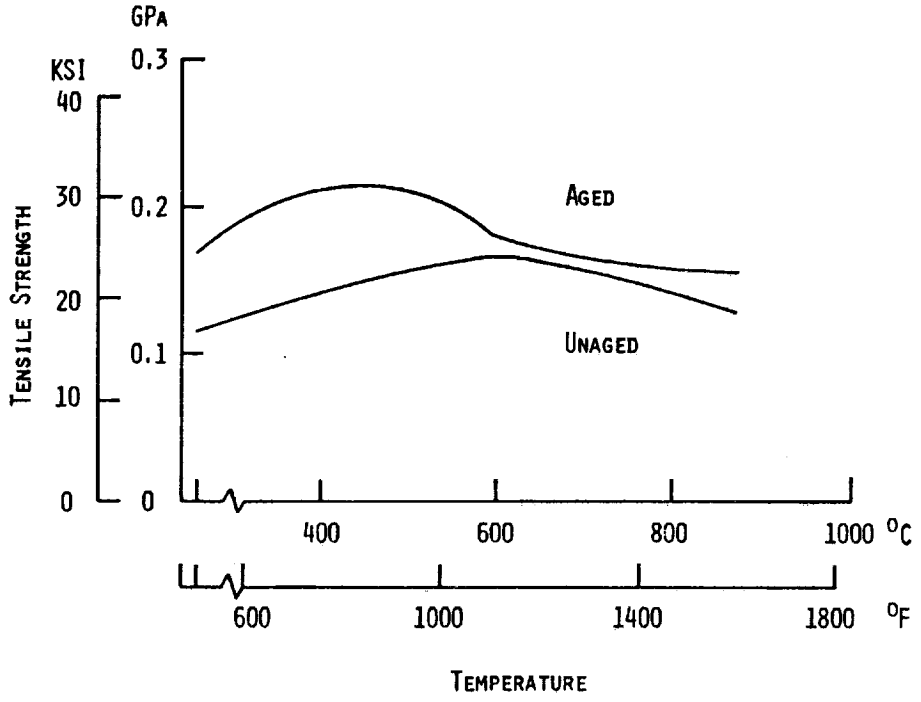

Figure B-7 Tensile Strength of the Baseline 40% Layer Aged for 500 Hours at 760°C (1400°F) is Slightly Higher than the Unaged 40% Layer

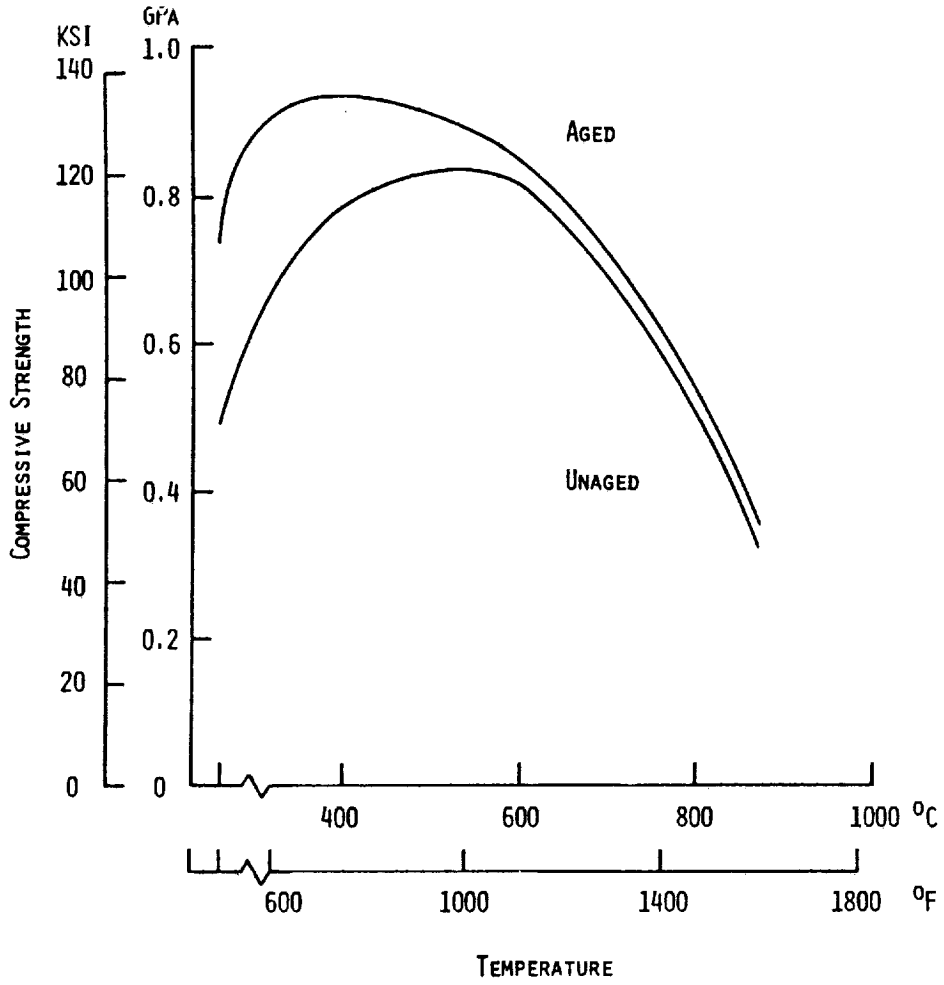

Figure B-8 Compressive Strength of the Baseline 40% Layer Aged for 500 Hours at 760°C (1400°F) is Slightly Higher than the Unaged 40% Layer

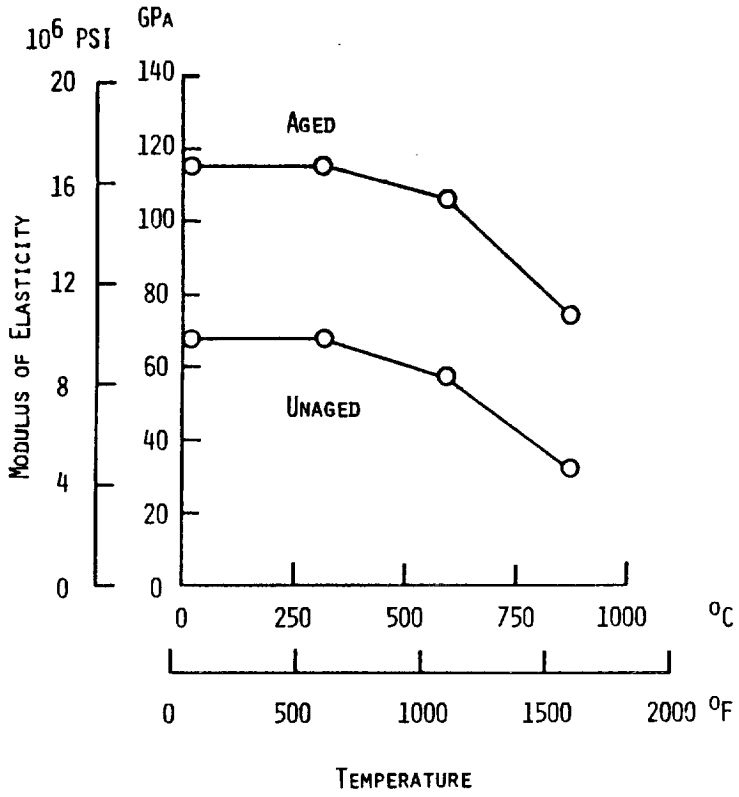

Figure B-9 Aging for 500 Hours at 760°C (1400°F) Increases the Modulus of Elasticity of the Baseline 40% Layer

II Effect of Spray Parameter Changes on Material Properties

The effect of spray parameters on internal properties was determined by varying four selected spray parameters from the baseline system. The spray parameters varied were gun distance, powder feed rate, primary gas flow and power to the gun. These variations were applied to both the 100% and 85% layers. Variations were as follows:

	Gun Distance cm (in)	Powder Feed Rate gm/min (lb/hr)	Primary Gas Flow CMH (CFH)	Gun Power kw
100% Layer				
Baseline	12.7 (5.0)	90 (11.9)	2.1 (75)	36
Variation	6.3 (2.5)	60 (7.93)	2.8 (100)	29
		120 (15.87)	1.7 (60)	46
85% Layer				
Baseline	12.7 (5.0)	45 (5.95)	2.1 (75)	36
Variation	6.3 (2.5)	90 (11.9)	2.8 (100)	46
	15.2 (6.0)	20 (2.64)	1.4 (50)	26

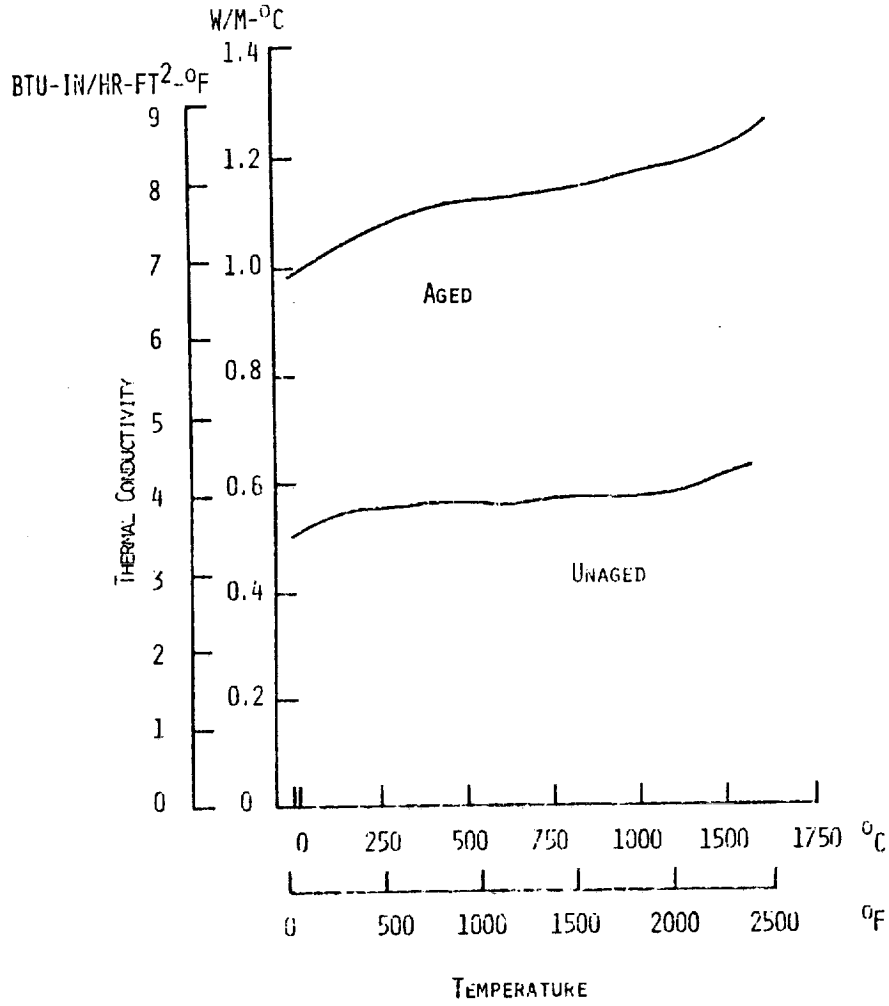

Figure B-10 Aging, 50 Hours at 1371°C (2500°F), of the Baseline 100% Layer Increases the Thermal Conductivity at Least by a Factor of Two

One ring representing each spray parameter variation was fabricated, from which single-layer flat plate specimens were machined. Machined specimens were subjected to property measurements for modulus, tensile strength, compressive strength, and thermal expansion.

Figure B-16 represents tensile strength data for the 100% layer spray parameter variations. With the exception of gun power of 29 kW, all of the spray parameter variations increased the tensile strength of the specimen. The most dramatic increase in tensile strength, approximately 42% over the baseline, was seen in the ring fabricated with a gun standoff of 6.3 cm (2.5 in) which was the parameter change selected for the improved system. Compressive strength data show the same trend in improvement. The ring fabricated with a gun standoff of 6.3 cm (2.5 in) showed an approximate increase of 100% over baseline parts in the temperature range of 537°C (1000°F) to 1371°C (2500°F).

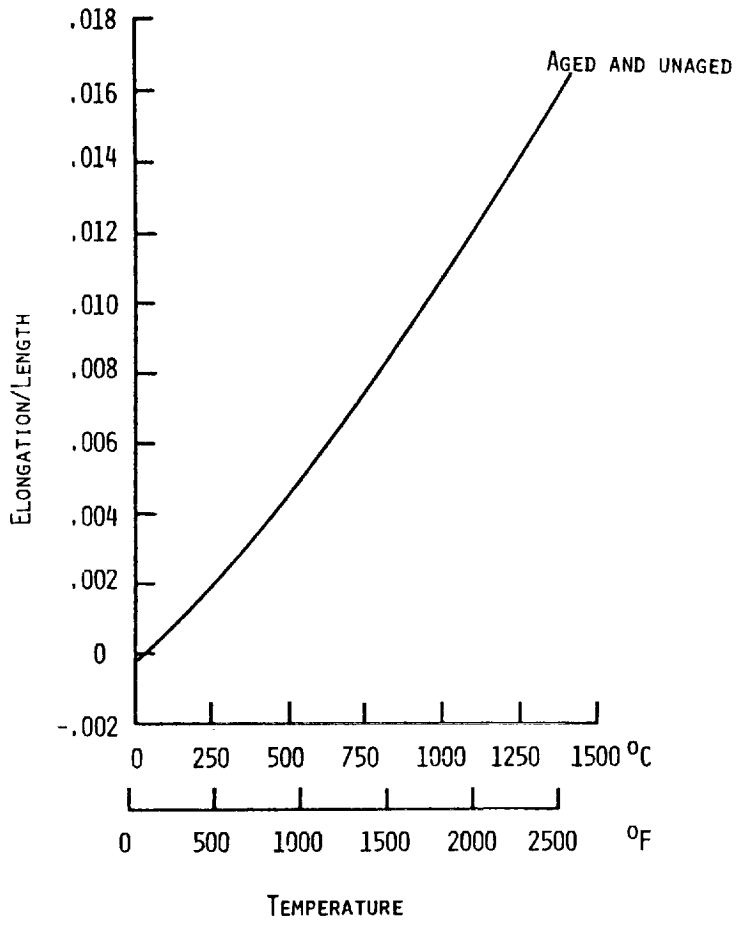

Figure B-11 Aging Does Not Change the Thermal Expansion Values of the Baseline 100% Layer

The elastic modulus of the 100% layer, determined from the tensile and compressive testing, increased for every ring except the one fabricated with a reduction in gun power to 29 kw. The data is plotted in Figure B-17. Since the greater the modulus the greater the stress generated in the thermal environment, and considering both Figures B-16 and B-17, the parameter change selected for the improved system offered the greatest improvement in strength with only a minimal effect on stress.

Figure B-18 shows the average tensile strength for each of the spray parameter variations for the 85% layer. Increasing the gun standoff to 15.2 cm (6.0 in) demonstrated the greatest increase in tensile strength. The compressive strength showed no significant increase over the baseline except for the ring fabricated with a gun standoff of 6.3 cm (2.5 in).

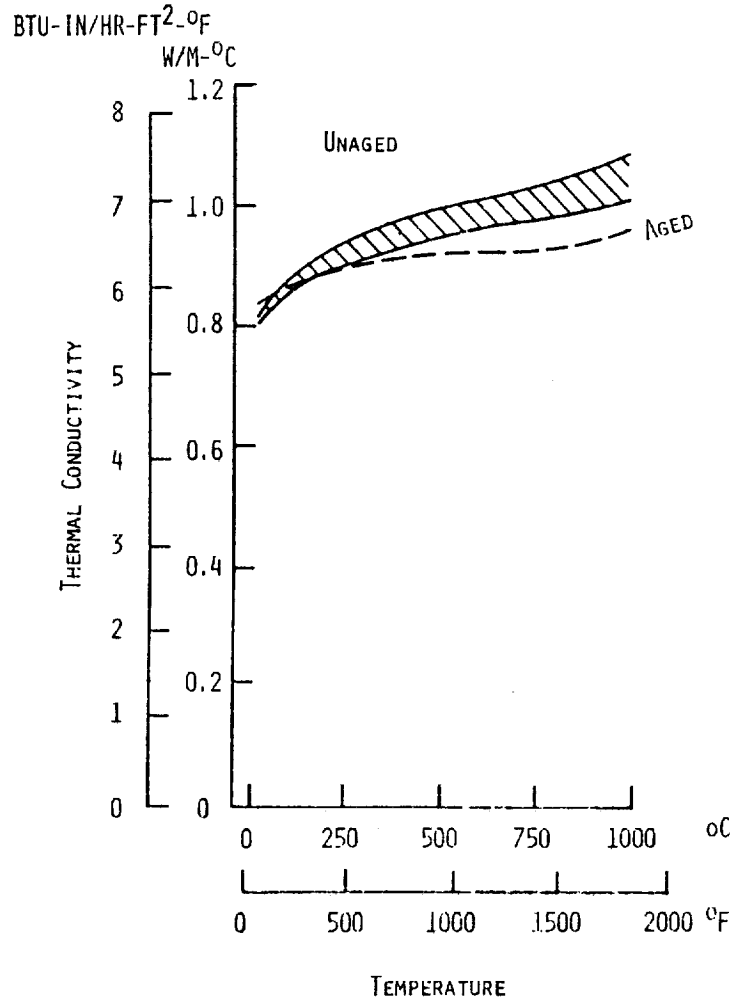

Figure B-12 Aging Did Not Appreciably Change the Thermal Conductivity Values of the Baseline 85% Layer

The elastic modulus of the 85% layer, determined from tensile and compressive testing, decreased for all the spray parameter variations. The ring fabricated with the 6.3 cm (2.5 in) gun standoff showed the most consistent decrease, a constant 18 to 24% over the entire testing range. The data is plotted in Figure B-19.

It is interesting to note that the 85% layer parameter change selected for the improved system, as a result of thermal rupture testing, had little if any effect on the strength of the layer but has the greatest effect in terms of reducing modulus.

Thermal conductivity of the 100% layer for most of the spray parameter changes was measured and are plotted in Figure B-20. Results show that the baseline value was close to the nominal of all the values measured for the parameter changes.

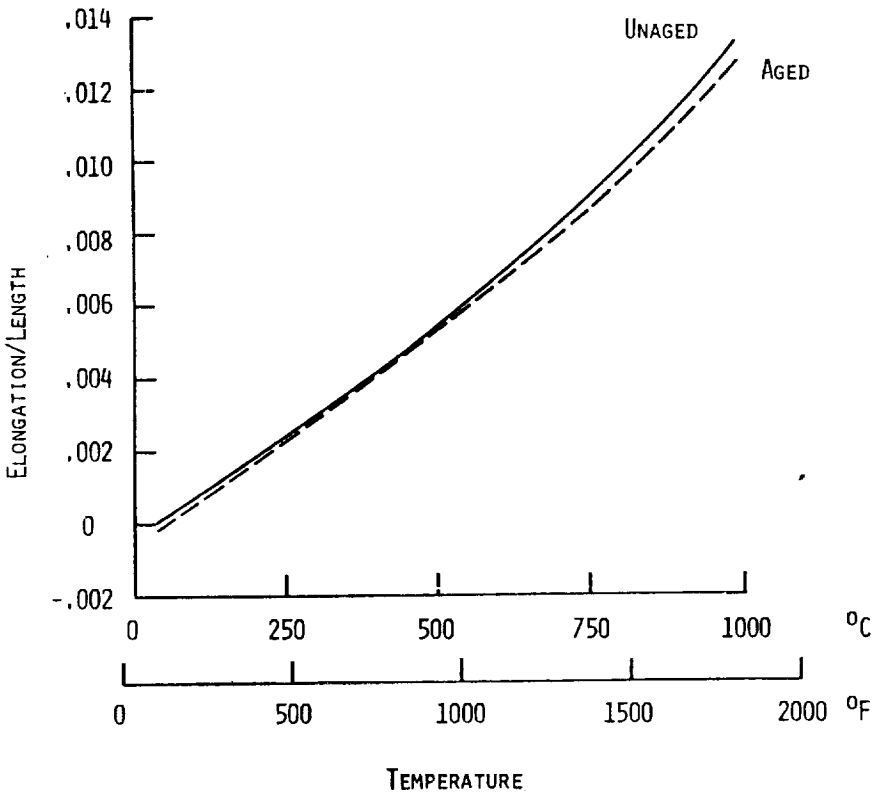

Figure B-13 Thermal Expansion Values of the Baseline 85% Layer Do Not Seem to be Dependent on Aging Effects

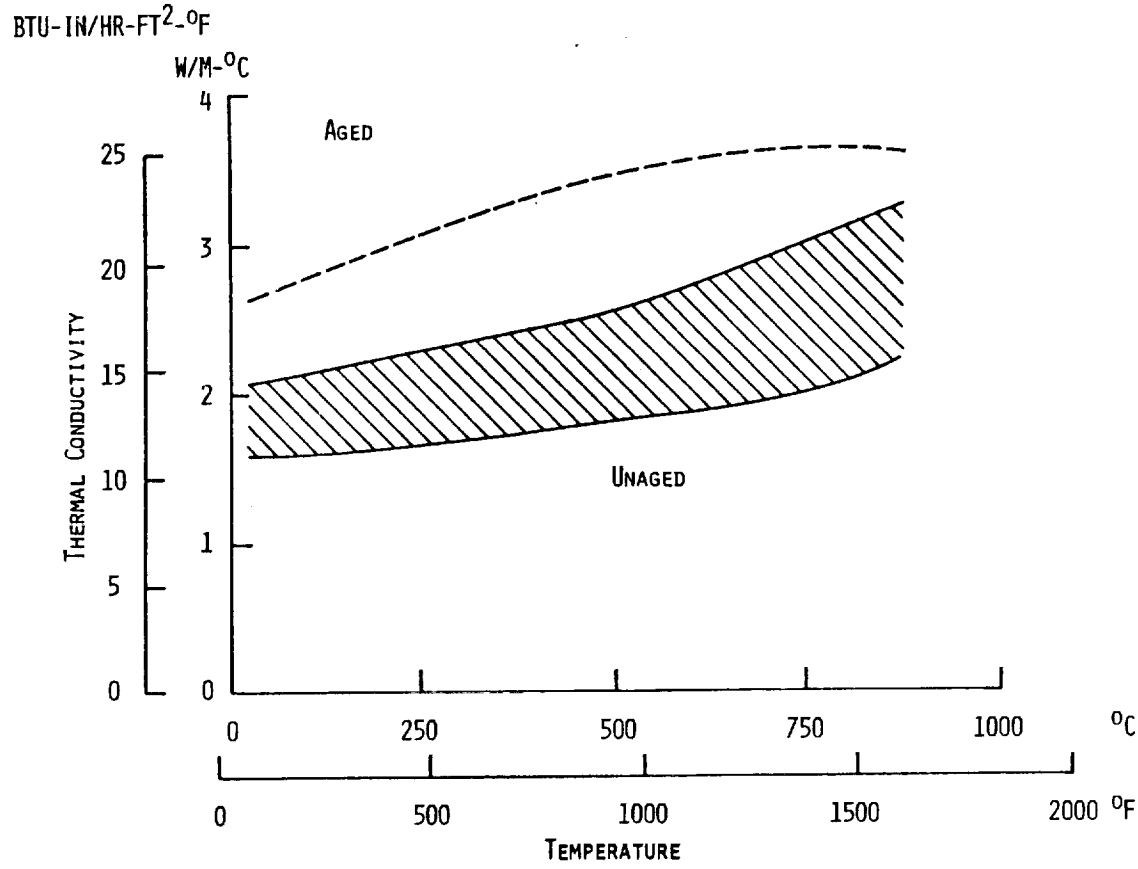

Figure B-14 Thermal Conductivity Increases With Aging, 500 Hours at 760°C (1400°F) of the Baseline 40% Layer

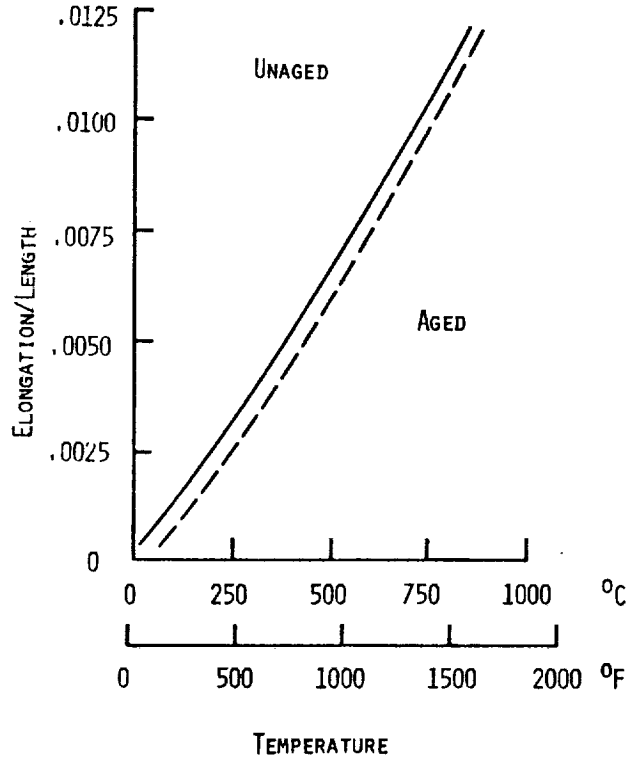

Figure B-15 Aging, 500 Hours at 760°C (1400°F) Marginally Decreased the Thermal Expansion Values of the Baseline 40% Layer

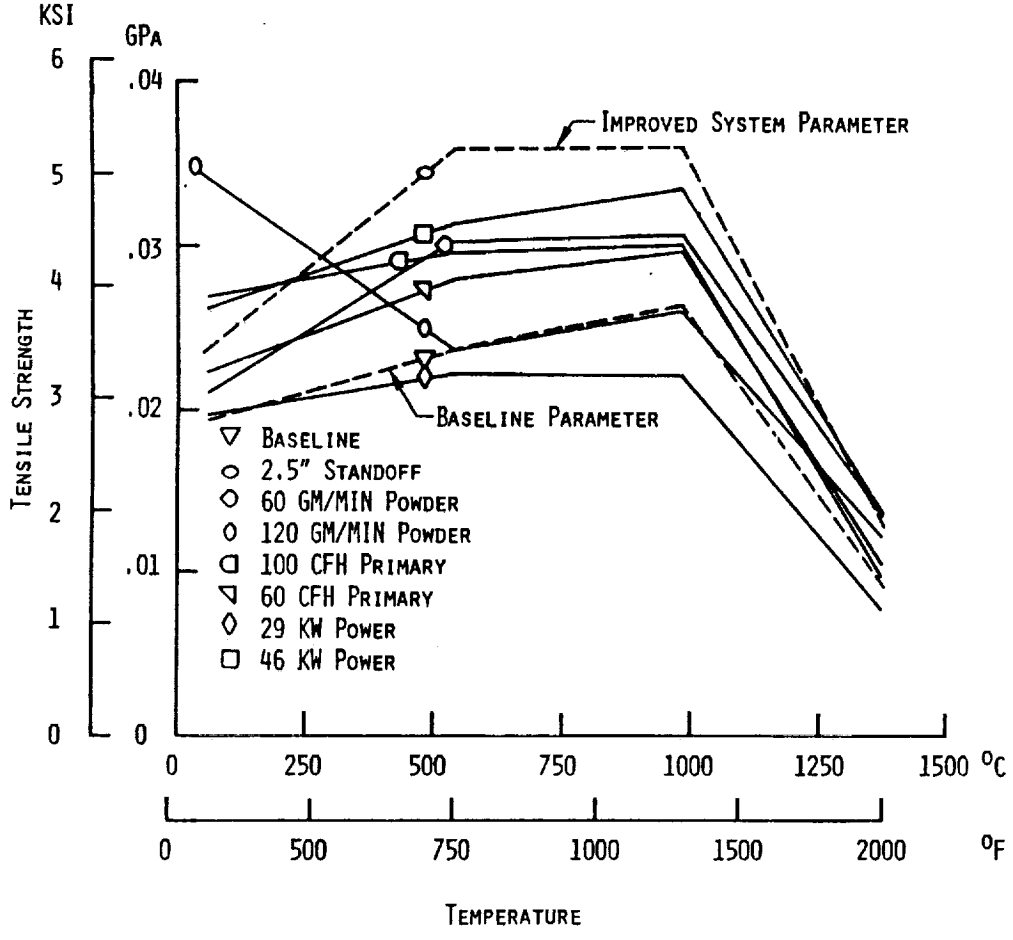

Figure B-16 The Majority of Spray Parameter Changes Resulted in an Increase in Tensile Strength of the 100% Layer

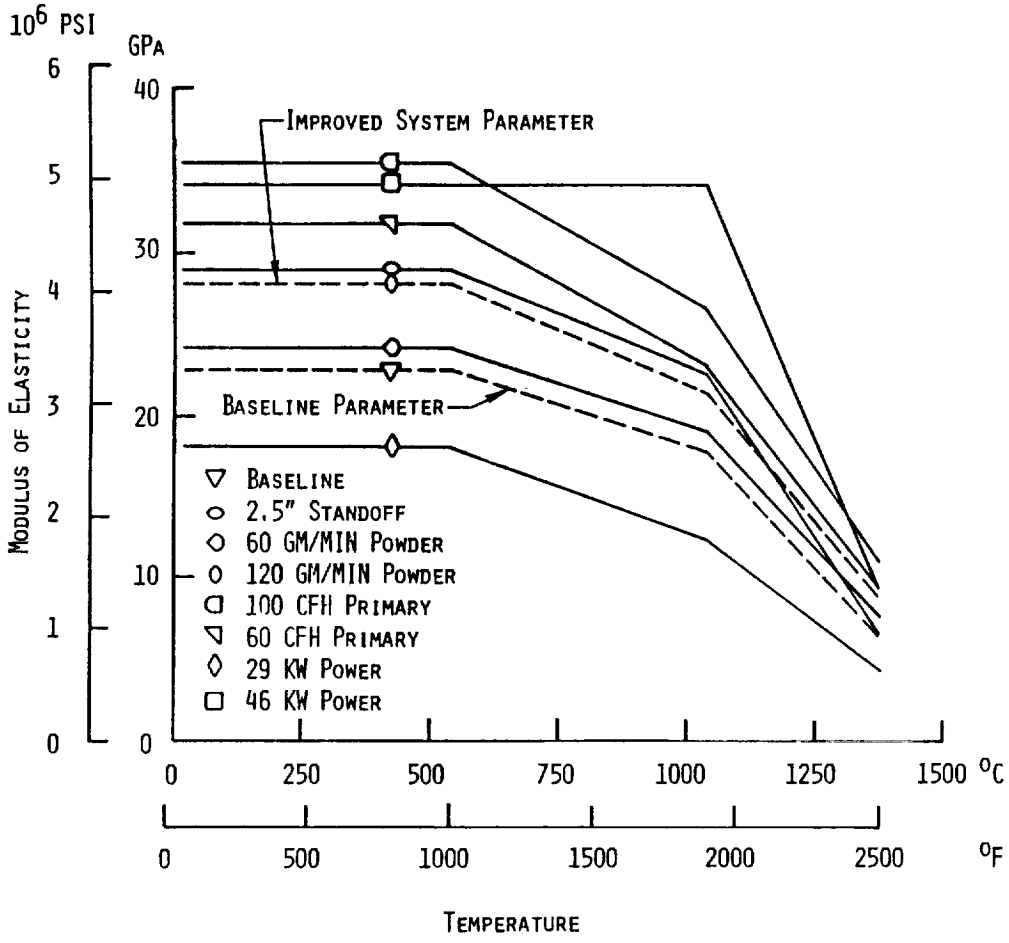

Figure B-17 Spray Parameter changes Generally Increased the 100% Layer Modulus of Elasticity

The elongation due to thermal expansion was measured for each of the spray parameter variations for the 100 % and 85 % layers. The results, presented in Figures B-21 and B-22, show no significant effect of spray parameter variations on thermal expansion.

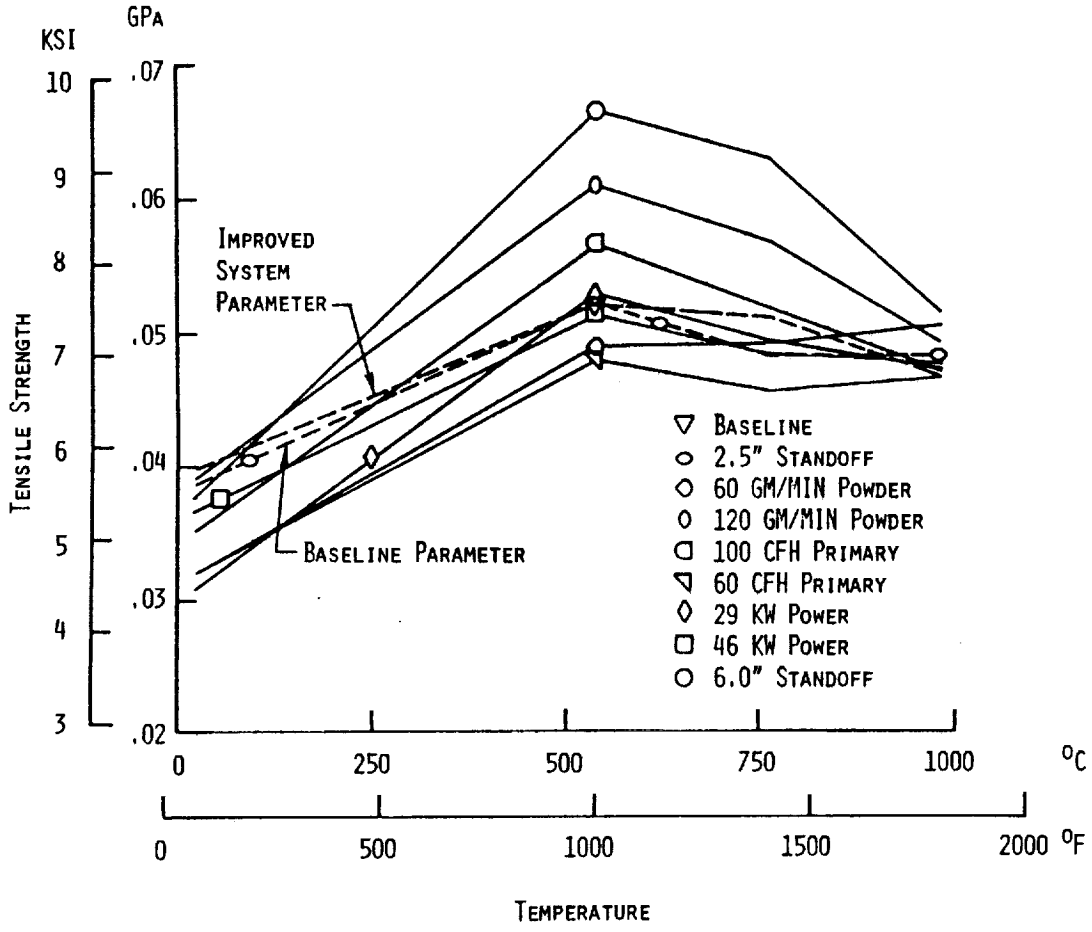

Figure B-18 15.2 Cm (6.0 In) Standoff Resulted in the Greatest Increase in the Tensile Strength of the 85% Layer

III Material Properties and the Effect of Aging of Improved Ceramic Seal System

Test specimens for each of the ceramic/metallic layers used in the improved seal system were thermally aged at temperatures and times representative of their exposure in the JT9D engine environment. The aged specimens were then subjected to property measurements for modulus, tensile strength, compressive strength, thermal conductivity, and thermal expansion.

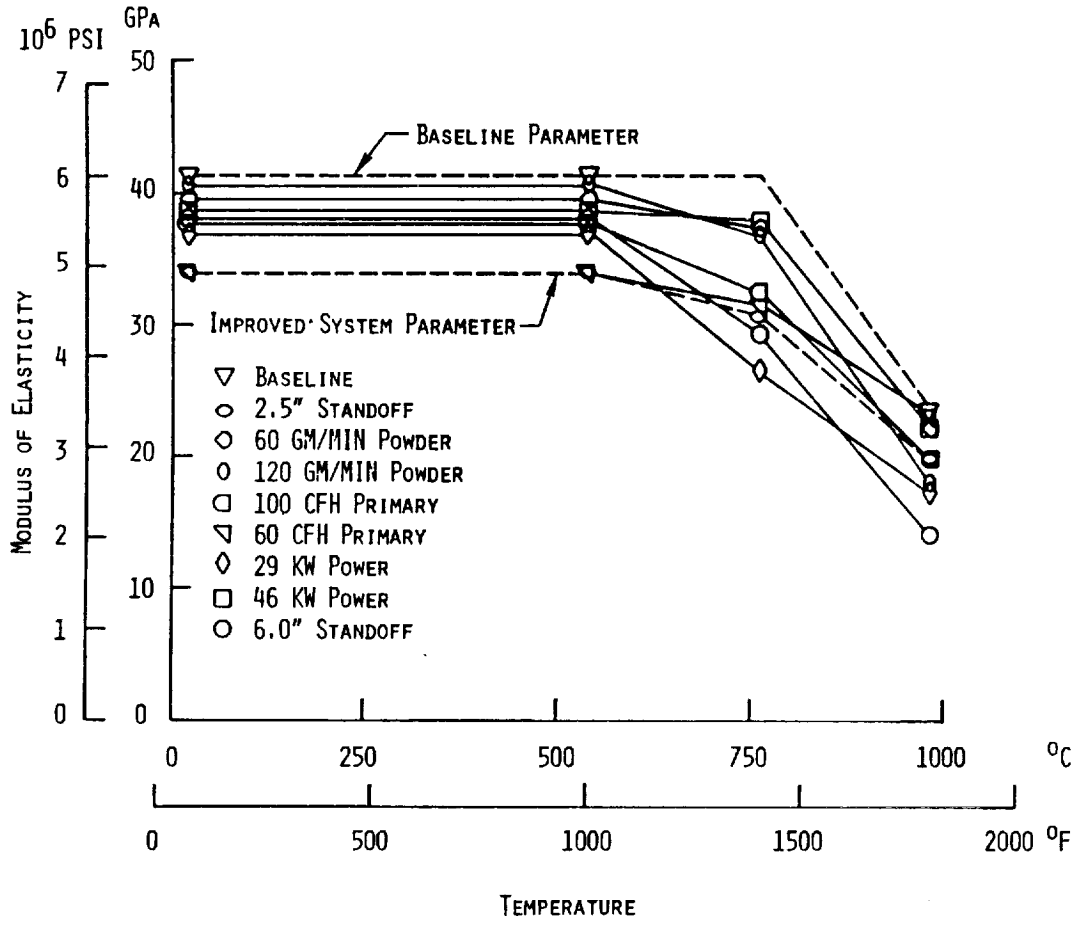

Figure B-19 2.5 Inch Standoff Provided the Greatest Reduction in Modulus for the 85% Layer

Property measurements for the porous zirconia layer were evaluated after being thermally aged at a temperature of 1371°C (2500°F) for 50 hours. Figure B-23 shows the effect of aging on the tensile strength of the material. In the temperature range of 1037°C (1900°F) to 1371°C (2500°F) the strength of the unaged material was at least three times greater than that of the aged material. Only at room temperature was the aged material greater in strength (approximately 3.5 times). The compressive strength as seen in Figure B-24 shows aged specimens to be stronger than the unaged specimen except at the maximum temperature. At all temperatures the modulus of the aged material is higher than the unaged as shown in Figure B-25.

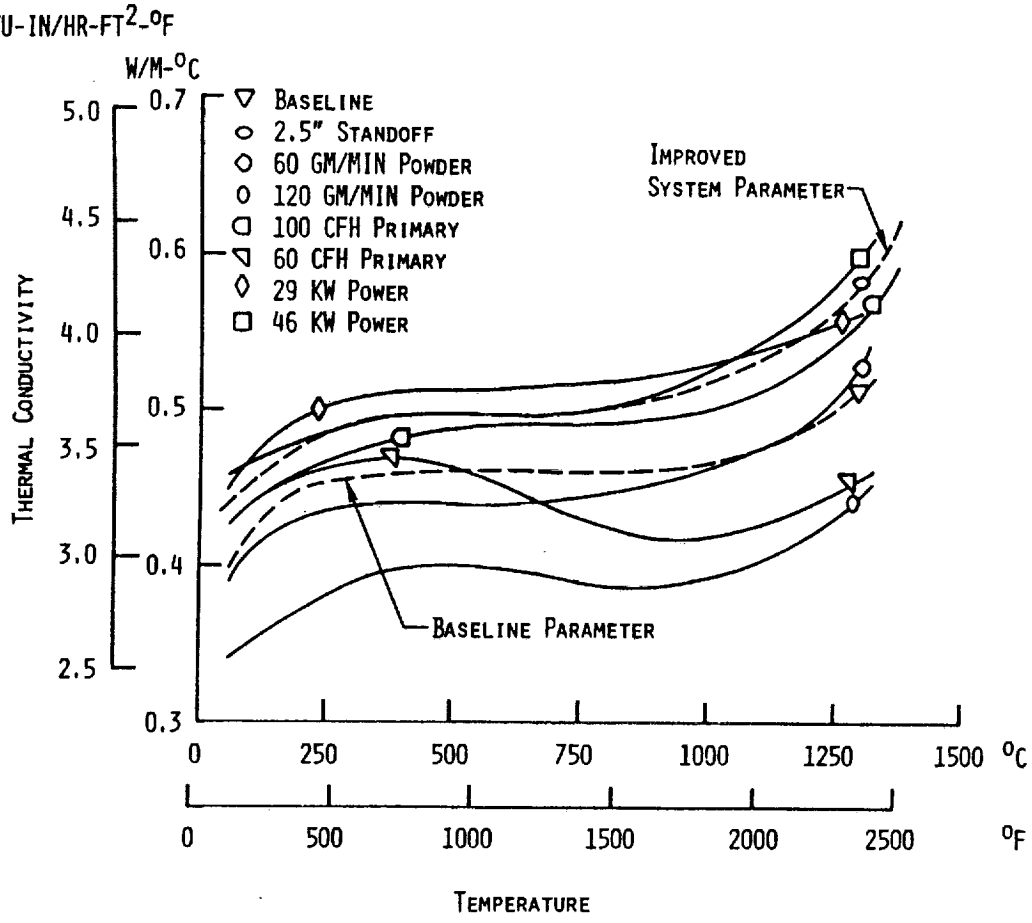

Figure B-20 Thermal Conductivity of Improved 100% Layer Is Similar to Baseline Value

Property measurements were evaluated on the 100% layer after a fifty hour aging period at a temperature of 1371°C (2500°F). Figure B-26 is a comparison of the aged and unaged tensile strength. At room temperature and 1371°C (2500°F) the aged material shows an increase in strength of almost twice that of the unaged material. At the intermediate temperatures, 537°C (1000°F) to 1037°C (1900°F), the unaged material appears to be stronger. This difference is inconsistent with the aging of the baseline specimens and is probably due to testing accuracy.

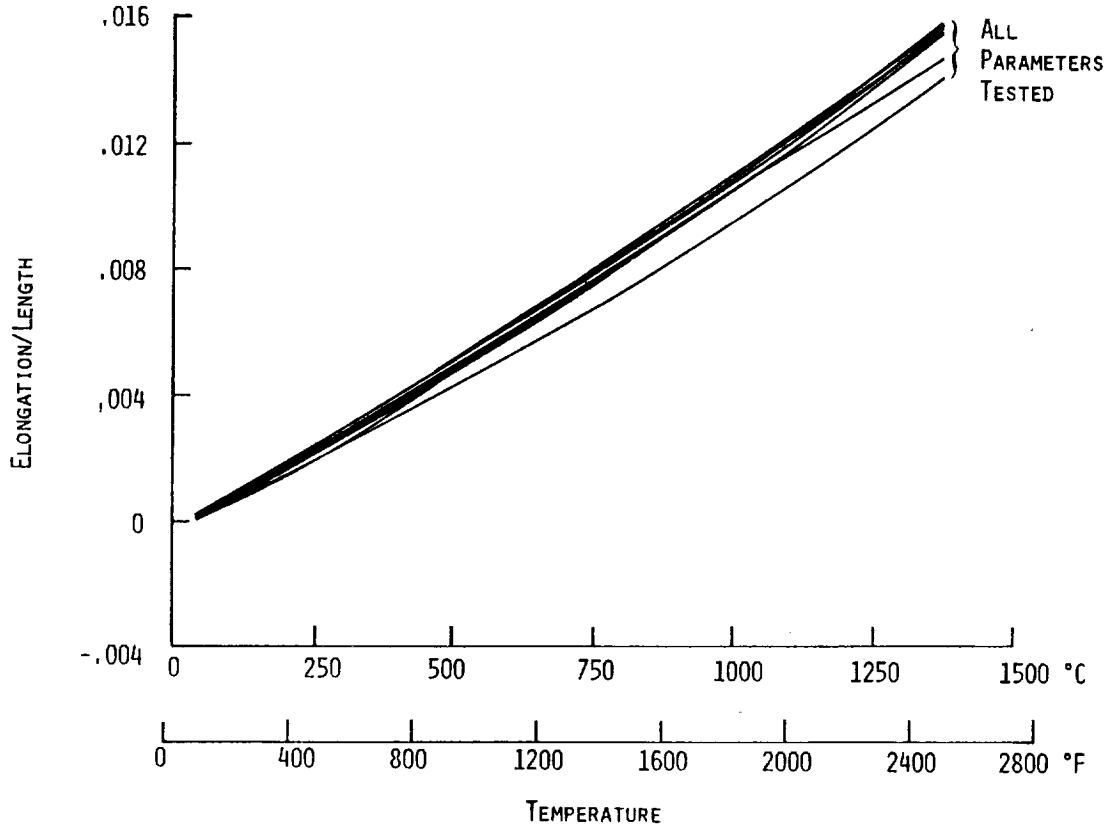

Figure B-21 Spray Parameter Variations Had no Significant Effect on Thermal Expansion in the 100% Layer

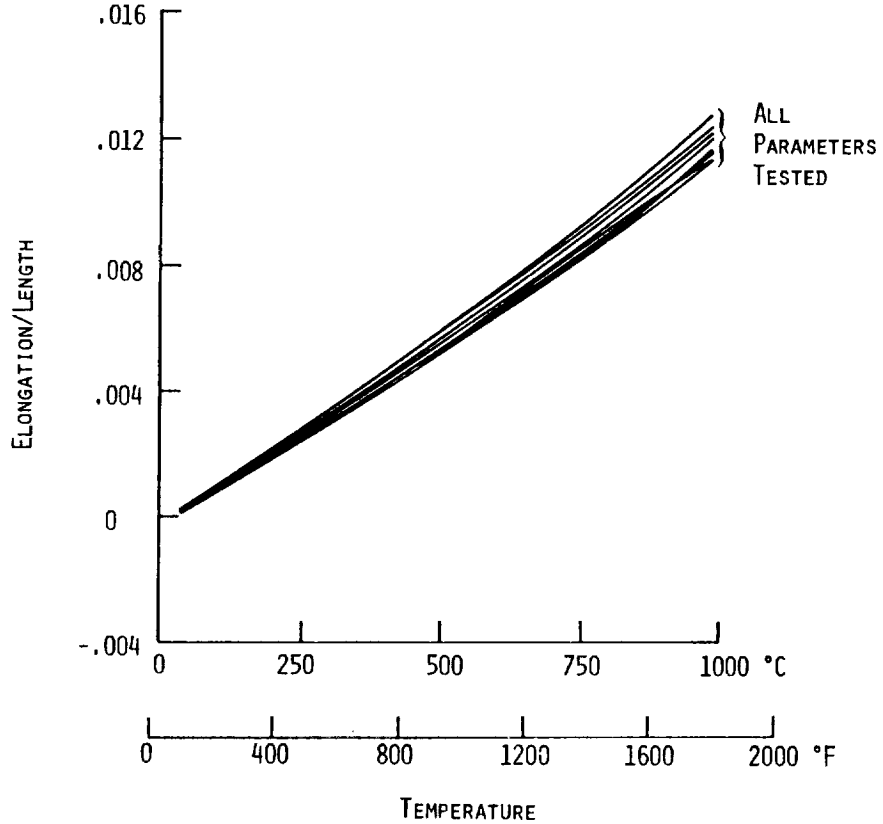

Figure B-22 Spray Parameter Variations Had no Significant Effect on Thermal Expansion in the 85% Layer

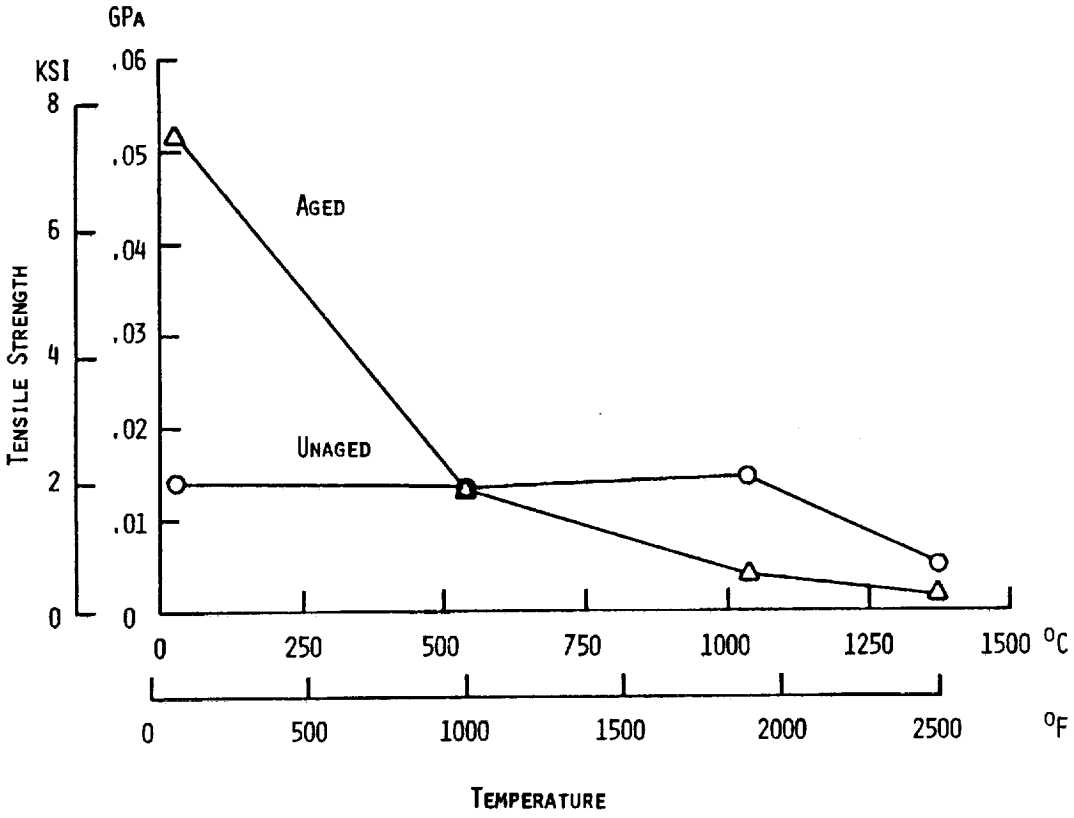

Figure B-23 Aging for 50 Hours at 1371°C (2500°F) Does Not Appreciably Change the Tensile Strength of the Porous Zirconia Layer

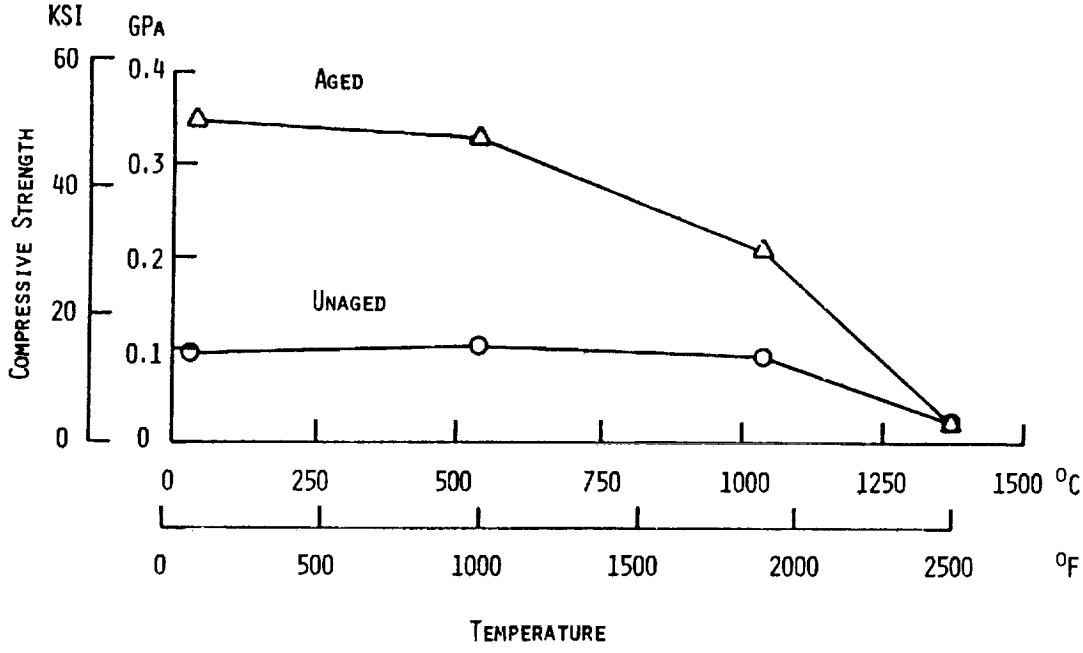

Figure B-24 Aging, 50 Hours at 1371°C (2500°F), of the Porous Zirconia Layer Increases the Compressive Strength

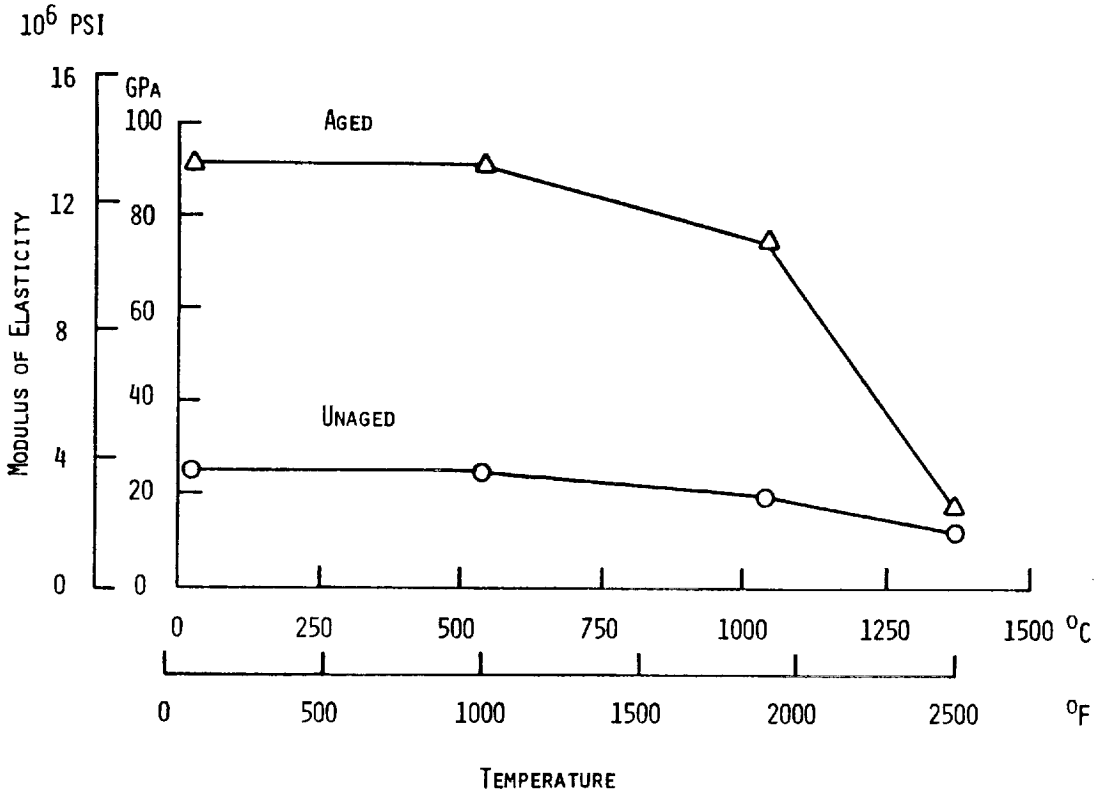

Figure B-25 Aging, 50 Hours at 1371°C (2500°F), of the Porous Zirconia Layer Increases the Modulus of Elasticity

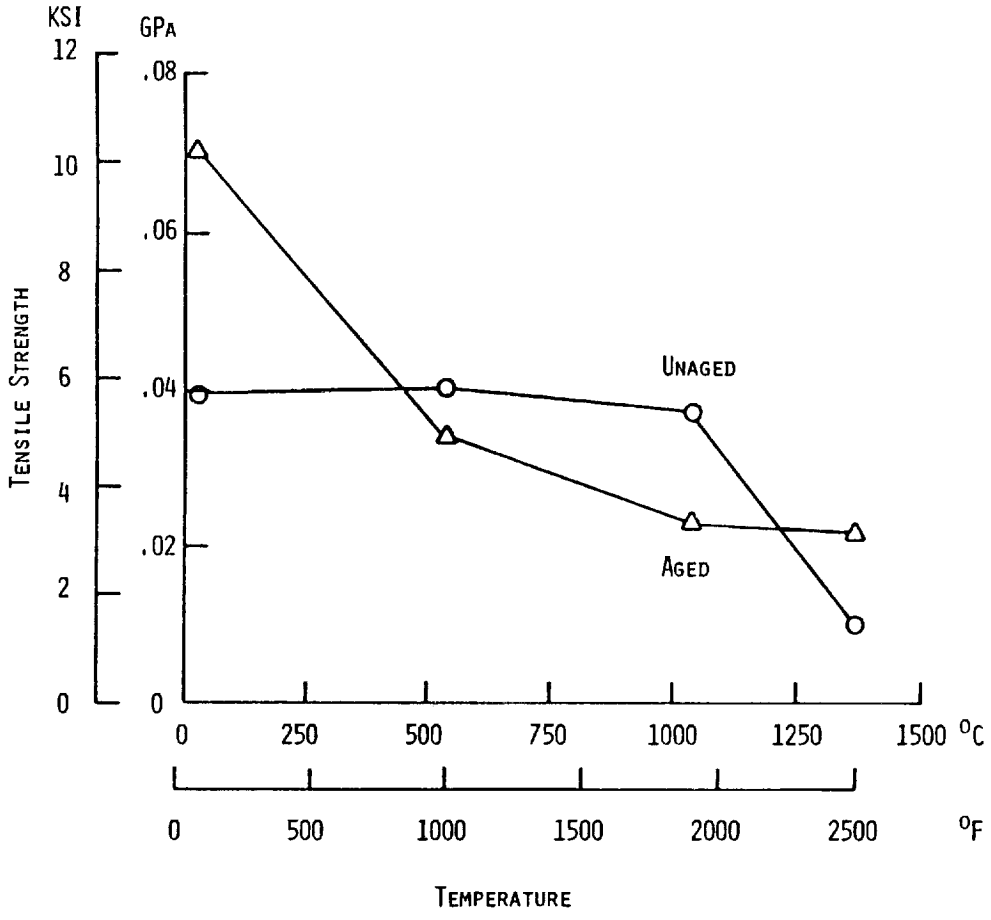

Figure B-26 Aging, 50 Hours at 1371°C (2500°F), of the Improved 100% Layer Decreases the Tensile Strength in the 537°C (1000°F) to 1093°C (2000°F) Range

Figure B-27 gives a comparison of the compressive strength of the aged and unaged material. Maximum increase in strength of the aged material occurs at 537°C (1000°F) where it is almost twice the strength of the unaged material. At 1037°C (1900°F) the aged material is still stronger than the unaged material but only by a factor of 1.3. At 1371°C (2500°F) the trend reverses itself and the unaged material is 1.1 times greater in strength than the aged material.

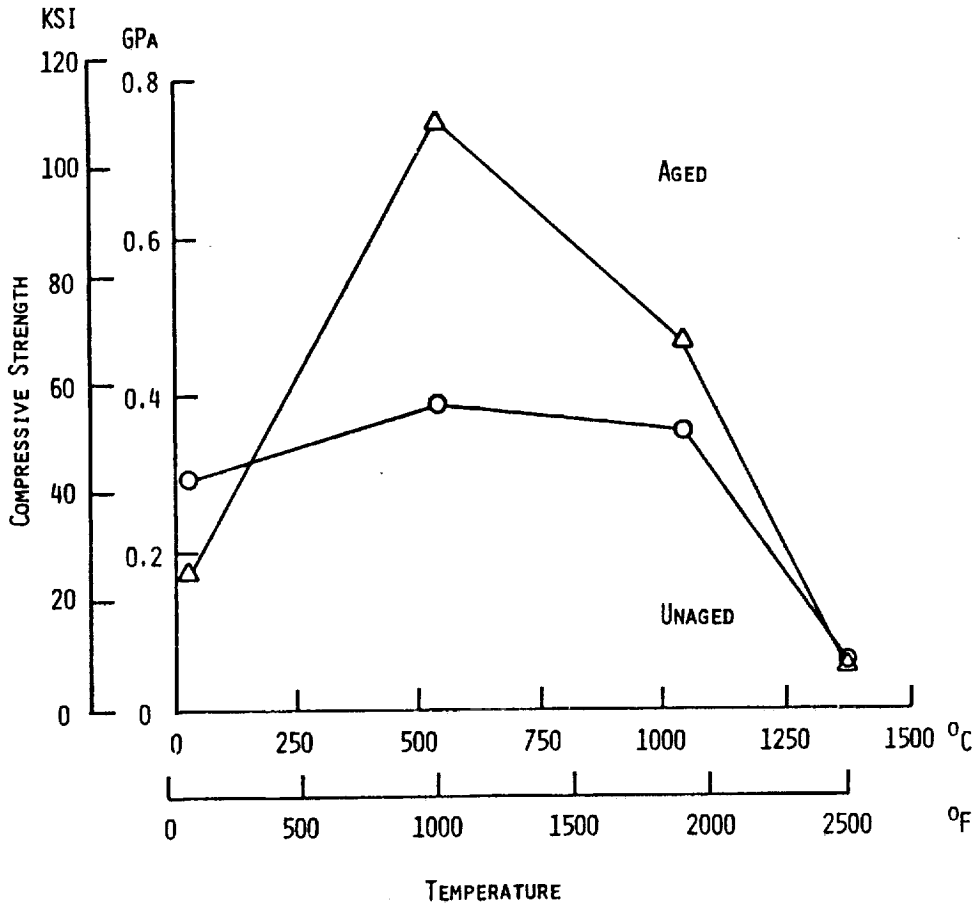

Figure B-27 Aging, 50 Hours at 1371°C (2500°F), of the Improved 100% Layer Increases the Compressive Strength Over the Majority of the Temperature Range

At all temperatures the modulus of the aged material greatly exceeds that of the unaged material (Figure B-28). From room temperature to 1371°C (2500°F) the modulus of the aged material is three times that of the unaged material.

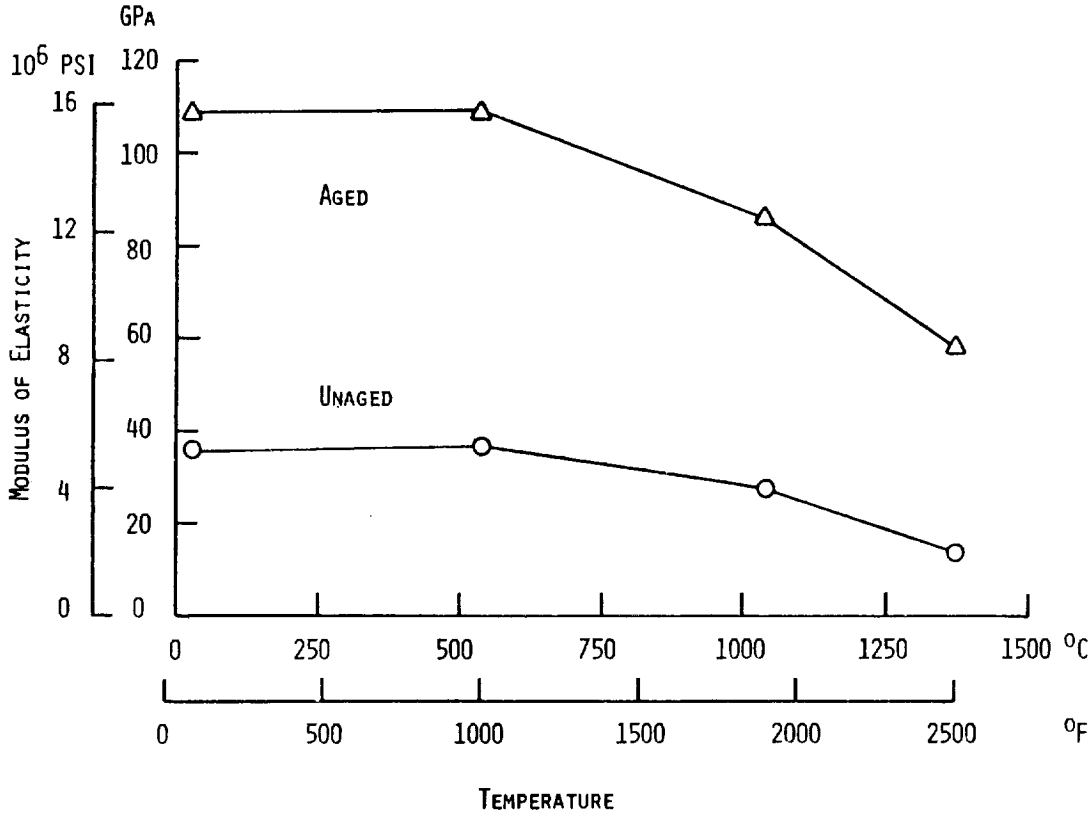

Figure B-28 Aging, 50 Hours at 1371°C (2500°F), Increases the Modulus of Elasticity of the Improved 100% Layer

Property measurements for the 85% layer were evaluated after an aging period of 300 hours at a temperature of 871°C (1600°F). Figure B-28 is a comparison of the tensile strength of the aged and the unaged material. As was noted with previous aging tests, the unaged material is stronger than the aged, in this case approximately 1.7 times stronger over the entire temperature range. Compressive strength was also consistently stronger for the unaged material by as much as 2.5 times that of the aged material in the temperature range from 537°C (1000°F) to 760°C (1400°F) as shown in Figure B-30. The modulus of elasticity of the aged material is always greater than the modulus of unaged material (Figure B-31).

The 40% layer was not changed for the improved system and therefore the property values and effect of aging is the same as reported in section I of this appendix.

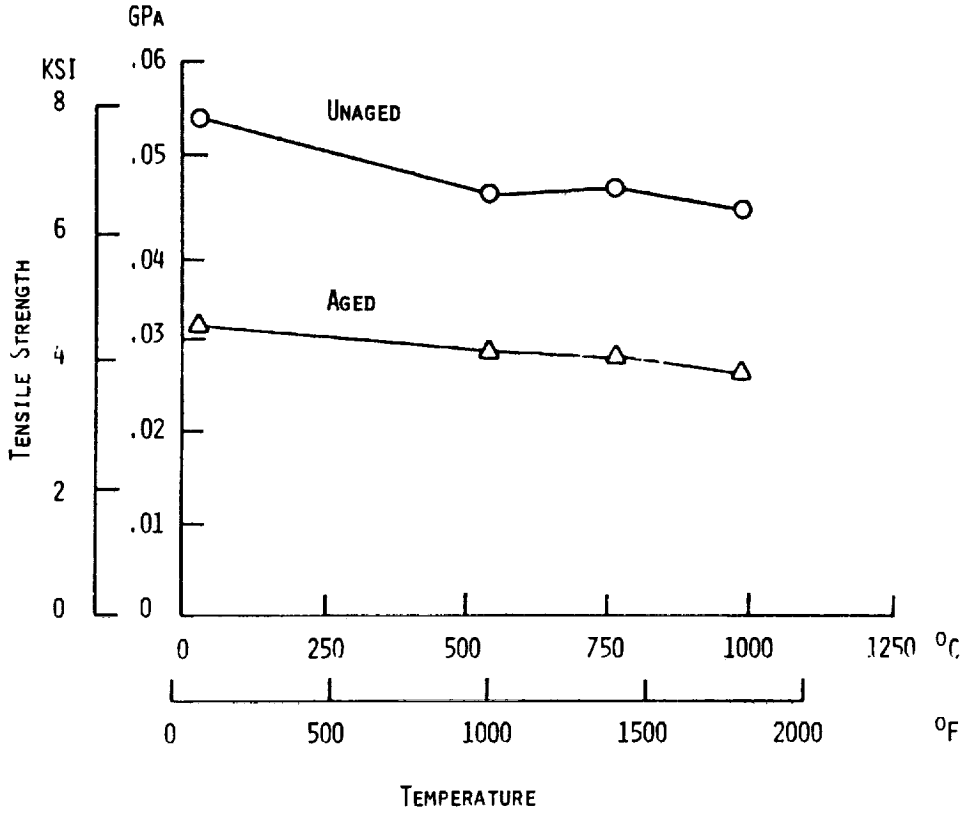

Figure B-29 Tensile Strength of the Improved 85% Layer Decreases After Aging for 300 Hours at 871°C (1600°F)

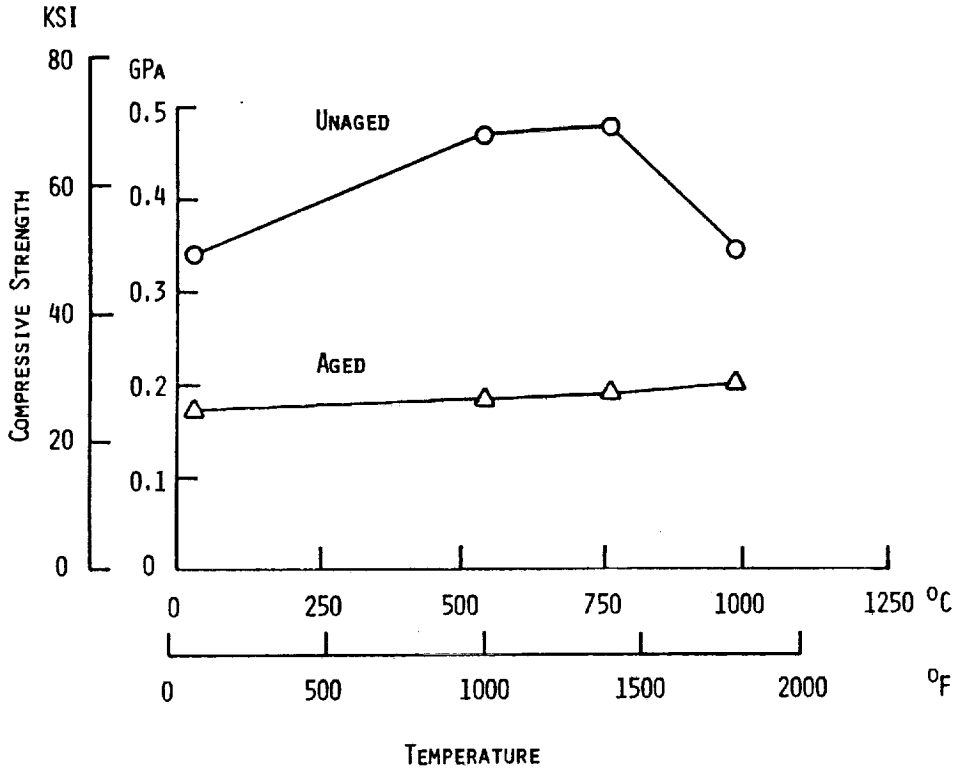

Figure B-30 Aging, 300 Hours at 871°C (1600°F), Decreases the Compressive Strength of the Improved 85% Layer

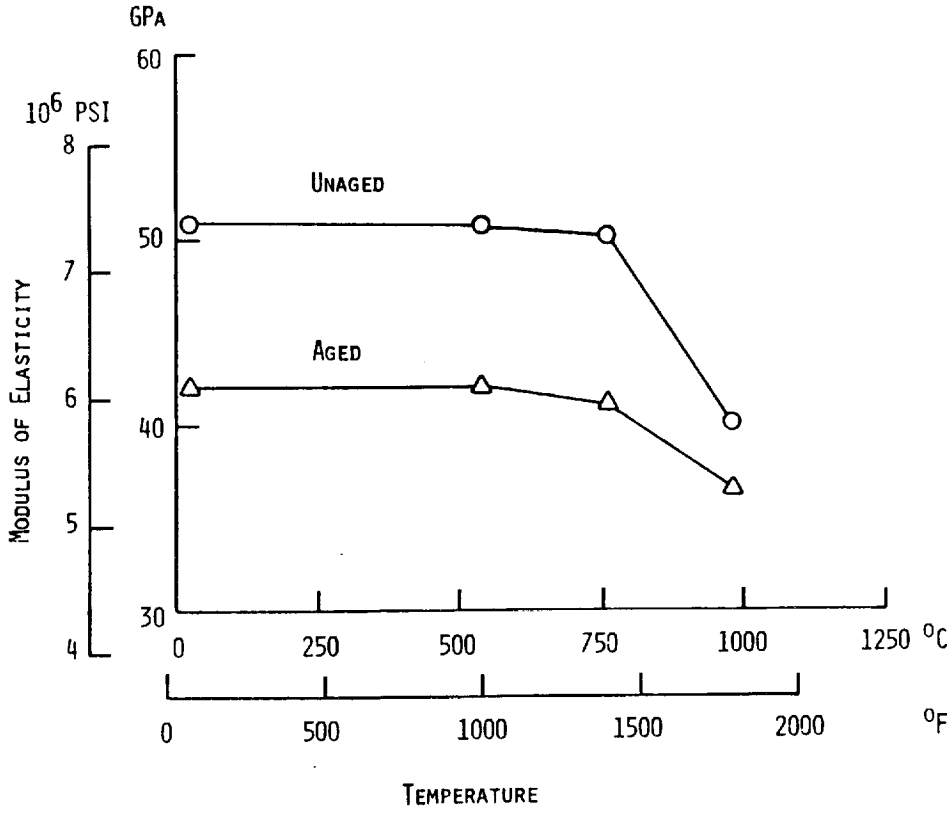

Figure B-31 Aging, 300 Hours at 871°C (1600°F), Decreases the Modulus of Elasticity at the Improved 85% Layer

Appendix C

Product Assurance

I Introduction

The Product Assurance system provided for the establishment of quality requirements and determination of compliance with these requirements, from procurement of raw material until the completion of the experimental test. The system ensures the detection of nonconformances, their proper disposition, and effective corrective action.

Materials, parts, and assemblies were controlled and inspected to the requirements of the JT9D Ceramic Outer Air Seal Program. A full production-type program requires inspection to the requirements indicated on the drawings and pertinent specifications. On experimental programs Engineering may delete or waive noncritical inspection requirements that are normally performed by Experimental Quality Assurance.

Parts, assemblies, components and end-item articles were inspected and tested prior to delivery to ensure compliance to all established requirements and specifications.

The results of the required inspections and tests were documented as evidence of quality. Such documents, when requested, were made available to designated Government Representatives for on-site review.

Standard Pratt & Whitney Aircraft Commercial Products Division Quality Assurance Standards currently in effect and consistent with Contractual Quality Assurance Requirements were followed during execution of this task. Specific standards were applied under the contract in the following areas:

1. Purchased Parts and Experimental Machine Shop
2. Experimental Assembly
3. Experimental Test
4. Instrumentation and Equipment
5. Data
6. Records
7. Reliability, Maintainability and Safety

II Purchased Parts And Experimental Machine Shop

Pratt & Whitney Aircraft has the responsibility for the quality of supplier and supplier-subcontractor articles, and effected its responsibility by requiring either control at source by Pratt & Whitney Aircraft Vendor Quality Control or inspection after receipt at Pratt & Whitney Aircraft. Records of inspections and tests performed at source were maintained by the supplier as specified in Pratt & Whitney Aircraft Purchase Order requirements.

Quality Assurance made certain that required inspections and tests of purchased materials and parts were completed either at the supplier's plant or upon receipt at Pratt & Whitney Aircraft.

Receiving inspection included a check for damage in transit, identification of parts against shipping and receiving documents, drawing and specification requirements, and a check for Materials Control Laboratory release. Positive identification and control of parts was maintained pending final inspection and test results.

The parts manufactured in Pratt & Whitney Aircraft Experimental Machine Shop were subject to Experimental Construction procedures to ensure that proper methods and responsibilities for the control of various quality standards were followed.

Drawing control was maintained through an engineering drawing control system. Parts were identified with the foregoing system. Quality Assurance personnel are responsible for reviewing drawings to ensure that the proper inspection requirements are indicated.

Non-conforming experimental articles involved in this program were detected and identified by Experimental Construction, by vendors, or by Experimental Quality Assurance. Non-conforming articles were reviewed by Engineering and Experimental Quality Assurance personnel in deciding disposition. Records of these decisions, including descriptions of the non-conformances were maintained by Experimental Quality Assurance and reviewed by the cognizant Government Quality Assurance Representative.

III Instrumentation And Equipment

Instrumentation and equipment were controlled under the Pratt & Whitney Aircraft Quality Assurance Plan which includes controls on the measuring and test equipment in Experimental Test to specific procedures. All testing and measuring equipment carries a label indicating its status (controlled, monitor or calibrated) and, when applicable, the date of calibration and next due date.

The accuracy of gages and equipment used for quality inspection functions was maintained by means of a control and calibration system. The system provided for the maintenance of reference standards, procedures, records, and environmental control when necessary. Gages and tools used for measurements were calibrated utilizing the aforementioned system.

Reference standards were maintained by periodic reviews for accuracy, stability, and range. Certificates of Traceability establish the relationship of the reference standard to standards in the National Bureau of Standards (NBS). Calibration of work standards against reference standards was accomplished in environmental-controlled areas.

Initial calibration intervals for gaging and measuring equipment were established on the basis of expected usage and operating conditions. The computerized gage control system provided a weekly listing of all gages and equipment requiring calibration, highlighting overdue items.

IV Records

Quality Assurance personnel ensured that records pertaining to quality requirements were adequate and maintained as directed in Experimental Quality Assurance procedures and in accordance with contractual requirements.

Rig build and operating record books were maintained in accordance with Engineering Department requirements. In addition, a consolidated record of operating times for each component test article used in the experimental program was maintained.

V Reliability, Maintainability And Safety

Standard production engine design techniques and criteria, which consider product reliability and maintainability in context with all other requirements (such as performance, weight and cost), were used in defining the parts for the JT9D Ceramic Outer Air Seal Program. The significant stress areas of the modified parts were analyzed to ensure that their structural margins were equal to or better than those of the bill-of-material parts.

The safety activities at Pratt & Whitney Aircraft are designed to fully comply with the applicable sections of the Federal Aviation Regulations, Part 33 Air Worthiness Standards: Aircraft Engines, as established by the Federal Aviation Administration.

REFERENCES

1. Gaffin, W. O. and Webb, D. E., "JT8D and JT9D Jet Engine Performance Improvement Program - Task I Feasibility Analysis - Final Report", NASA CR-159449, April 1979 (PWA-5515-38)

2. Shiembob, L. T., "Development of Improved High Pressure Turbine Outer Gas Path Seal Components," NASA CR 159801, January 1980 (PWA-5568)

DISTRIBUTION

AVCO Lycoming Division
550 South Main Street
Stratford, CT 06497
Attn: A. Bright, Eng. Perform. (1)

Aerojet Manufacturing Company
601 S. Placentia
Fullerton, CA 92634
Attn: J. Kortenhoeven, VP Eng. (1)

Air California
Oakland Intl. Airport
Oakland, CA 94614
Attn: L. Wuth Director Engineering (1)

Air Research Mfg. Co. of Arizona
Dept. 93-200/503-3S
402 South 36th Street
Phoenix, AZ 85010
Attn: K. Fledderjohn (1)

Air Research Mfg. Co. of Arizona
Dept. 93-010/503-4B
P.O. Box 5217
Phoenix, AZ 85010
Attn: Dr. M. C. Steele (1)

Air Transport Association
1709 New York Ave., NW
Washington, DC 20056
Attn: E. Thomas, Asst. VP. Eng. (1)

Alaska Airlines,Inc.
Box 68900
Seattle, WA 98188
Attn: J. S. Bracelen Eng. & Maint.Admin. (1)

American Airlines, Inc.
Tulsa Maint. & Engineering Center
3800 N. Mingo Road
Tulsa, Oklahoma 74151
Attn: Keith Grayson (1)

Arnold Engineering & Development Center
AEDC/XRFX
Arnold AFS, TN 37389
Attn: Dr. James G. Mitchell, Director of
Facility Plans and Programs (1)

Arnold Engineering & Development Center
AEDC/XRFX
Arnold AFS, TN 37389
Attn: R. Roepke (1)

Boeing Company
P.O. Box 3707
Seattle, WA 98124
Attn: R. Martin MS: 73-07 (2)

Braniff International, Braniff Tower
P.O. Box 35001
Exchange Park, Dallas, TX 75235
Attn: Hank Nelson, Director - Powerplant
Engineering (1)

Civil Aeronautics Board
Washington, DC 20428
Attn: J. E. Constantz, Chief, Economic
Analysis Division, B-68 (1)

Continental Airlines, Inc.
Los Angeles International Airport
Los Angeles, CA 90009
Attn: Frank Forster, Director - Powerplant
Engineering (1)

Cooper Airmotive, Inc.
4312 Putman Street
Dallas, TX 75235
Attn: Terry Harrison (1)

Delta Airlines, Inc.
Hartsfield-Atlanta International Airport
Atlanta, GA 30320
Attn: Jim Goodrum (1)

Dept. of Transportation
21000 Second St., SW
Washington, DC 20591
Attn: Harold Ture (1)

Dept. of Transportation, FAA
21000 Second St., SW
Washington, DC 20591
Attn: R. S. Zuckerman, ARD 550, Aircraft Noise
Project Manager (1)

Detroit Diesel Allison Div. GMC
P.O. Box 894
Indianapolis, IN 46206
Attn: R. A. Sulkoske, Dept. 8896 MS: V19 (1)

Eastern Air Lines, Inc.
Miami International Airport
Miami, FL 33148
Attn: M. Dow, Director Pwrplnt Eng.-MIAEW,
Bldg. 21 (1)

Eastern Air Lines, Inc.
Miami International Airport
Miami, FL 33148
Attn: Arthur Fishbein, Pwr. Plnt. Eng.-MIAEW,
Bldg. 21 (1)

Eastern Air Lines, Inc.
Miami International Airport
Miami, FL 33148
Attn: P. M. Johnstone V.P., Engineering (1)

Federal Aviation Administration DOT/FAA/NAFEC
ANA-410, Bldg. 211
Atlantic City, NJ 08405
Attn: Gary Frings, Project Engineer (1)

Federal Express Corp.
Box 727
Memphis, TN 38194
Attn: J. R. Riedmeyer, Maint. and Engrg (1)

Flying Tiger Line, Inc.
7401 World Way West, L. A. Intl. Airport
Los Angeles, CA 90009
Attn: J. Dimin, Powerplant Eng. (1)

Flying Tiger Line, Inc.
7401 World Way West, L. A. Intl. Airport
Los Angeles, CA 90009
Attn: B. Lewandowski (1)

Frontier Airlines, Inc.
8250 Smith Rd.
Denver, CO 80207
Attn: W. B. Durlin Engineering (1)

General Electric Company, Aircraft Engine Group
1 Neumann Way
Evandale, OH 45215
Attn: Mr. A. F. Shexnayder (10)

Hamilton Standard Div. UTC
Windsor Locks, CT 06096
Attn: Louis A. Urban - Senior Design Project
Engineer MS 3-2-36 (1)

Hughes Airwest
San Francisco Int'l Airport
San Francisco, CA 94128
Attn: W. G. Drechsler, Maintenance and
Engineering (1)

Lockheed-California Co.
P.O. Box 551
Burbank, CA 91520
Attn: T. F. Laughlin Jr., Director Aircraft
Oper. - Tech. (1)

McDonnell Douglas
3855 Lakewood Blvd.
Long Beach, CA 90846
Attn: F. L. Junkermann MC 36-41 (1)

McDonnell Douglas
3855 Lakewood Blvd.
Long Beach, CA 90846
Attn: Ronald Kawai MC 36-41 Powerplant
Engineering (1)

McDonnell Douglas
3855 Lakewood Blvd.
Long Beach, CA 90846
Attn: Tech. Lib. ADTL 246-75 (1)

NASA
Washington, DC 20546
Attn: W. S. Aiken/R (1)

NASA
Washington, DC 20546
Attn: Dr. R. S. Colladay/RT-6 (3)

NASA
Washington, DC 20546
Attn: P. G. Johnson/RJT-2 (1)

NASA
Washington, DC 20546
Attn: Dr. J. L. Kerrebrock/R (1)

NASA
Washington, DC 20546
Attn: C. R. Nysmith/R (1)

NASA
Washington, DC 20546
Attn: Dr. W. B. Olstad/R (1)

NASA
Washington, DC 20546
Attn: R. L. Winblade/RJT-2 (1)

NASA - Ames Research Center
Moffett Field, CA 94035
Attn: J. Zuk/MS 237-11 (1)

NASA - Hugh L. Dryden Flight Research Ctr.
P.O. Box 273, Edwards CA 93523
Attn: Dr. J. Albers MS E-PE (1)

NASA - Hugh L. Dryden Flight Research Ctr.
P.O. Box 273, Edwards CA 93523
Attn: F. V. Olinger MS E-EAP (1)

NASA - Hugh L. Dryden Flight Research Ctr.
P.O. Box 273, Edwards CA 93523
Attn: Harold Washington, Chief - Propulsion
Systems Branch MS E-EA (1)

NASA - Langley Research Center
Hampton, VA 23665
Attn: Dr. R. W. Leonard/MS 158 (1)

NASA - Langley Research Center
Hampton, VA 23665
Attn: L. J. Williams/MS 249A (1)

NASA - Lewis Research Center
21000 Brookpark Road
Cleveland, OH 44135
Attn: Chief, Fluid Mechanics & Acoustics
Division MS 5-3 (1)

NASA - Lewis Research Center
21000 Brookpark Road
Cleveland, OH 44135
Attn: Chief, Mechanical Components Branch
MS 23-2 (1)

NASA - Lewis Research Center
21000 Brookpark Road
Cleveland, OH 44135
Attn: Head, Seals & Rotor Dynamics Section/MS
23-2 (1)

NASA - Lewis Research Center
21000 Brookpark Road
Cleveland, OH 44135
Attn: Calvin L. Ball/MS 5-9, Chief - Fan &
Compressor Branch (1)

NASA - Lewis Research Center
21000 Brookpark Road
Cleveland, OH 44135
Attn: Milton A. Beheim/MS 3-5, Director of Aeronautics (1)

NASA - Lewis Research Center
21000 Brookpark Road
Cleveland, OH 44135
Attn: Milton A. Beheim/MS 86-1, Chief, Propulsion Systems Div. (1)

NASA - Lewis Research Center
21000 Brookpark Road
Cleveland, OH 44135
Attn: Carl C. Ciepluch/MS 301-4, Mgr. Energy Efficient Engine Program (3)

NASA - Lewis Research Center
21000 Brookpark Road
Cleveland, OH 44135
Attn: Melvin J. Hartmann/MS 3-7, Director of Science & Technology (1)

NASA - Lewis Research Center
21000 Brookpark Road
Cleveland, OH 44135
Attn: Lewis Library/MS 60-3 (2)

NASA - Lewis Research Center
21000 Brookpark Road
Cleveland, OH 44135
Attn: J. E. McAulay/MS 301-4, Mgr. ECI Program (3)

NASA - Lewis Research Center
21000 Brookpark Road
Cleveland, OH 44135
Attn: D. L. Nored/MS 301-2, Chief, Transport Propulsion Office (1)

NASA - Lewis Research Center
21000 Brookpark Road
Cleveland, OH 44135
Attn: D. J. Poferl/MS 500-207 Chief, Engine Systems Div. (1)

NASA - Lewis Research Center
21000 Brookpark Road
Cleveland, OH 44135
Attn: R. M. Purgert /MS 500-305, Contracting Officer (1)

NASA - Lewis Research Center
21000 Brookpark Road
Cleveland, OH 44135
Attn: Lonnie Reid /MS 5-9 (1), Head, Multistage Compressor Section

NASA - Lewis Research Center
21000 Brookpark Road
Cleveland, OH 44135
Attn: Report Control Office/MS 5-5 (1)

NASA - Lewis Research Center
21000 Brookpark Road
Cleveland, OH 44135
Attn: I. E. Sumner/MS 301-4 (13)

NASA - Lewis Research Center
21000 Brookpark Road
Cleveland, OH 44135
Attn: J. A. Ziemianski/MS 49-6, Chief - Structures and Mechanical Technologies Division (3)

NASA Scientific & Technical Info. Facility
P.O. Box 8757
Baltimore/Washington Intl. Airport, MD 21240
Attn: Accessioning Dept. (30)

National Airlines, Inc.
P.O. Box 592055, Airport Mail Facility
Miami, FL 33159
Attn:R. A. Starner, Director-Engrg. (1)

Naval Air Propulsion Center
1440 Parkway Avenue
Trenton, NJ 08628
Attn: W. L. Pasela - PE 63, Project Engineer-Test & Eval. (1)

Northwest Airlines, Inc.
Minneapolis-St. Paul Int'l. Airport
St. Paul, MN 55111
Attn: A. Radosta - MS 838, Assistant Director, Powerplant Maint. (1)

Ozark Air Lines Inc.
Box 10007
St. Louis, MO 63145
Attn: E. E. Boock, Maint & Engineering (1)

Pacific Airmotive Corp.
2940 N. Hollywood Way
Burbank, CA 91503
Attn: Oddvar Bendikson, Director, Project Engineering (1)

Pacific Airmotive Corp.
2940 N. Hollywood Way
Burbank, CA 91503
Attn: J. R. Gast, Sr. Director Engrg. (1)

Pacific Southwest Airlines
3225 Harbor Dr.
San Diego CA 92101
Attn: L. Norwood, Engineering (1)

Pan American World Airways, Inc.
John F. Kennedy International Airport
Jamaica, NY 11430
Attn: Niels Andersen, Project Engineer (1)

Pan American World Airways, Inc.
John F. Kennedy International Airport
Jamaica, NY 11430
Attn: Angus MacLarty, Director - Powerplant Engineering (1)

Pan American World Airways, Inc.
John F. Kennedy International Airport
Jamaica, NY 11430
Attn: VP & Chief Engineer (1)

Pan American World World Airways
John F. Kennedy International Airport
Jamaica, NY 11430
Attn: Robert E. Clinton, Jr. (1)

Piedmont Airlines
Smith Reynolds Airport
Winston-Salem, NC 27102
Attn: H. M. Cartwright, V.P. Maint. & Engineering (1)

Piedmont Airlines
Smith Reynolds Airport
Winston-Salem, NC 27102
Attn: Paul M. Rehder, Supervisor - Power Plant Engineering (1)

Pratt & Whitney Aircraft Group
400 Main St.
East Hartford, CT 06108
Attn: J. P. Murphy, Chief Quality Performance Branch, AFPRO - OL-AA, Det. 8 (1)

Republic Airlines, Inc.
3500 Airline Dr.
Minneapolis, MN 55450
Attn: D. W. Atwood, Maintenance & Engineering (1)

Seaboard World Airlines, Inc.
Seaboard World Building, JFK Intl. Airport
Jamaica, NY 11430
Attn: J. Farrah, VP Maintenance & Engineering (1)

Seaboard World Airlines, Inc.
Seaboard World Bldg., JFK Intl. Airport
Jamaica, NY 11430
Attn: R. Barba, Manager - Powerplant Engineering (1)

Southwest Airlines, Co.
Box 37611
Dallas TX 75235
Attn: J. A. Vidal, Maintenance & Engineering (1)

Texas International Airlines, Inc.
Box 12788
Houston TX 77017
Attn: R. Stephenson, Engineering (1)

Trans World Airlines
P.O. Box 20126, Kansas City Intl. Airport
Kansas City, MO 64195
Attn: Ken Izumikawa 2-280 MCI (1)

Trans World Airlines
P.O. Box 20126, Kansas City Intl. Airport
Kansas City, MO 64195
Attn: W. D. Sherwood (1)

USAir
International Airport
Pittsburg, PA 15231
Attn: W. G. Peppler, Development Engineering (1)

United Airlines, Inc.
San Francisco International Airport
San Francisco, CA 94128
Attn: John Curry (1)

United Airlines, Inc.
San Francisco International Airport
San Francisco, CA 94128
Attn: James Uhl (1)

Western Air Lines, Inc.
6060 Avion Dr. Box 92005, World Way Postal Ctr.
Los Angeles, CA 90009
Attn: Walter Holtz (1)

Wien Air Alaska, Inc.
4100 Int'l Airport Rd.
Anchorage, AK 99502
Attn: J. E. Colburn, Operations & Maintenance (1)

World Airways,Inc.
Box 2330
Oakland CA 94614
Attn: R. L. Funk, Maintenance & Engineering (1)

Wright Patterson AFB
Dayton, OH 45433
Attn: E. Bailey, AFWAL/NASA PO (1)

Wright-Patterson AFB
Dayton, OH 45433
Attn: Lt. Col. D. S. Dickson, ASD/YZI (1)

Wright-Patterson AFB
Dayton, OH 45433
Attn: C. M. High, ASD/YZE (1)

Wright-Patterson AFB
Dayton, OH 45433
Attn: Maj. C. Klinger, ASD/YZET (1)

Wright-Patterson AFB
Dayton, OH 45433
Attn: E. C. Simpson, AFAPL/TB (1)